Nanometric cutting: mechanisms, practices and future perspectives

Abstract

Nanometric cutting removes material at nanoscale and generates high-quality surfaces with a nanometric finish. In past decades, it has thrived as a mainstream manufacturing technology to produce critical components to advance scientific discovery and promote innovation in various fields, such as astronomy, aerospace, microelectronics, optics and photonics, biology and quantum technology. Therefore, it is timely to develop a review article capturing such developments and establishing directions for future advancement. This article systematically reviews the fundamental issues such as cutting models, material deformation mechanisms and tool wear mechanisms in nanometric cutting. It also presents the working principles of innovative ion implantation-assisted, laser-assisted and ultrasonic vibration-assisted nanometric cutting methods to overcome the challenges of machining difficult-to-cut materials. Practical techniques for the generation of high-quality complex or structured surfaces are also discussed. Finally, challenges and future perspectives of nanometric cutting, as well as the evolution towards atomic and close-to-atomic scale manufacturing, are outlined.

Nomenclature			
UCT	Undeformed chip thickness	LCM	Laser confocal microscopy
BDT	Brittle-to-ductile transition	WLI	White light interferometry
SCD	Single crystal diamond	EBSD	Electron backscatter diffraction
SPDT	Single point diamond turning	LRS	laser Raman spectroscopy
DOC	Depth of cut	GND	Geometrically necessary dislocation
AFM	Atomic force microscope	TB	Twinning boundary
PZT	Piezoelectric ceramic	HAB	High angle boundary
MD	Molecular dynamics	GB	Grain boundary
RGMD	Renormalization group MD	DTL	Dislocation trace line
MPM	Material point method	NiIM	Nanometric machining of ion-implanted materials
MPM-MD	MPM coupled with MD	LAC	Laser-assisted nanometric cutting
FEM	Finite element method	UVAC	Ultrasonic vibration-assisted cutting
QC	Quasicontinuum method	STS	Slow tool servo
SEM	Scanning electron microscope	FTS	Fast tool servo
TEM	Transmission electron microscope	EUV	Extreme ultraviolet
FIB	Focused ion beam	TBNC	Tip-based nanometric cutting
NOSC	No observed surface cracks	ACSM	Atomic and close-to-atomic scale manufacturing

1. Introduction

Since the 1960's, ultra-precision machining technologies have played an increasingly important role in the manufacturing of high-end mechanical, optical and electronic components and products, such as air bearings, spectrometers and range

devices, to name a few. As a mainstream ultra-precision machining technology, nanometric cutting relies on extremely high fidelity in transferring precise machine tool motion and tool profile onto workpieces to produce macroscale components with sub-micrometre form accuracy, nanometre or even sub-nanometre surface finish, and high-precision micro or nano structures. Nanometric cutting is therefore a key enabler in meeting the ever-increasing demand for performance enhancement, light weight and function integration of these high-end components and products, which are becoming established in all major areas of the daily life and can already been found across a broad spectrum of applications in sectors such as automotive, aerospace, photonics, renewable energy, medical device and scientific instruments.

The achievable precision of cutting is determined by the minimum scale of controllable material removal, which can be characterised by a minimum undeformed chip thickness (UCT). Nanometric cutting is the cutting process with the UCT less than 100 nm, and the surface roughness (Ra) on a nanometre or even sub-nanometre scale can be achieved. This distinguishes nanometric cutting from traditional macro cutting, where UCT is usually larger than 100 μm, while the surface roughness (Ra) is 0.1-10 μm [1], and micro cutting, where the UCT is 0.1-100 μm and the surface roughness (Ra) can usually reach 10 to several hundred nanometres. The last three decades have seen remarkable advancements in nanometric cutting, expanding workable materials from non-ferrous metals and polymers to brittle infrared materials and even stainless steels. Employing nanometric cutting, damage-free nano-smooth surfaces on various brittle materials, such as Si [2], Ge [3] and CaF_2 [4], which would be impossible through macro

and micro cuttings due to the nature of brittle fractures, can be constantly achieved. This is done by means of a so-called 'brittle-to-ductile transition' (BDT) phenomenon enabled by setting up appropriate operational conditions, which is discussed in Section 3. Recently, innovative approaches such as ion implantation-assisted, laser-assisted, and ultrasonic vibration-assisted nanometric cutting methods have also been developed to improve the machinability of difficult-to-cut materials, such as brittle and hard materials and ferrous metals.
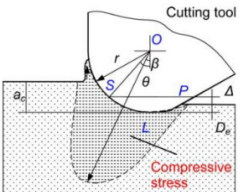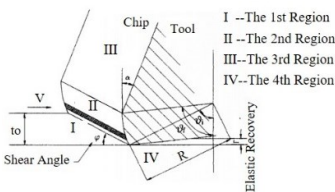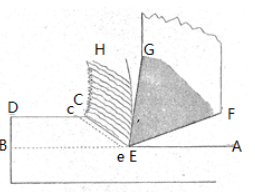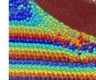
To remove nanoscale material in nanometric cutting, a cutting tool with an extremely sharp edge is required. A single crystal diamond (SCD) tool is considered as the perfect choice for nanometric cutting, since diamond has super-high hardness and heat conductivity and, most importantly can be sharpened to an edge radius of 30–100 nm for commercial use. In nanometric cutting, the UCT of material removal achieved can be tens of nanometres or even lower [5], which determines the surface finish to be obtained. There are mainly two ways to achieve the machining of practical surfaces through nanometric cutting. The first one is using the ultra-precision lathe and diamond tool with nanoscale edge, including single point diamond turning (SPDT), ultra-precision fly-cutting, milling and so on. This method can achieve the nanoscale surface roughness and sub-microscale form accuracy of the products, which are tens of millimetres or even bigger size. The nanometric cutting can be realized through synergistic motions of the tool and workpiece which are precisely controlled. For a specific machining setup, the UCT can be calculated according to the geometrical relationship given the depth of cut (DOC), feed rate and tool nose radius (see Equation

2 in Section 5). The other method is using the atomic force microscope (AFM) and a sharp silicon or diamond tip [6], which is an emerging nanometric cutting technique to remove materials and generate smooth surfaces and/or 2D/3D structures at the nanoscale. The nanoscale UCT is realised by piezoelectric ceramics (PZT)-driven motion of the tip/workpiece and the force feedback control. AFM-tip-based nanomachining will be included in the discussions in this paper (see Section 5.2).

As nanoscale material removal occurs in nanometric cutting, its machining mechanism would fundamentally differ from those in macro and micro cuttings. **Table 1** illustrates the primary characteristics of nanometric, micro and macro cuttings based on current understanding. It shows that the workpiece material cannot be regarded as homogeneous as in macro and micro cuttings in nanometric cutting. With a decrease in UCT to tens of nanometres, the removed material would contain only dozens or hundreds of atomic layers, and the subsurface deformation is usually confined to the superficial layer at nanoscale thickness [7, 8]. For some brittle materials, a crack initiated in the subsurface might extend several micrometres long at most [9]. Thus, it is essential to analyse material deformation based on atomic and micro structures such as point defects, crystal orientation, dislocation, phase transformation and crack initiation. An important feature of nanometric cutting is that the tool edge radius and UCT are both in nanoscale. The edge radius of diamond tools used in practice is commonly larger than the UCT, inducing a large negative effective rake angle and significantly influencing the chip formation [10]. Moreover, with the combined effects of the tool edge, nanoscale UCT and material deformation, ploughing and surface

recovery of the workpiece against the tool flank face become essential in nanometric cutting [11], which in turn influences primary tool wear pattern [12, 13] and the machined surface topography. This is usually neglected in macro cutting. In addition, the size effect from workpiece material behaviour, chip-tool friction [14] and tool edge profile [15] leads to a unique nano-level cutting mechanism, which is quite different from the shearing model widely used in micro and macro cuttings.

Table 1. Primary characteristics among nanometric, micro, and macro cutting (Pictures are reused from Ref. [2, 16, 17])

Characteristics	Nanometric cutting (UCT ≤ 100 nm)	Micro cutting (100 nm < UCT ≤ 100 μm)	Macro cutting (100 μm < UCT)
Material removal model	Round edge tool (nanoscale) Extrusion or shearing	Round edge tool Shear zone	Sharp tool Shear plane
Material mechanics	Atomic/molecular, Heterogeneous	Microstructure, Heterogeneous	Continuum, Homogeneous
Simulation method	Molecular dynamics Multiscale simulation	Finite element Dislocation dynamics	Finite element
Tool wear	Flank face (abrasion, chemical wear)	Flank face & rake face	Rake face (abrasion, adhesion, thermal wear
Surface generation	Elastic recovery apparent	Elastic recovery apparent	Transfer of tool profile (dominant)
Specific cutting energy	Significantly high	High	Low

Current understanding of the mechanisms involved in nanometric cutting remains inconclusive. Some important issues, such as the manner of chip formation, initiation of brittle fracture in defect-free work material, and various tool wear mechanisms for different work materials, still need further understanding. For some difficult-to-cut

materials, such as brittle crystals, ceramics and ferrous metals, it is still hard to obtain the high-quality surface by common nanometric cutting technique because of fracture damage, serious diamond tool wear, or low efficiency. Thus, improving the machinability of these materials is essential for increasing the machining efficiency and promoting the application of nanometric cutting. As shown in **Figure 1**, this paper presents a review of the state-of-the-art nanometric cutting mechanisms, innovative approaches to improve machinability of hard-to-cut materials and practical applications of nanometric cutting techniques. It also goes further to identify future research trends in nanometric cutting. Section 2 introduces the numerical simulation and experimental methods commonly used for the study of nanometric cutting mechanisms. Section 3 presents a systematic study of the state-of-the-art nanometric cutting mechanisms considering cutting models, cutting limit, material deformation and tool wear. Since the mechanical and inner-material structural responses in nanometric cutting are strongly dependent on the type of workpiece material, the subject of material deformation mechanism is divided into two parts for ductile metals/alloys and brittle crystals, respectively. Innovative approaches to improving the machinability of difficult-to-cut materials are presented in Section 4, including surface modification via ion implantation, laser-assisted and ultrasonic vibration-assisted nanometric cuttings. To this end, Section 5 briefly introduces typical and practical nanometric cutting processes and their applications. Finally, the challenges and future perspectives of nanometric cutting are outlined in Section 6.
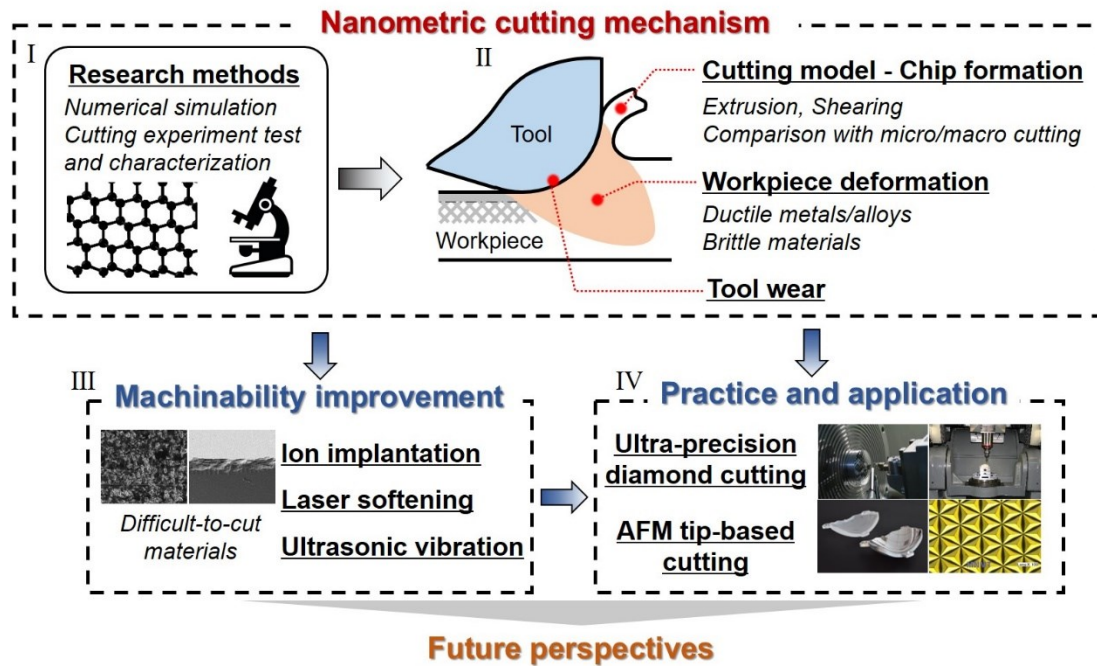
Figure 1. The topics discussed in this paper.

2. Methods to study nanometric cutting mechanism

Current methods in studying nanometric cutting mechanism can be divided into two categories: numerical simulation and experimental investigation. Numerical simulation provides an effective way to obtain the microscopic insight of the cutting process with low cost and high repeatability. It is especially useful for overcoming the limitation of experimental observation, especially for the transient phenomena in nanometric cutting. The local area of nanometric cutting contains at least hundreds of atoms and is normally confined to nanoscale or sub-microscale. Therefore, molecular dynamics (MD) and multiscale modelling are appropriate solutions to numerical simulation of nanometric cutting. Several experimental approaches have also been employed to reveal the material behaviour. For example, taper cutting tests are designed by researchers to study the BDT phenomena of brittle materials in nanometric cutting

[18-20]. Nanoindentation and scratching are also often used to study the material response to nanoscale loading. Force acquisition and high resolution in-situ observation of orthogonal cutting can provide comprehensive information about chip formation process. In addition, experimental characterizations of the machined surface topography, subsurface lattice structural deformation, residual stress, and tool edge wear are also extensively performed as they are essential to understand the cutting mechanism.

2.1   Numerical simulation for studying nanometric cutting mechanism

2.1.1 Molecular dynamics simulation for studying nanometric cutting mechanism

MD simulation is an efficient approach to predict the motion of molecules and atoms in an interacting system to obtain detailed structural evolution at nanoscale. On the basis of well-evaluated potential function or the molecular force field, the motion trail of all the atoms and thus the structural change during the process can be subsequently obtained. Meanwhile, specific physical properties of the system can be calculated. Despite the difference between the MD simulation model and the practical system, this method is still an effective approximation for many materials [21]. As early as the late 1980s, MD simulation was pioneered by researchers in Lawrence Livermore National Laboratory to study the micro-friction and nanometric cutting mechanism on monocrystalline Cu [22, 23]. In the 1990s, researchers explored the nanometric cutting mechanism of monocrystalline Cu and Si using MD simulation [24-28]. These studies accelerated the application of MD simulation in nanometric machining. The subsurface

structural deformation in atomic detail and the physical quantities such as force, energy, stress and temperature during the process can be easily obtained from the simulation. At present, MD simulation has been used to study the nanometric cutting mechanism of monocrystalline or polycrystalline metals and alloys [29-40], semiconductors [41-52], oxide optical materials [53-55], metallic glasses [56, 57] and composite materials [58, 59]. The deformation mechanism of different materials in nanometric cutting is related to the specific atom type and crystal structures. **Table 2** summarizes the typical workpiece materials studied so far by MD simulation, as well as characteristic topics of nanometric cutting mechanism.

Table 2. Nanometric cutting on various workpiece materials by MD simulation.

Categories of workpiece	Materials	Main topics of mechanism & material deformation concerned
Crystalline metal and alloy	Cu [29-32], Al [33, 34], Fe [35, 36], Ni [37], Ce [38], Cu-Be alloy [39], WC [40]	Monocrystalline: (1) Dislocations and stacking faults (2) Nano-sized twin boundary (3) Lattice orientation effects Polycrystalline/alloy: (1) Stacking fault inside the grain (2) Dislocation nucleation accumulation at the grain boundary (GB) (3) Slippage and rotation of the grains

		(4) Sub-grain formation
Brittle crystalline materials	Si [41-45], Ge [46-48], SiC [49-51], GaAs [52], Lu_2O_3 [53], Al_2O_3 [54], SiO_2 [55]	(1) High pressure phase transformation and amorphization (2) Dislocations (3) Crack initiation (4) Lattice orientation and rake angle effects (5) Tool wear mechanism
Other materials	Cu_xZr_y metallic glass [56, 57], composite materials [58, 59], silica glass [60]	(1) Shear band (2) Densification in the local region (3) Composition effects

Nowadays, MD simulation has become a main numerical simulation method in the study of nanometric cutting mechanism. Despite great advantages and potentials, it still faces many challenges. First of all, MD simulation relies heavily on the accuracy of the potential functions. For materials without appropriate potential functions at present, it is hard to conduct the simulation, which restricts the practical use for a wider range of materials. In addition, potential function may not precisely predict all the material properties since it is usually semi-empirical or simplified from the first-principles calculation. For example, the commonly used Tersoff potential would overestimate the melting temperature of monocrystalline Si and Ge [61, 62], which might lead to deviation in the study of thermodynamic issues in nanometric cutting.

Hence, developing more reliable potential functions for nanometric cutting is one of the primary targets in the future. Another issue is the limits of spatial and time scale in MD simulation. An excessively small model may cause a huge discrepancy between simulation and experimental results. In practical nanometric cutting, the tool edge radius and the UCT are always much larger than those in an MD model. Due to the strong size effect at nanoscale, this issue seriously restricts the capability of simulation to reveal the cutting mechanism and reproduce critical phenomena, such as the fractures during the nanometric cutting of brittle materials. Because of heavy computing burden, the feature size of most nanometric cutting models in MD simulation are tens to hundreds of nanometres at most, and the cutting speed is usually much faster than the real cutting speed. Solving this problem may rely on the development of high-performance computation and multiscale simulation.

2.1.2 Enhanced molecular dynamics modelling and multiscale simulation for studying nanometric cutting mechanism

Enlarging the model size is the key to diminish the gap between simulation and experiment in the aspect of size effect in nanometric cutting. However, it requires a dramatic increase in computing resource. The first solution is to accelerate the conventional MD simulation (**Figure 2**a) in two ways. In the aspect of hardware, the graphics processing unit is suitable for increasing the computation speed because the MD algorithm is parallelizable [63]. Another method is dynamic modelling (**Figure 2**b), in which only the material in the vicinity of the tool edge is modelled and adjusted through periodic extension and truncation to keep up with the tool motion [48]. This

helps to optimize the utilization of computer memory and thus enable a larger model. These methods have been successfully adopted to accelerate the simulation of crack formation in nanometric cutting of SiC [64-65].

The second solution is the multiscale simulation, which involves basic principles at various spatial scales and more complex algorithms than MD. The atomic description is only applied where large deformation occurs, such as the local deformation zone near the tool edge. The remaining region can be handled by approximation or empirical theories to reduce the data volume and accelerate the computation. The renormalization group MD (RGMD) and material point method (MPM) coupled with MD (MPM-MD) are two representative methods for particle-based multiscale simulation. In RGMD, the atoms are packaged into clusters (virtual atoms) to reduce the total particle number [66], and the interaction between all particles is described based on the atomic potential function (**Figure 2**c). The analytical solution or finite element method (FEM) result from the elastic region can be used as the reference in RGMD simulation [67, 68]. MPM is a particle-based method that represents the material as a collection of material points, which is effective to handle large deformation. Different from MD, the points here stand for small material elements whose volume are determined by the point density. Their deformation and motion are determined by Newton's laws and constitutive model, instead of atomic potentials. In MPM-MD (**Figure 2**d), a smooth transition of stress/strain from the MPM region to the MD region is important [69]. This "hand-shaking" issue is also critical for the multiscale simulation coupling the mesh-based method and MD simulation, such as the dynamic coupled atomistic/discrete dislocation

method [70] and MD-FEM coupled method (**Figure 2**e) [71, 72]. The quasicontinuum method (QC) is an important MD-FEM coupled approach used in the study of nanometric cutting. In QC, a FEM mesh is constructed based on the "representative atoms" (repatoms) covering the elastic deformation zone in order to reduce the degree of freedom of the system (**Figure 2**f). The density of the repatoms increases with the deformation degree until a fully atomic description is reached [72]. This method has been used to analyse the nanometric cutting mechanism on Cu [73, 74]. Despite the advantage in enlarging the simulation model size, these multiscale simulation methods haven't been widely used in mechanism study of nanometric cutting by now because of the difficulties from theory and programming which are more complex than MD method. In addition, the open source Large-scale Atomic/Molecular Massively Parallel Simulator (LAMMPS) is widely used and easy to extend with new features and functionality, making MD simulation easy to use in research of nanometric cutting mechanism. For multiscale simulation, the few open-source sophisticated code packages available at present creates higher barriers to use in study of nanometric cutting.
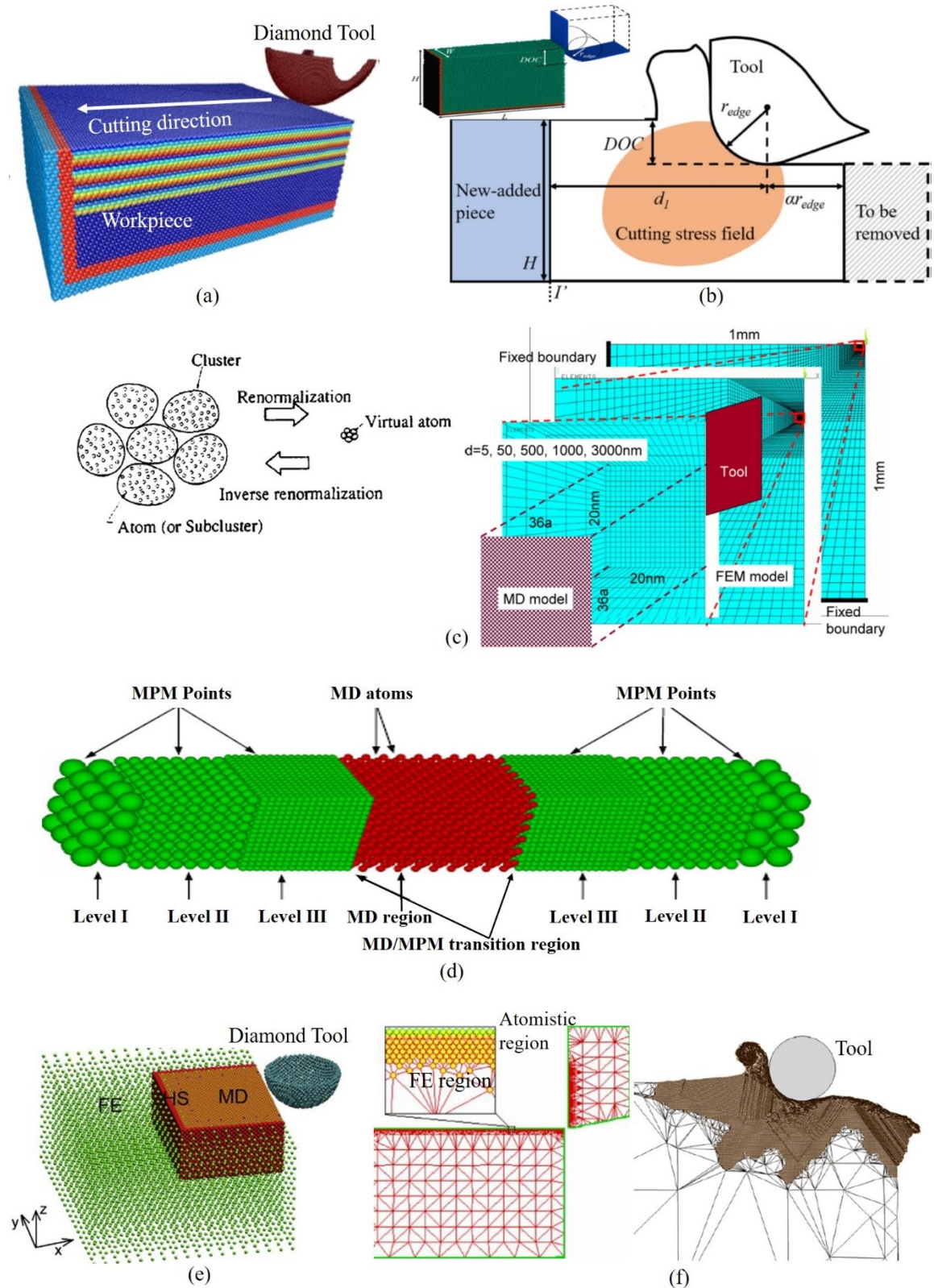
Figure 2 Numerical simulation models. (a) 3D conventional MD model of

nanometric cutting [46]; (b) Dynamic modelling of MD model in nanometric cutting

[48]; (c) RGMD model of nanometric cutting [66, 68]; (d) MPM-MD model of

workpiece in tensile test [69]; (e) MD-FEM model of nanometric cutting using an overlapped handshake region [71]; (f) QC model of nanometric cutting [72, 73].

2.2   Experimental cutting test and characterization for studying nanometric cutting mechanism

Conducting nanometric cutting tests is the foundation to study the mechanism experimentally. Ordinary nanometric cutting practices such as SPDT, fly-cutting and diamond milling have complicated motion patterns to form the machined surfaces, making it hard to distinguish the effects from individual process parameter in the cutting process. In addition, it is difficult to obtain characteristics such as cutting force and chip formation during these processes, which is significant for mechanism analyse. Theoretically speaking, the material removal model of different types of nanometric cutting in the local area around tool edge can all be simplified into an orthogonal cutting model with the key parameters including UCT and tool edge radius. Therefore, carrying out nanometric cutting experiments in a way with parameters specifically designed, and monitoring the process conveniently is in great demand to study the cutting mechanism. Furthermore, the results from numerical simulation also need to be validated by experiments, which is necessary for testing the rationality and applying them to guide the practice.

Until now, nanoindentation, nanoscratching, orthogonal nanometric cutting with customized straight-edge tool and tapper cutting are the most often reported experimental methods for mechanism study. Table 3 summarizes the major features of

these methods in the aspects of tool shape, cutting speed, UCT, as well as their advantages and disadvantages. **Figure 3** presents the shape of various tools used in nanometric cutting experiments.

Table 3. Comparison among different nanometric cutting experiments for mechanism study.

Experimental method	Nanoindentation and nanoscratching	AFM-tip nanoscratching	Taper cutting	Orthogonal cutting enable Scanning electron microscope (SEM) in-situ observation
Device	Nano indenter	AFM	Ultra-precision lathe	Customized in-situ cutting device or nano indenter
Tool	Berkovich indenter or spherical indenter	AFM tip with pyramid shape	Diamond lathe tool	Customized straight-edge diamond tool
Usual reported cutting speed	0.1-100 μm/s	1-240 μm/s	16.7 μm /s -20 m/s	23.5 nm/s -1.4 mm/s
Reported UCT	20 nm	Dozens to	0-several μm	3 nm

	-several μm	hundreds nm	(continues)	-several μm
Advantages	Force and displacement control and acquisition;	High resolution force and displacement control and acquisition; extreme small scale; In-situ AFM measurement	Large range of cutting speed	Basic cutting and In-situ observation of chip formation with SEM
Disadvantages	Slow strain rate; Tool shape	Slow strain rate; Tool shape	Unachievable constant UCT	Slow strain rate
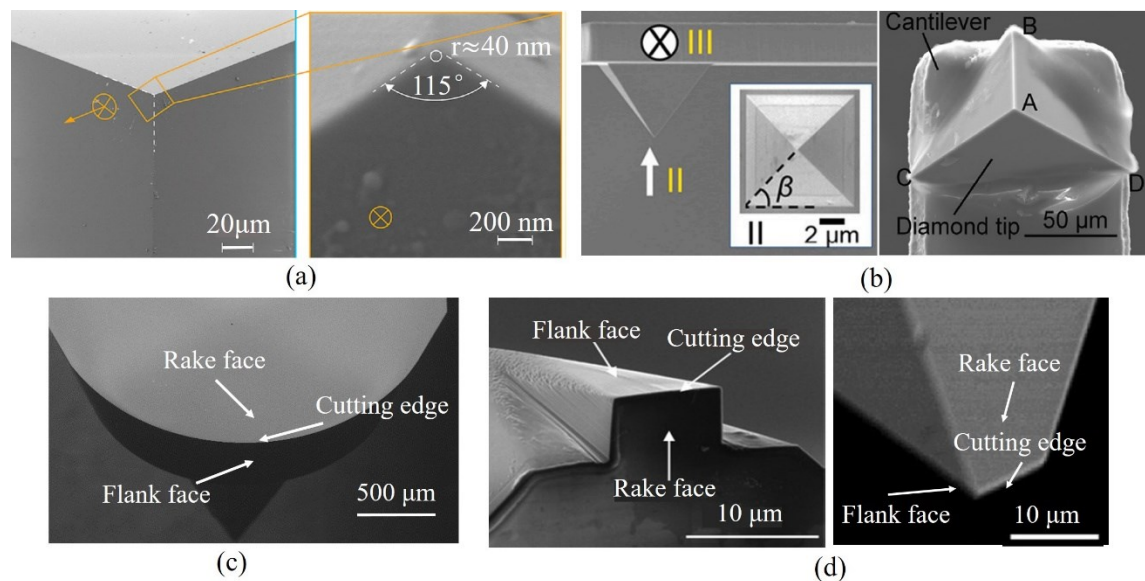
Figure 3 Diamond tools used in nanometric cutting experiments. (a) Berkovich indenter for nanoscratching [75]. (b) AFM diamond tip with pyramid shape [76, 77].

(c) Commercial diamond lathe tool with a round tool nose for SPDT (See **Figure 19**).

(d) Customized diamond tool with straight edge for orthogonal cutting [78, 79].

2.2.1 Nanoindentation and nanoscratching

Nanoindentation is usually used to study materials mechanical properties, such as nanohardness and Young's modulus. Since it can acquire controllable loading and nano-precision displacement of the indenter during process, nanoindentation is applied to characterise the nanomechanical behaviour of materials under nanoscale loading. For example, the "pop-in" event in the load-displacement curve of monocrystalline Si [80] and GaAs [81] implies a high-pressure phase transformation during plastic deformation, which can be used as the experimental evidence for high pressure phase transformation found in MD simulation of nanometric cutting [82]. This method is also devoted to study the fracture toughness (or BDT load) of materials in nano and micro scale machining [20, 83]. Based on the same instrument, nanoscratching experiments are widely carried out to imitate the loading condition and material removal process of nanometric cutting nowadays. Combined with post-characterization such as AFM, SEM and cross-sectional transmission electron microscope (TEM), it was usually adopted to study the ductile deformation [84-86], BDT phenomenon [83, 87, 88], cracks formation [9, 84, 89], and material removal mechanism [90] . Though a lot of nanoscratching tests employed a scratching depth of more than 100 nm or even several micrometres [9, 83, 85, 87, 88, 90, 91], the knowledge of subsurface deformation is still instructive for nanometric cutting. The Berkovich type indenter was mostly used in the nanoscratching experiments, which has the triangular pyramid shape and a tip with

radius ranging from 20 -100 nm [9, 84, 91], as shown in **Figure 3**a. The AFM tip is also used to conduct nanometric scratching, to study the mechanism such as material flow, material removal, chip and surface formation in nanoscale [76]. The tip usually has a shape of pyramid or triangular pyramid, as shown in **Figure 3**b. The loading force is usually set less than 100 μN and the UCT of several to tens of nanometres can be achieved. The UCT and tool size in these experiments are very close to the scale in MD simulation, making it a suitable method to verify the simulation results experimentally. Except for mechanism study, AFM tip-based nanometric cutting (TBNC) is also a promising technique to fabricate nanostructures with smaller feature size than using diamond tools (see Section 5.2).

The materials removal behaviour (e.g., chip formation, pile-up and ploughing) in nanometric cutting is strong connected with the tool geometry. For a pyramid shape tool, the continuous ribbon chips are easy to form in front of the tool with the face-forward scratching, while the short segmental chip or serious side pile-up/chip will form with the different scratching directions, as shown in **Figure 4**a. However, the commercial diamond tool used in nanometric cutting practice has a different geometry (rake face, flank face and tool edge radius, see **Figure 3**c), which may lead to a great difference in subsurface stress condition and materials flow including chip formation, pile-up and ploughing. Furthermore, the loading and scratching speeds were usually set as 0.1 to hundreds μm/s, which are several orders of magnitude smaller than the cutting speed in practice such as SPDT and fly-cutting (10^{-3}-10^{1} m/s) [92], as well as in the MD simulation (1-10^{2} m/s). This leads to a misfit of the strain rate in the study on nanometric

cutting mechanism of diamond tool-based nanometric cutting practice. In addition, the low stiffness of scratching equipment could reduce the correlation between captured force signal and material deformation, which disturbs the understanding of phenomena associated with material deformations [78]. Despite the shortcomings mentioned above, nanoindentation and nanoscratching are still important methods to reveal material deformation mechanism at micro/nano scale, providing valuable references for studying nanometric cutting mechanism in term of materials response.
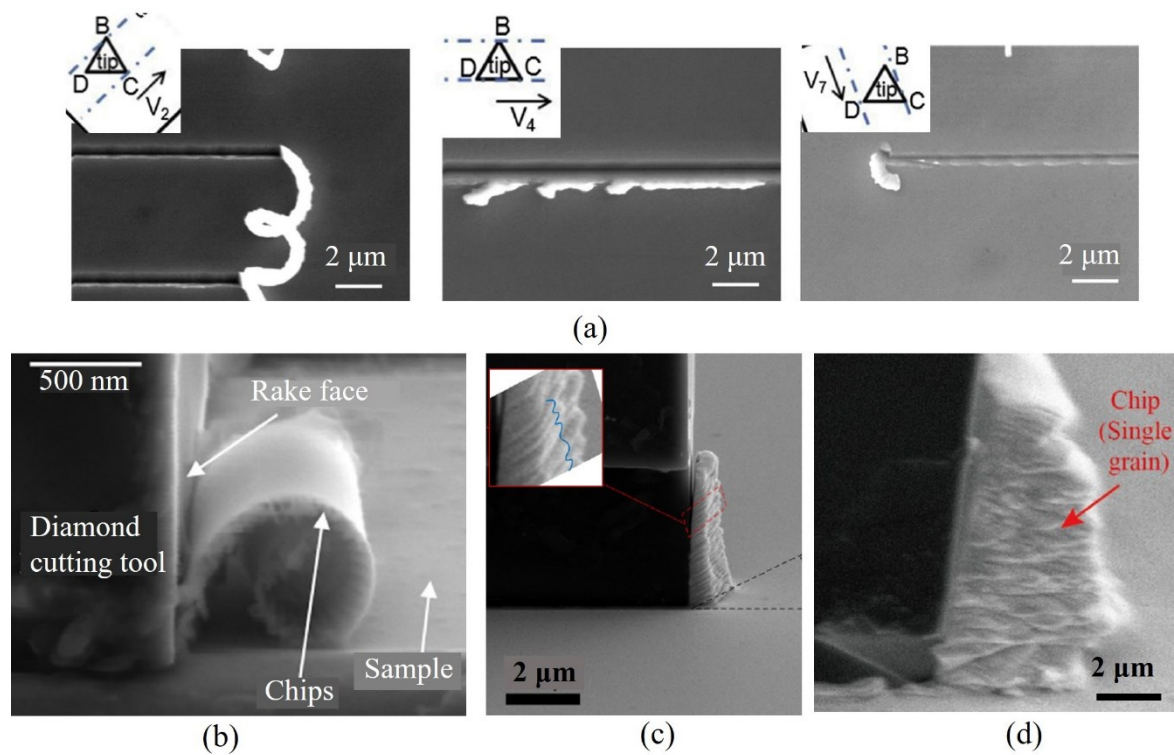
Figure 4. Chip and pile-up formation in different nanometric cutting experiments. (a) SEM image of machined surfaces with AFM pyramid tip along different scratching directions, UCT < 200 nm [77]; (b)-(d) In-situ SEM observation of chip formation in orthogonal cutting: (b) monocrystalline Cu, UCT< 100 nm, cutting length is 7µm and cutting speed is 23.5 nm/s [79]; (c) monocrystalline Cu, UCT is 500 nm, cutting length is 7 µm and cutting speed is 70 nm/s [93]; (d) Ni-based superalloy, UCT is 1 µm, cutting length is 12 µm and cutting speed is 2 µm/s [78].

2.2.2 Orthogonal nanometric cutting enable in-situ SEM observation

Orthogonal cutting is considered to be the basic cutting process, and most of the cutting models and theory are based on the orthogonal cutting configuration. Conducting the orthogonal nanometric cutting experiments and observe the nanometric cutting process such as chip and surface formation can provide visualized and experimental evidences for theoretical and numerical analyses, and contribute to a deeper understanding of fundamental mechanism. However, the highly localized deformation zone and nanoscale chip formation make the in-situ observation of nanometric cutting by conventional nondestructive optical microscopy impossible. SEM can be employed to observe surface topography with a lateral resolution of 1 nm. It also has a large depth of field and wide amplification range, which can provide sharp images with a nanoscale resolution on a large scale. These features make SEM a promising method to characterize the critical phenomena during nanometric cutting.

A nanometric cutting device with the merits above was developed in 2015 to acquire detailed material deformation and chip formation during nanometric cutting [79]. The relative motions of the diamond tool and workpiece in orthogonal tri-axial directions are all driven by PZT actuator with a closed-loop moving resolution of 0.6 nm, to realise the nanoscale UCT. The cutting speed ranges from 23.5 nm/s to 1.4 mm/s, and the UCT from several nanometres to several microns can be achieved. The dimension of this system is 30 mm×30 mm×42 mm, allowing it to be easily mounted in the vacuum chamber of the SEM microscope. In order to capture the dynamic process during cutting with SEM, the cutting speed should be set as slow as possible (e.g., 23.5

nm/s) to match the electron scanning speed [79]. Recently, a commercial in-situ indenter was used to perform cutting experiments in the SEM chamber. It has a tri-axial piezo-electric force measurement device and a lateral-move PZT stage is used to realise the micro/nanoscale UCT, and the measurable force range is 0.1-0.2 N [78]. The straight-edge diamond tools used in orthogonal cutting experiments are specially fabricated using focused ion beam (FIB), which have the well-defined geometry including rake angle/face, flank angle/face and straight edge with nanoscale radius, as shown in **Figure 3**d.

The orthogonal cutting experiments and in-situ characterization on various materials such as monocrystalline Cu [93, 94], Si [95], SiC [96, 97], Ni-based superalloy [78] are carried out by means of these devices. The chips formation in front of the rake face during cutting are observed by SEM, as illustrated in **Figure 4**b-d. The curved chip of Cu forms when the UCT is less than 100 nm with the cutting length of 7μm (**Figure 4**b), and the clear shear bands show up on the free side of the chips (**Figure 4** b-d). However, chips of monocrystalline Si are smooth without any shear bands on both sides with UCT of 100 nm. In addition, the chip deformation coefficient (the ratio of chip thickness to UCT) becomes larger with an increase in tool edge radius from 15 to 30 nm and the decrease of UCT to below 15-20 nm [95], which presents the size effect and extrusion model in nanometric cutting (See Section 3.1). Besides, this instrument enabled the cutting tests on a single grain and across a GB, proving the experimental evidence of material crystal texture variation in orthogonal micro/nanometric cutting (See Section 3.2).
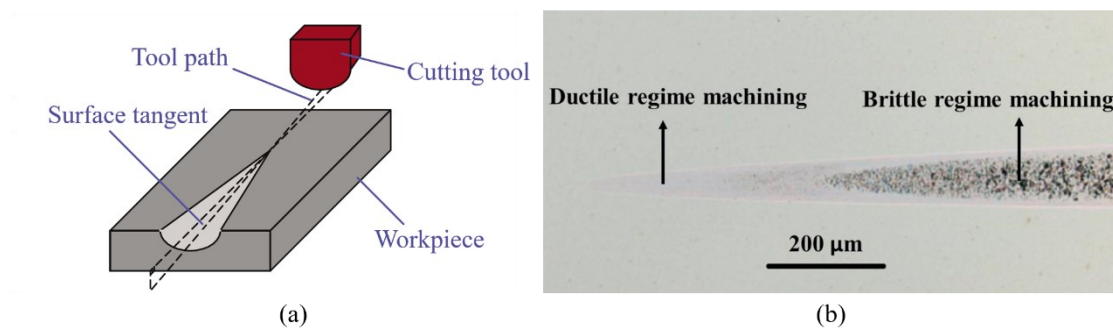
2.2.3 Taper cutting

Brittle materials can be machined in ductile-regime without crack formation when the UCT decreases to nanoscale. Therefore, it is important to determine the critical UCT and to study the mechanism for BDT of brittle materials in nanometric cutting. Taper cutting (or plunge cutting) is an efficient method to achieve a machined surface with a large range of UCT values from several nanometre to several micrometre in a single groove, which helps understand ductile and brittle machining areas. The machined surface topography and subsurface deformation with different UCTs can also be characterized and analysed on this inclined groove. In addition, the taper cutting experiments can be employed to achieve a large range of cutting speed from 1 mm/min [52] to 20 m/s [92], or even wider range through planing, turning, and fly cutting by ultra-precision machining lathe. As early as the 1990s, this method was first used to study the ductile-regime machining of Si [18-20]. **Figure 5** shows a schematic of taper cutting and a typical machined surface with ductile and brittle areas. The inclined groove can be realized using an ultra-precision lathe in two ways. One is to feed the workpiece or the cutting tool in a straight line with increasing DOC, and the other is to use the rotation of a fly cutter to achieve the inclined groove [92, 98, 99].

In fact, the critical UCT for BDT determined from surface cracks by optical microscope in taper cutting was usually overestimated. The cracks initiate in the subsurface region and propagate along specific directions during machining until they extend to the surface to form visible cracks, which has been proved by experiments on monocrystalline Si [100, 101] and GaAs [52], as well as MD simulation [52, 53]. In

practice, the fracture toughness of some brittle materials, such as Si and Ge, is close to the yield strength, which makes the boundary between ductile- and brittle-regime machining ambiguous [102, 103]. Therefore, ductile and brittle deformation can exist simultaneously in the nanometric cutting of these materials. Ductile- or brittle-regime machining should be determined by the dominant deformation pattern. Thus, by inspecting the surface cracks and fractures on the surfaces in the taper cutting experiment, the so-called "critical UCT for BDT" should rather be named as "critical depth of no observed surface cracks" (NOSC depth).

Figure 5. Taper cutting test. (a) Schematic illustration [2]. (b) Surface topography of the groove on monocrystalline Ge showing the transition of cutting mode [102].

2.2.4   Characterization methods for studying nanometric cutting mechanism

During or after nanometric cutting experiments, it is essential to characterise the machined surface topography, subsurface structural deformation, residual stress, and tool edge for the mechanism study. The characterization can be categorized into the methods for morphology (surface topography and tool edge) and material microstructure. In terms of the 3D micro/nanoscale morphology characterization, laser confocal microscopy (LCM), white light interferometry (WLI), AFM and SEM are

mostly used because of their sub-nanometric resolution in specific direction. In terms of material lattice structural characterization, especially the nanoscale or microscale local area of subsurface deformation, the techniques of TEM, electron backscatter diffraction (EBSD) and laser Raman spectroscopy (LRS) are frequently used. The characterization methods in nanometric cutting mechanism study and their capacity are summarized in **Table 4**.

Table 4. Characterization methods used in nanometric cutting.

| Categories	Methods	Capacity
Characterization of morphology	LCM	Micro 3D reconstruction of machined surface; NOSC depth [52, 102]
	WLI	Surface roughness and micro-topography
	SEM	Surface micro-topography [4, 79]; Tool wear [12, 104]; Chip morphology [95, 105]; In situ observation of cutting process [93-97]
	AFM	Micro-nano 3D topography; Surface roughness; NOSC depth; Tool edge profile [106-108]
Characterization of deformed microstructure	TEM	Subsurface structure (point defect, dislocation, phase transformation, micro crack, etc.) [3, 7, 65]
	EBSD	Crystallization orientation (map) [78, 109, 110]; Geometrically necessary dislocation (GND) density [111]; Grain
	LRS	Phase transformation [112-116]; Residual stress [113]; In situ

		measurement

The measurement of tool edge by AFM is an intricate process requiring a professional operation. One way is to scan the tool edge directly with the AFM cantilever, through the assistance of an optical alignment system [106]. An alternative method is impressing the tool into a soft material such as copper and then scanning the transferred mark of the edge with AFM tip [107, 108]. In this case, the influence of elastic deformation during the indentation must be considered and the AFM tip radius effect should be eliminated in the evaluation result [107].

TEM is effective in enabling direct observation of subsurface structures, including phase transformations, dislocations and microcracks, as well as the quantitative measurement of their sizes in nanometric cutting [7] (**Figure 6**a). It can also provide subsurface information reflecting the atom arrangement or even the real atoms image (**Figure 6**b) [3, 65]. However, this method is destructive and the subsurface damage distribution is difficult to characterize over a large area.

LRC is a powerful nondestructive method for characterizing the lattice information of insulators and semiconductors [112], which is widely used to detect the crystalline–amorphous phase transformation in machining of silicon [113, 114] and germanium [102, 117]. It can also provide on-machine measurement, selective measurement of a specific surface area, mapping measurement of a large surface area [116] since it is quick and can be performed at room temperature in the air. The Raman intensity ratio was proposed as a parameter to represent the relative significance of

crystalline and amorphous phases for a quantitative measurement of amorphous Si layer after nanometric cutting (**Figure 6**c) [115].
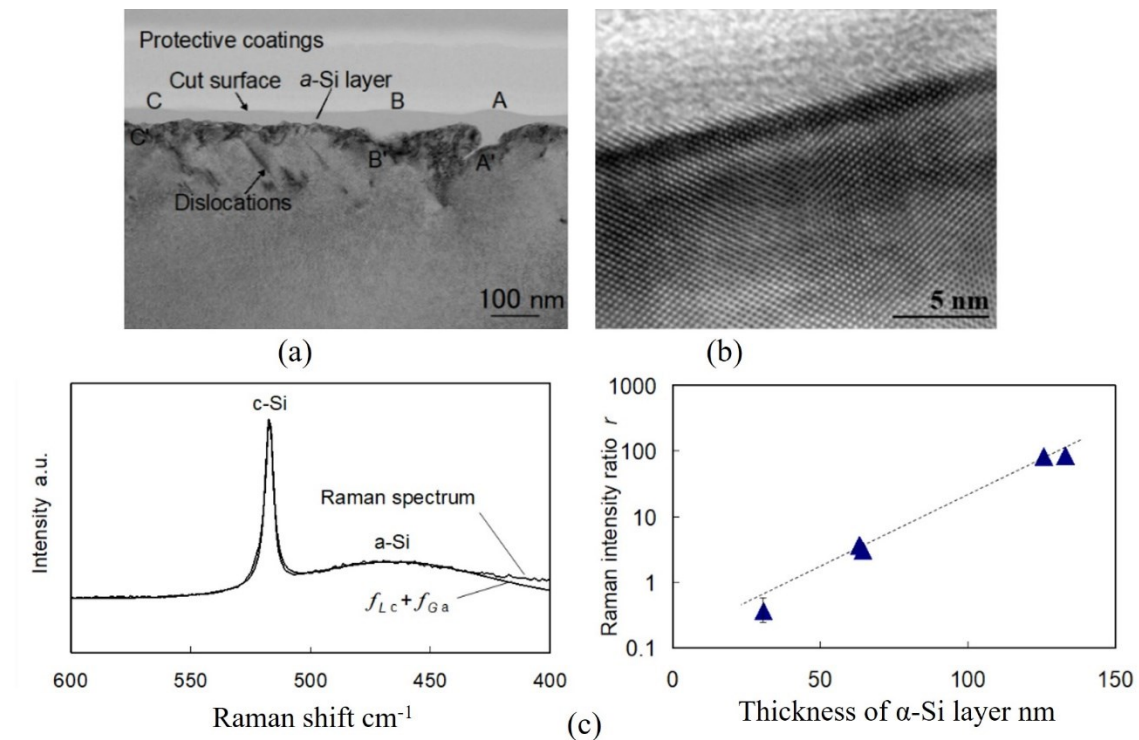
Figure 6. Subsurface information in nanometric cutting revealed by TEM and Raman spectra. (a) Subsurface deformation of machined Si [7]. (b) High-resolution TEM observation of machined Ge surface lattice [3]. (c) Quantitative evaluation of amorphous layer thickness using Raman intensity ratio [115].

3. Nanometric cutting mechanism

Workpiece, tool, and their interaction are basic elements of a cutting process. Nanometric cutting mechanism consists of chip and surface generation, subsurface deformation, and tool wear, which is significant for improving the surface integrity of final products. As aforementioned, nanometric cutting has distinctive mechanism in the aspects of material removal model, lattice structural deformation and tool wear pattern.

In this section, relevant research progresses in this area are systematically discussed. These investigations have provided the foundation of the technologies for improving machinability and efficiency in practice.

3.1   Nanometric cutting model

One of the most important factors changing the cutting model from macro to nanometric scale is the significance of tool edge geometry. In macro cutting model, the edge is assumed to be perfectly sharp and the cutting forces are derived from the forces acting on a single shear plane and rake face [118]. As the UCT decreases, the edge profile and the elastic recovery of machined surface cannot be neglected at all. Similar to the classical shearing model, it is possible to establish an analytical description of round-edge cutting, where the shear plane is replaced by an extensive shear zone [16]. This zone, accompanied with other two near the round edge and the rake face, also occurs in the slip-line field model for micro cutting [119]. Although the size effect introduced by the tool edge exists in both micro and nanometric cutting, there are still several distinctions between those two processes. Firstly, the UCT of nanometric cutting is usually smaller than a single grain. Therefore, the workpiece material properties are strongly dependent on crystal orientation rather than isotropic. With a decrease of lattice defects in the range of UCT, mechanical strength approaches to the theoretical value, which is another source of size effect [14]. The strong intragranular deformation makes the nanometric cutting has the highest specific cutting energy than macro and micro cutting. Secondly, the tool must be sharp enough to generate a

nanometric thin chip. Those having edge radius at micro scale, which are widely used in micro cutting, would not realize stable material removal at nanometric scale. Furthermore, the ratio of UCT to edge radius in nanometric cutting is always smaller than that in micro cutting. As a result, the effective rake angle becomes more negative and the shear plane/zone may disappear. It is supported by feeding the process parameters into the shearing model and getting a negative shear angle contrary to an actually cutting action, which finally leads to the chip formation mechanism of nanometric cutting termed as extrusion [2].

The highly negative effective rake angle leads to a compressive stress state and triggers the localized phase transition of workpiece material, which enhances plastic deformation and is significant for the ductile-regime machining of non-metallic crystals. For example, as a typical material extensively investigated, Si transforms to a metallic phase when the hydrostatic pressure excesses 10-13 GPa, and changes into other phases after unloading [7], which is used to interpret the formation of lattice structure in the chip and the machined surface. This well-known model comes from the knowledge of indentation and scratching tests, but the loading condition is quite different from that in nanometric cutting with much higher strain rate and complex tool geometry. Besides, there has been no direct observation showing how the workpiece lattice changes in front of the edge. By contrast, the extrusion model presents the understanding of phase transition and material removal mechanism. As illustrated in **Figure 7**a, recent study indicates that a narrow amorphous zone contacting with the tool edge occurs during the cutting, which does not transform from the metallic phase [41]. The phase transition to

other crystalline structures, if happened, is always beneath that zone, as supported by MD simulations [120, 121]. What is important in the extrusion model is that the chip comes from the amorphous zone, which leads to a natural result of amorphous chip without the necessity of metallic phase (TEM images in **Figure 7**a). In addition, there exist some evidences implying the fluid-like character of this zone. For example, fluid dynamics is used to calculate the forces of nanometric cutting on Cu, where the tool edge radius and the elastic rebound at flank face are explicitly considered [122]. It is based on a hypothesis that the high temperature in the cutting zone makes solid like fluid, and a satisfactory fit between the simulated and the experimental force values can be achieved. Keeping it in mind that the shear stress in fluid is more dependent on strain rate rather than strain itself as in solid, it is also interesting to note that the fluid hypothesis seems to be valuable for brittle materials as well, because the shear stress, as shown in simulations, concentrates in the crystalline substrate undergoing elastic deformation, rather than the amorphous zone with larger deformation [41]. In brief, material removal in the extrusion model is realized from an amorphous zone that surrounds the tool edge and behaves like (viscoelastic) fluid, accompanied with other types of deformation in the subsurface.

Various experimental results and fundamental issues can be explained and understood based on the extrusion model. First of all, the stagnation region [46], that is the branching point of material flow up to the chip and down to the substrate (ploughing), locates in the amorphous zone (the blue zones in **Figure 7**). Therefore, the topmost layer of the machined surface is amorphous too, as shown in TEM observations

[7]. In other words, the stagnation region divides the material in the amorphous zone to form the chip and the machined surface separately. With an increase in UCT (**Figure 7**b), the chip would not be totally amorphous [123], thus the cutting may not be dominated only by extrusion. MD simulation reveals that some localized amorphous bands would originate from the boundary of the amorphous zone of extrusion [41]. They can propagate upwards and after reaching the free surface, a piece of crystalline material would slide along them to become a part of the chip. These amorphous bands act as the shear plane/zone in the macro/micro cutting, so the chip formation mechanism can now be a combination of extrusion and shearing. This concept successfully interprets the polycrystalline lattice and the morphology of the chip [123, 124]. The amorphous bands can also evolve down into the workpiece and induce the subsurface deformation, which is similar to the TEM observation. With the help of advanced simulation method, the subsurface deformation layer thickness could even be quantitatively predicted [65].
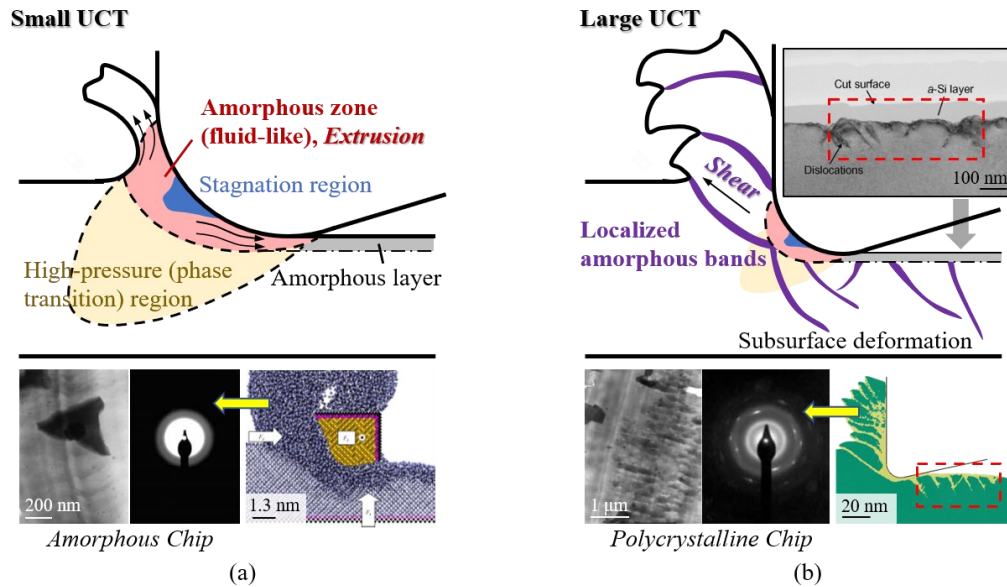
Figure 7. Schematic illustration of nanometric cutting model with evidences from experiments and simulations [7, 123, 125]. (a) Cutting under small UCT is dominated by extrusion. The chip and the machined surface layer are amorphous. (b) Larger UCT results in the coexistence of extrusion and shearing. Polycrystalline structure is observed in the chip and the machined surface.

The weight of extrusion or shearing mechanism in nanometric cutting is mainly influenced by the ratio of the UCT to the edge radius. The sharper the tool, the larger this ratio, thus shearing becomes dominant. This could be understood from the aspect that extrusion means a total amorphization of the material to be removed and requires more and more energy than shearing for larger UCT. As the ratio decreases for blunter tool, the above process reverses and the amorphous phase in the chip increases. Meanwhile, the stagnation region moves up, so more material in the range of UCT would be depressed into the machined surface which enhances the thrust force [11]. Once the stagnation region reaches the free surface, there is no chip formation and

cutting turns into sliding. **Figure 8** shows an in-depth comparison of the chip morphology between nanometric and micro cutting. At nanoscale (**Figure 8**a), the chips of brittle material (Si) have no trace of shearing when the ratio of the UCT to the edge radius is small [126]. At this stage, extrusion becomes the dominant cutting mechanism. While for ductile metal such as Cu, experimental evidences of the chip crystallinity are still lack. MD simulations (3.6-5 nm edge radius, 0.1-14 nm UCT) indicate a small degree of extrusion as dislocation activity becomes easier which enhances the shearing [34, 127]. Although the edge radius in the model is much less than that of a real SCD tool, it can be confirmed that the shearing-dominated chip formation takes place much earlier in metals as the tool edge becomes sharper [93, 128]. In the micro cutting (**Figure 8**b), the chip surfaces of two types of workpieces are full of lamella structure or serrated shape, and no amorphous phase is detected (in the Cu chip), indicating the dominance of shearing [129-131]. In particular, there is no extrusion-like chip even under the nanometric UCT when the edge radius increases to micro scale for hard Ni-Cr alloy [129]. Therefore, the extrusion process would occur only when the UCT and the edge radius are all at nanoscale, and the characteristic ratio between them should be smaller than a threshold. It is a distinctive phenomenon of nanometric cutting, which disappears in micro and macro cutting. On the other hand, the shear band configuration indicates an unsteady plastic flow, i.e., shear banding [132] irrespective of the cutting scale. This similarity is more apparent as shown in **Figure 8**c, where a shear band evolution is followed. In both cases, the shear band is severely deformed and the nearby material keeps its crystallinity. It contains many nanocrystals during the macro cutting,

but is totally amorphous in the nanometric cutting. Another difference is that the shear band direction is mainly determined by the cutting geometry (rake angle, UCT, etc.) at macro/micro scale, in contrast, it is strongly influenced by the lattice orientation of the workpiece at nanoscale. In addition, the steady laminar flow from classical shearing model does not occur at nanoscale, although the speed of nanometric cutting in **Figure 8**a,b is less than 6 mm/s. It implies the "continuous chip" is only a macroscopic concept. For nanoscale, the chip is always serrated-like as long as shearing happens, which is independent on the material property or cutting speed. Such a continuous chip may be only possible to form by extrusion. Despite the phenomenological similarity of shearing, the extrusion zone and complex material behaviour are two sources affecting the feasibility of classical shearing model at nanoscale.
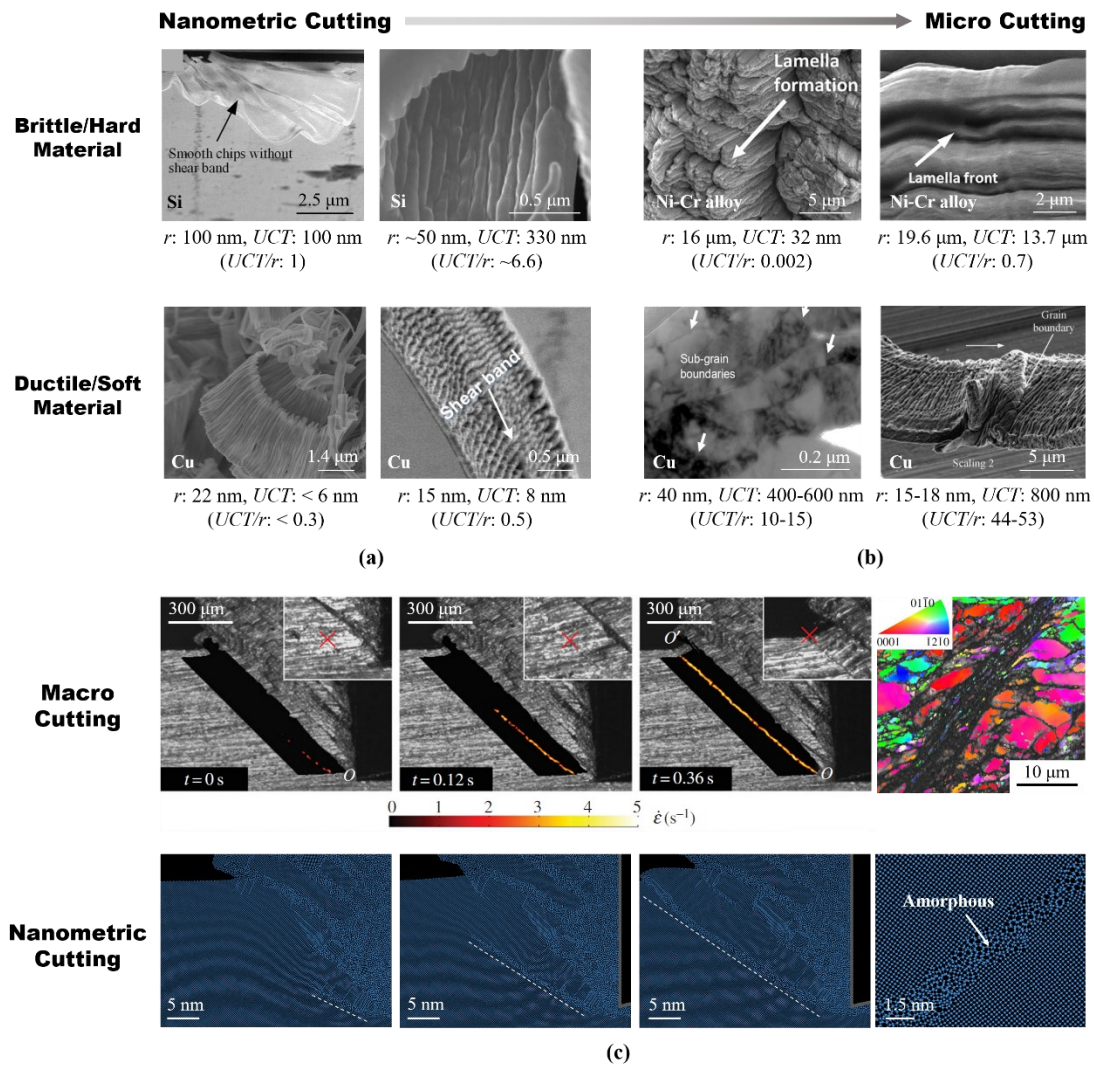
Figure 8. Comparison of chip formation at different scales. Chip morphology of two kinds of materials from (a) nanometric [95, 105, 126, 128] to (b) micro scale [129-131]. (*r*: edge radius) (c) Shear banding process. Up: High-speed camera images of cutting on cold-worked brass (UCT: 600 μm) and EBSD map of the shear band in titanium alloy chip (UCT: 125 μm). (Edge radius: 10 μm) [132] Below: MD simulation on Si using a sharp tip (UCT: 20 nm).

How small the UCT can be reduced to form a continuous chip is another interesting topic, which is termed as the nanometric cutting limit, reflecting the highest achievable machining precision [133]. Theoretical studies indicate the ratio of the minimum UCT

to edge radius is 0.05 to 0.1 [24, 134, 135]. It is also found that the critical rake angle for chip formation is −60° to −75° regardless of whether a sharp edge or a round edge is employed in the model [29, 136]. According to the definition of the effective rake angle [29], it corresponds to such a ratio of 0.03-0.13. This characteristic range is recently found to be valid even for the cutting at atomic and close-to-atomic scale [137], which implies an extremely sharp tool whose edge radius should be at least less than ~8 nm is necessary to remove only one atomic layer. The tool sharpness, accompanied with the wear problem, is also a challenge for experimental validation. An edge radius less than 50 nm can be realized through many approaches, including lapping, polishing and oxidative etching [138]. FIB milling is also a commonly used method, with the advantage of in-situ monitoring of the edge profile and capability for complex tool geometry at micro scale [139, 140]. Using such a customized diamond tool with the edge radius of 22 nm, extremely thin chip of Cu with a ~6 nm thickness can be generated, as shown in **Figure 8**a. The chip thickness is about one-third of the edge radius, while the UCT should be smaller because material structural change could increase the chip volume. Finally, although the orthogonal cutting model is employed to investigate the cutting limit theoretically, diamond turning is always the experimental approach due to its better controllability and stability to realize a nanometric UCT.

3.2 Material deformation mechanism

The nanometric cutting process mainly involves the materials removal, surface generation and subsurface deformation. Material deformation, including the

microstructural defects in nanometric cutting, is one of the most important aspects influencing the machined surface integrity, and consequently plays a critical role in determining the product's functional performance. Understanding the deformation mechanism can help optimize the process conditions in nanometric cutting, such as setting the appropriate parameters, adopting material modification-assisted machining and environmental control. For example, the anisotropy behaviour of the subsurface deformation in single crystals provides a reference for choosing the optimal lattice orientations in nanometric cutting [47]. As another example, the amorphous phase transformation found in the ductile-regime nanometric cutting of Si and Ge inspires the enhancement of the machinability of brittle materials via modifying the surface lattice into amorphous state [141-143].

The workpiece deformation mechanism in nanometric cutting is related to the microstructures and varies with material types, such as ductile metals/alloys and brittle crystal materials. For ductile metals and alloys, attentions are mainly focused on the intragranular crystal defects such as dislocations and stacking faults, as well as the GB effects of polycrystalline materials. In terms of brittle crystals, concerns are focused on the BDT and crack formation, except for the ductile deformation mechanism in nanoscale. In addition, effect of process parameters such as cutting velocity and UCT is also usually considered in mechanism study for all the materials.

3.2.1 Subsurface deformation mechanisms in nanometric cutting of metals and alloys

It is revealed that ductile metals such as monocrystalline Cu, Al and Fe mainly

undergo dislocation, stacking fault and twin-based subsurface deformation in nanometric cutting. MD simulations provide the atomic detail on the structural change during the processing. For monocrystalline Cu, defects evolution including point defects, perfect dislocations, Shockley dislocations, stair-rod dislocations, Frank dislocations, dislocation loop, stacking faults and twinning boundary (TB) are all observed during the machining (**Figure 9**a) [30, 31, 144]. After cutting, vacancy defect, atomic cluster defect, stacking fault tetrahedral, and stair-rod dislocation remain in the subsurface [31], which contributes to the work hardening [30]. As the material with FCC lattice structure, monocrystalline Al undergoes a similar structural deformation, such as perfect dislocations, Shockley partial dislocations, stair-rod dislocations, Frank partial dislocations and stacking faults [33, 34], as shown in **Figure 9**b. Although Al has a high stacking fault energy, twin deformation is still observed in simulation [34, 145]. For the BCC structure metal Fe, edge dislocations, partial dislocations, vacancies, and nano-twin are identified in the subsurface deformation during nanometric cutting [35]. The abundant dislocation networks, dislocation loops, dislocation cells and stacking faults are experimentally observed in the subsurface of monocrystalline Cu after nanoscratching with AFM tip in a recent study, as shown in **Figure 9**c [131]. A sharp boundary between high dislocation density (abundant dislocation networks) and low dislocation density (dislocation loops) areas in the subsurface is also observed [131]. The anisotropy of the crystal is another important feature of subsurface deformation since dislocations and stacking fault tend to propagate along the slip systems, which is determined by the Miller indices and cutting direction [32, 34, 36].

The propagating direction and distribution of subsurface deformation, cutting force, as well as the shape and surface roughness of pile-up (chip) are observed varied with lattice orientations [32, 36]. In addition, attentions are also focused on effects of rake angle, UCT, tool edge radius, cutting speed etc. on the subsurface deformation [29, 146, 147]. Aside from simple metals, materials reinforced with hard particles also play an important role in the industry. For example, the metal alloy and metal matrix composite could have a crystalline structure with hard particles. MD simulation studies show that the depth of hard particles determines the way they move and the machined surface quality, as well as the evolution of subsurface defects [33, 144].

Nanometric cutting imposes a complicated loading condition on materials involving large sliding or rubbing process [148], which means that the subsurface microstructural evolution in sliding friction experiments would be an appropriate reference. It is observed that the misorientation of the lattice structure (e.g., lattice rotation) appears in the early deformation of sliding contact and microscale shear test on metals [109, 110, 131, 148], while this event is rarely reported in the MD simulation of nanometric cutting on monocrystalline metals. The reason might be the UCT adopted in the simulation is normally several nanometres and the cutting length is dozens of nanometres. Thus, the load imposed on the materials is too small and the cutting length is too short to induce visible lattice rotation. However, the UCT in nanometric cutting practice would be dozens of nanometres, leading to a much larger loading and friction force, as well as abundant dislocations. Thus, the lattice rotation could occur in enduring nanometric cutting [36]. The orthogonal cutting experiment with a straight-line-edge

tool on Ni-based superalloy reveals that the crystal rotation inner grain occurs relative to the cutting direction and normal direction, while almost no lattice rotation is observed relative to the transverse direction. When the misorientation reaches a threshold, a clear horizontal line of high angle boundary (HAB) appears, above which is the area with a complex array of line defects and misorientation from the bulk material, as shown in **Figure 9**d. The misorientation value up to 45° is detected in the subsurface after machining [78].
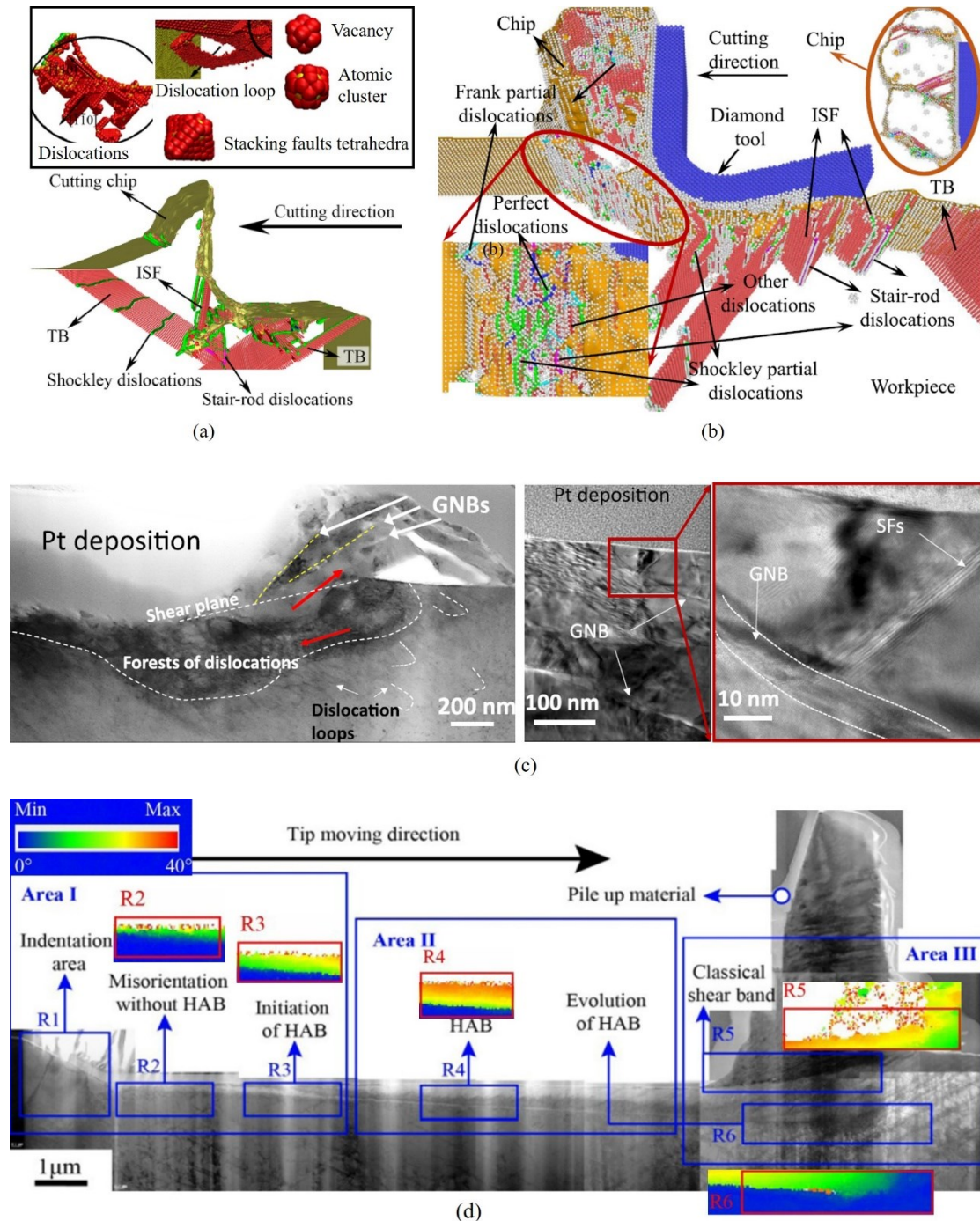
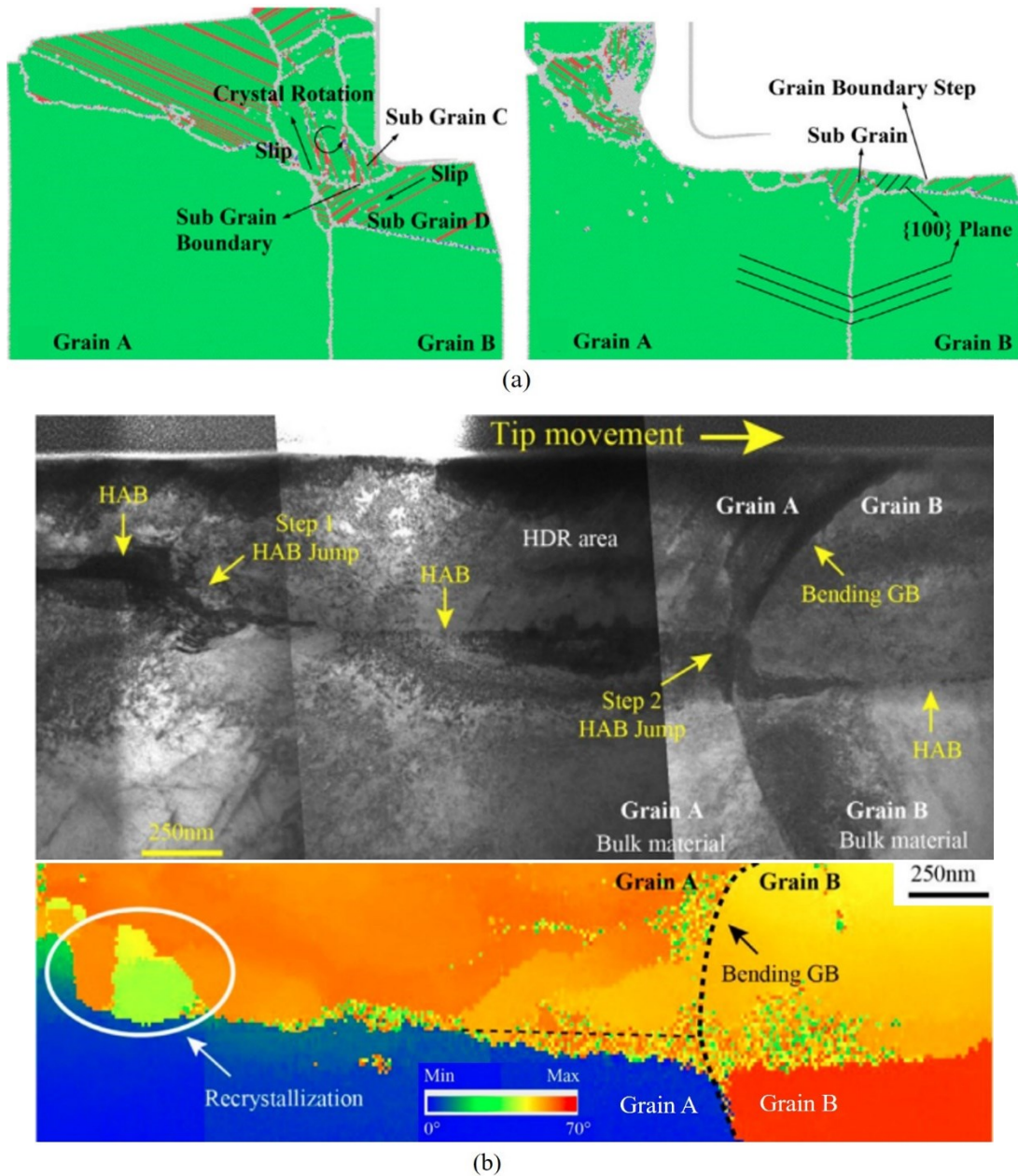**Figure 9. Structural deformation during the nanometric cutting on metals.** (a) MD simulation of microstructure evolution of monocrystalline Cu [31, 144]; (b) MD simulation snapshot of microstructure evolution of monocrystalline Al [34]; (c) TEM image of microstructural change in sub-surface areas after AFM-tip based nanoscratching in monocrystalline Cu [131]; (d) TEM image and misorientation map

of various crystal structures in subsurface areas from orthogonal cutting experiment with a straight-line-edge tool on a single grain of Ni-based superalloy [78].

Different from single crystals, metallic and alloy materials usually have polycrystalline structure with GB, which would bring great influence on the plastic deformation mechanism. Unlike dislocation-dislocation interactions which is the dominant deformation mechanism of nanometric cutting on monocrystalline metals, the dislocation-GB interaction is another important plastic deformation mechanism in polycrystalline metals and alloys [149]. During the processing, partial dislocations nucleate and extend from free surface and GBs, connected by stacking faults [145, 149, 150]. Following the complete nucleation, the dislocations travel along the slip planes to across the grain, until they reach another side of the grain and are terminated by GBs [145, 149]. As shown in **Figure 10**a, the dislocations are confined in the grains during nanometric cutting. For the cutting at larger scale, although GB and TB usually act as the obstacles for dislocation transmission, abundant dislocations move forward and attribute to the formation of dislocation trace line (DTL) and HAB from lattice rotation, which might bring sufficient local stress to activate continuous travel of DTL and HAB across the GBs [78]. It should be noted that the dislocations and DTL seems to transmit across a TB more easily than an ordinary GB [110, 149]. Under the combined interaction of dislocations and GBs, as well as the deformation twin, the new grains (sub-grain) would occur [110, 149, 150]. It is experimentally observed that the recrystallization shows up at the local area of HAB (see **Figure 10**b), which is

considered to be the result of significant dislocation accumulation along the HAB [78].

In the meantime, the nanometric cutting process would also lead to the shift and bending

of GB [40, 78, 110, 149], as well as grain rotation [78, 109, 149]. It is discovered that

GB step occurs on the machined surface both in MD simulation and experiments [40,

150, 151], which deteriorates the surface roughness [151]. **Figure 10**b shows the TEM

image and misorientation map of the subsurface structural variation when the tool cuts

across the GB of Ni-based superalloy [78]. It reveals the existence of local

recrystallization, bending of GB, lattice rotation and the interaction between HAB and

GB in the subsurface after micro/nanoscale shearing based material removal. It should

be noted that although the UCT in this experiment is around 1 μm which actually falls

into the regime of micro cutting, the comprehensive information of subsurface

deformation in micro and nanoscale is valuable and provides a reference for

understanding nanometric cutting. When the grain size decreases from micro to

nanoscale, the nucleation and slip of dislocations are no longer operational and the

dominant deformation mechanism is GBs-based interactions and evolution [145].

(a)

(b)

Figure 10. **Dislocations in nanometric cutting.** (a) MD simulation snapshot of microstructure evolution of polycrystalline Cu (UCT: 14.46 nm) [150]; (b) TEM image and misorientation map of structural variation in subsurface areas from orthogonal cutting across the GB of Ni-based superalloy [78].

Deformation mechanism of ductile metals and alloys in nanometric cutting strongly depends on the initial surface state. The nucleation location and extension

direction of dislocations, stacking faults, etc. are closely related to the crystallization orientation, cutting direction, GB and even the grain size. It should be noted that many results of subsurface deformations of lattice misorientation, DTL, HAB and grain rotation come from the sliding test and micro cutting experiments. For the typical UCT in nanometric cutting (< 100 nm), whether the abundant dislocations could evolve into the distinct DTL or HAB is still unclear. The magnitude and complexity of the subsurface deformation therefore need further study.

3.2.2 Subsurface deformation mechanisms in nanometric cutting of brittle materials

Generating crack-free surface on brittle materials is one of the most prominent contributions of nanometric cutting, which fulfils the large demands from optical, microelectronics, and biomedical fields. BDT and subsurface deformation are two critical fundamental issues in improving the machined surface quality and are still hotspots under investigation.

Research on the brittle and ductile nature of materials can be traced back to 1950s. It was found that plastic deformation is involved in the frictional wear of rock salts, although some cracks and surface fragmentations appear [152], and plastic flow plays an important role in the fracture of glass [153]. It was also realized during that time that almost any material, including the hardest diamond, can be deformed plastically even at low temperatures under the influence of large hydrostatic stress [154]. To characterize brittleness quantitatively, an empirical parameter, brittleness index, was defined as the ratio of hardness to fracture toughness. Then, the maximum load and flaw size that a

solid might sustain without fracture can be estimated [155]. Based on the research about

indentation, critical scale of BDT was formulated as [156]

$$d_c = \alpha(\frac{E}{H})(\frac{K_c}{H})^2 \qquad (1)$$

where E, H, K_c are the elastic modulus, hardness and stress intensity factor respectively.

It reflects the critical DOC of ductile-regime grinding with α of 0.15. However, due to

the strong size effect and anisotropy of material at nanoscale, it is probably to fix this

expression while applying it to specific situations [157], and accurate prediction of BDT

is still difficult. Another question comes from the difference in the loading condition

between indentation and cutting, where a much higher strain rate and asymmetric

process configuration arise in later case. Therefore, investigations aiming at the

nanometric cutting process were conducted. Considering the shear zones and

lateral/median crack system, analytical expressions of specific cutting energy, which

concern the work-material intrinsic properties, tool geometry and process parameters,

are constructed [158]. The critical UCT for BDT can then be obtained at the intersection

point of energy curves standing for the material removal through ductile and brittle

modes respectively. It should be noted that the brittle-regime cutting is still modelled

based on indentation fracture mechanics with pre-existing crack. Difficulties for an

accurate model come from not only the asymmetric tool edge geometry and process

configuration, but also the complexity of crack nucleation which highly depends on

local lattice structure. Another model was recently developed based on the theoretical

fracture strength of specific crystal planes [159]. Stress distribution is calculated

considering the cutting force from classical shear model and the residual plastic

deformation in the subsurface, then is compared with the fracture strength to indicate

whether BDT would happen. This model takes into account the anisotropy of lattice

structure and gives an estimation of critical UCT with the error less than 29.8%. It may

be also possible to evaluate the speed effect by introducing strain rate into the cutting force terms. On the other hand, a ductile-regime diamond turning model for brittle materials was proposed in the early 1990s [160]. As shown in **Figure 11**a, the UCT increases from the bottom of the tool nose to the uncut shoulder. There is a special position of critical UCT (t_c), above which the material removal scale is large enough to induce fracture. (Of course, a slow feed rate might be used so that the maximum UCT, t_{max}, keeps less than the critical value.) As long as the microcracks do not propagate below the machined surface plane, a mirror surface without fracture damage can be obtained. Because properly enhancing the feed rate means a higher efficiency, material removal in diamond turning is always realized by a combination of brittle and ductile modes. While no matter how large the maximum UCT becomes, the critical UCT of brittle materials is in nanoscale and the machined surface integrity is significantly influenced by the nanometric cutting process near the nose radius center. It is clear that the configuration in **Figure 11**a is more complex than indentation or orthogonal cutting, but the model is convenient to use in practice and makes diamond turning, which will be discussed in the following section, as one of the most important technologies to achieve an ultra-smooth surface with a roughness even down to 1 nm (**Figure 11**b) [2, 18]. The BDT is also obviously indicated by the chip morphology which changes from fragmented type to continuous ribbon shape when the UCT decreases below the critical value, as shown in **Figure 11**c.
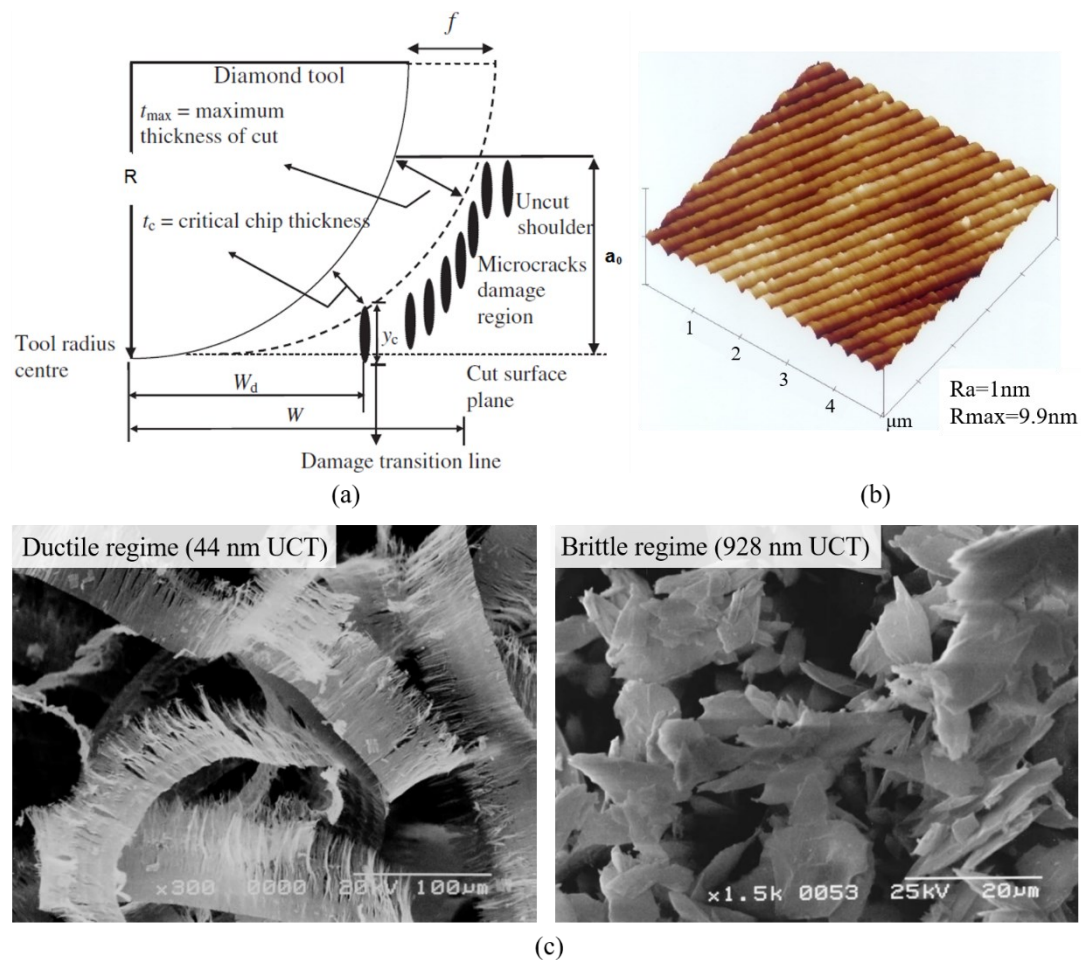
Figure 11. Machining of brittle materials in ductile and brittle regimes. (a) Schematic model of material removal in diamond turning [160]. (b) Si surface with a Ra of 1 nm by ductile-regime cutting [2]. (c) Si chip morphologies in various cutting regimes [161].

Generally speaking, the brittle behaviour can be considered as a result of that the tensile stress exceeds its critical value on specific crystal planes before the plastic yield happens. However, to gain more information about the BDT requires numerical simulation because the tool edge geometry and the change of workpiece lattice structure make the stress field too complex to analysis. Let's take a further consideration from the beginning of the amorphous layer on top of the machined surface. Because it has been experimentally confirmed not only on simple crystals (e.g., Si, Ge [102]), but also

on the material with complex unit cell (e.g., $Gd_3Ga_5O_{12}$ [162]) which is less likely to have a metallic phase transition, this top layer seems more likely to come from the fluid-like amorphous zone in the extrusion model. This argument is supported by the study of indentation on Si and Ge [163], where the direct amorphization under the indenter is proposed based on the fact that the fast unloading gives no enough time for the back transformation from metallic to amorphous phase. It also implies the occurrence of the liquid phase, which is coincidently in agreement with the extrusion model and simulation result [47]. Besides, it should be careful that the surface characterization method may confuse the analysis. For example, the amorphous layer on machined SiC surface is difficult to detect in Raman spectrum [157] but can be clearly seen by TEM [65], which is attributed to the small layer thickness and the transparency of SiC at the laser wavelength of Raman test. Under the amorphous zone of extrusion, high-pressure phase transition to other crystalline structure depends on the workpiece material, such as the bct5 and β-phases of Si and Ge [47]. It needs to mention again that these metastable phases can be directly verified only by MD simulation currently, which is sensible to the potential function used and the model size. As a consequence, some questions are still unclear, such as the ductile response origin and rock salt phase transition of SiC [51].

In TEM observations of the machined subsurface, there are inclined slip lines beneath the top amorphous layer, which are considered as dislocation slip. Another possible mechanism is considered to be the shear banding process, corresponding to the localized amorphous bands moving downwards (**Figure 7**b). The reason is that

dislocation slip would not seriously damage the lattice along the slip path. For example, in the nanometric cutting on SiC, dislocations can move along the basal plane parallel to the surface [65] (**Figure 12**a), and the lattice recovers to its original structure after they pass by. With an increase in the UCT, more shear banding and dislocations occur and intersect to form a network resulting in a concentration of tensile stress in the subsurface. Far from the hydrostatic pressure region, micro crack nucleation can be triggered here once the tensile stress is large enough, followed by a sudden propagation along cleavage plane. The picture above successfully interprets the subsurface lattice structure observed in TEM (**Figure 12**b), which is a mixture of amorphous and nanocrystals regions with micro crack under them [9, 52]. Recent study shows another interesting process that if the crack occurs in front of the edge, its surfaces could be closed as the tool passes by [65], which may also exhibit as a "dislocation slip line" in the TEM image. Nevertheless, it has been clear that the BDT in nanometric cutting of brittle crystals arises from the subsurface dislocation/shear banding layer without the occurrence of surface crack, just as the NOSC depth means.
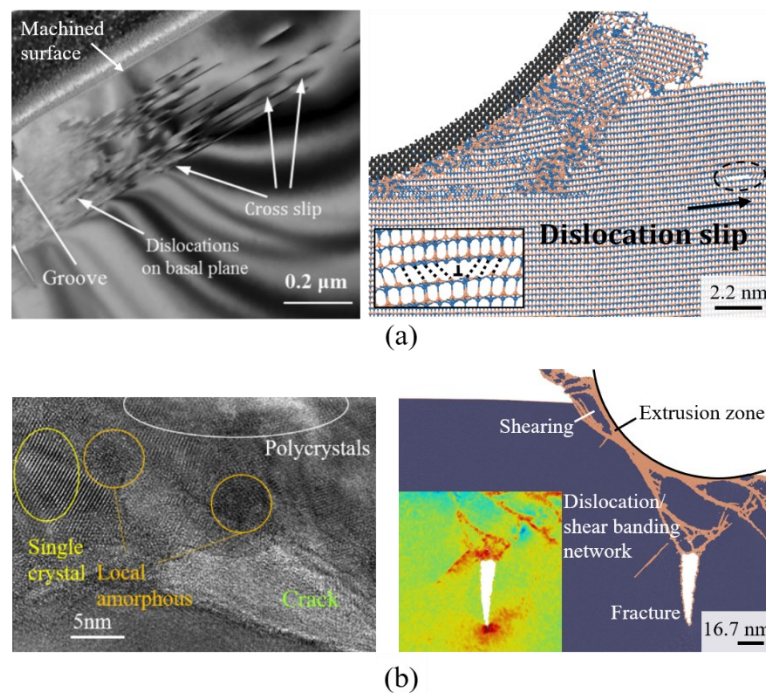
Figure 12. Comparison between MD simulations and TEM observations. (a) Basal dislocation slips in SiC [65, 164]. (b) Subsurface of GaAs (TEM) and Ge (MD) with similar lattice structure [48, 52]. The machined surface of GaAs locates in the upper left direction and the local view of simulation is the first principal stress distribution near the crack.

There are many reports about the effect of process parameters on the BDT and subsurface deformation. In practice, negative rake angle and slow feed are commonly employed to obtain higher hydrostatic pressure which increases the critical UCT, and reduce the maximum UCT (t_{max} in **Figure 11**a) in order to improve the ductile-regime cutting. However, when the rake angle is too much negative, it may decrease the NOSC depth [7]. As the rake angle reduces, the stagnation region moves up to the free surface and chip formation decreases, accompanied with an increase in the amorphous layer thickness [102]. More cutting energy imported into the workpiece has to be dissipated

through subsurface deformation, which in turn enhances the shear banding/dislocation density and the probability of crack nucleation. This is also the reason of why the machined surface would be torn under an excessively small UCT (i.e., highly negative effective rake angle) [165]. Such condition would also arise if a tool with the edge radius of several microns is used. It makes the plastic deformation more difficult because blunter tool reduces the stress intensity for extrusion or shearing, so the sharpest SCD tool is mostly employed in nanometric cutting. Similar to cutting on metal, the anisotropy from lattice orientation also has considerable influence on brittle crystals. For example, the NOSC depth of CaF_2 on the (111) plane is ~600 nm along the $[\bar{1}\bar{1}2]$ and $[1\bar{1}0]$ directions, which is three times larger than that along the $[0\bar{1}1]$ and $[1\bar{2}1]$ directions [166]. It was reported that mirror surface is easier to generate on the (001) plane of Si while cutting along the [100] orientation than the [110] orientation [98, 167], which can be explained by the slip orientation factor theory [102, 168, 169]. However, this trend on Ge is completely changed after the rake angle becomes much negative (−60°), which is probably caused by the phase transformation under large hydrostatic pressure [102]. For the tool speed, slow cutting (1-100 mm/min) has no obvious influence (for Si and Ge) [128, 143], but faster cutting (523-15700 mm/min) increases the NOSC depth of Si apparently [170]. Although it could be understood by thermal softening which prompts the transformation from cleavage to dislocation nucleation [171], details from the microstructure and stress field are still lack. It must be pointed out that current MD simulation is difficult to give a comprehensive interpretation, because the tool speed is several orders of magnitude greater than that in experiment

53

and an opposite result is always obtained. This issue becomes more serious for larger scale model, which has not been effectively resolved. Nanoindentation experiments reveal that the dynamic hardness of Si almost keeps constant in the range of 0.003-100 s^{-1}, which corresponds to a small strain rate sensitivity coefficient (< 0.01) and interprets the independence of NOSC depth on the normal cutting speed [172]. In addition to the single crystal, nanometric cutting on polycrystalline materials shows a lower propensity of amorphization [43]. It is the grain boundaries that further relax the strain energy and provide more sites where the shear slip can take place. Then, the extrusion and shear banding are weakened. As the pre-existing lattice imperfect structure, grain boundaries dominate the subsurface crack formation at the BDT as well [173]. Discussion above indicates the fact that the NOSC depth is not a constant and influenced by many factors. In fact, the ratio of the edge radius to the UCT is also important because it determines the stress field. However, such complete information is not always recorded, so the NOSC depths, which is mostly used in practice, reported in different literatures can have a dispersion even for the same workpiece material, and conducting a strict comparison is still difficult.

3.3   Tool wear mechanism

Chip formation and surface generation in nanometric cutting are influenced not only by the mechanical property of the workpiece, but also by the diamond tool edge status due to the strong size effect. Different from the topics above, knowledge on the tool wear is more empirical and phenomenological. Although the wear during
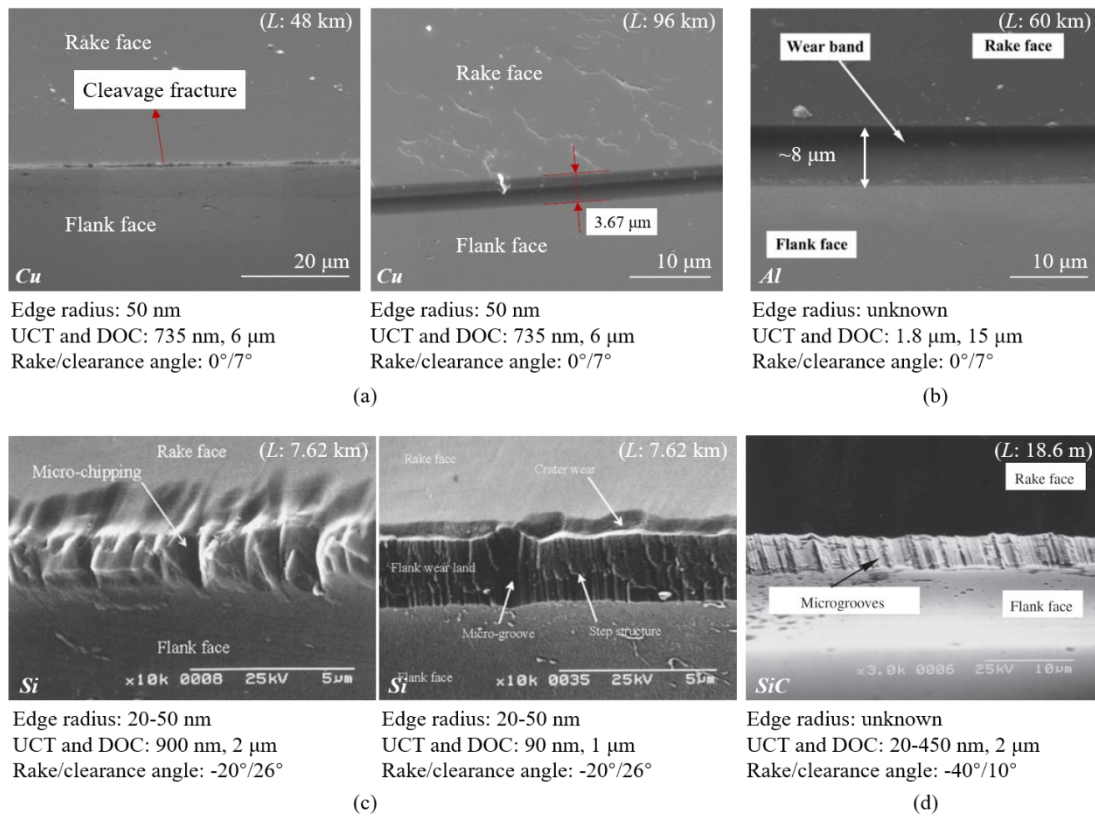
nanometric cutting can be classified from the perspective of mechanical, thermal, chemical, and hybrid modes, there has been no such well-developed wear models as those of chip formation. One reason is the huge uncertainty in the experiment, such as material microstructure, process parameter, quality of diamond crystal and edge profile, which can even lead to opposite conclusions. The other reason is that the MD simulation only gives interpretation from excessively small scale. This may be enough to understand the chemical wear, but is difficult to comprehensively reflect the role of mechanical action. As the tool wear itself is a large topic and according to the situation above, this section aims at only some typical materials encountered above, rather than an extensive discussion. Systematic review on this can be found in the references [174, 175].

For ductile metals, such as Cu and Al, the cutting length can be as long as tens of kilometres before serious wear occurs. As shown in **Figure 13**a, during the cutting of Cu, a uniform wear land on both the rake face and the flank face is formed, which evolves from individual micro breakages in the early stage [176]. Because the low hardness of Cu should not induce a strong stress, the edge chipping is attributed to the thermal-chemical erosion of oxygen where Cu acts as the catalytic agent [177]. In the cutting of Al, wear land locates on the flank face (**Figure 13**b) and energy dispersive X-ray spectroscopy detects carbon element in the chip, which indicates a diffusion wear and is verified by MD simulation [178]. It also shows a greater influence from clearance angle and feed rate than cutting speed. The blunter edge can increase the thrust force and the material flow, and the edge chipping mark would be replicated on the workpiece,

which finally deteriorate the surface quality.

Although smooth surface can be achieved on many brittle materials via the removal at nanoscale, the critical issue is that the ductile-regime cutting would not be stabilized once the tool edge is damaged, and BDT would happen. One example is the surface tearing, as a result of increased edge radius. Therefore, the wear mechanism attracted more attention for brittle materials. As shown in **Figure 13**c, the wear pattern is more complicated after cutting on Si than on ductile metals. Even for the ductile-regime machining, micro-chipping is serious after only several kilometres cutting length, accompanied with the crater and flank wear. It is intensified in the brittle-regime machining, where many microgrooves and steps occur [12]. MD studies reveal the thermo-chemical mechanism is due to the reduction in the cohesion energy of carbon under the high cutting temperature [13], as well as the graphitization of diamond lattice [125]. The formation of SiC hard particle from the dangling bonds at the tool flank face is considered as another source of abrasive wear during the nanometric cutting of Si [179], and the induced groove on flank face increases the subsurface damaged region and promotes the formation of polycrystalline structure [180]. Similar wear patterns are also observed in the machining of SiC (**Figure 13**d), while the cutting length the tool edge can sustain is only tens of metres due to the great hardness of the workpiece [181]. Efficient production of such material is still a challenge although negative rake angle has been employed.

Edge radius: 50 nm
UCT and DOC: 735 nm, 6 μm
Rake/clearance angle: 0°/7°

Edge radius: 50 nm
UCT and DOC: 735 nm, 6 μm
Rake/clearance angle: 0°/7°

Edge radius: unknown
UCT and DOC: 1.8 μm, 15 μm
Rake/clearance angle: 0°/7°

(a)

(b)

Edge radius: 20-50 nm
UCT and DOC: 900 nm, 2 μm
Rake/clearance angle: -20°/26°

Edge radius: 20-50 nm
UCT and DOC: 90 nm, 1 μm
Rake/clearance angle: -20°/26°

Edge radius: unknown
UCT and DOC: 20-450 nm, 2 μm
Rake/clearance angle: -40°/10°

(c)

(d)

Figure 13. Tool edge wear of cutting on typical materials with cutting length (L) in each subfigure. (a) Cu [176], (b) Al [178], (c) Si (left: ductile-regime, right: brittle-regime) [12], (d) SiC [181].

The last example discussed in this section is ferrous metals, a representative of difficult-to-cut materials due to the chemical reaction of diamond. There is a hypothesis showing that the diamond-to-graphite transition could be catalysed by those elements who have unpaired d-shell electrons [182]. It is also interesting to note in recent studies [183, 184] that pure iron actually does not make the major contribution to the wear. Instead, the minority elements in steel, such as Cr and W, are critical. The existence of oxygen also plays an important role because the oxidation of those elements in the workpiece hinders their reaction with carbon atoms. Therefore, an oxygen-enriched

environment is beneficial.

4. Approaches to improving machinability of difficult-to-cut materials

Brittle materials, such as crystals and ceramics, find wide applications in various fields such as advanced optics, biomedical engineering, and precision engineering. As seen in previous sections, it is difficult to maintain a stable ductile-regime cutting status due to the surface damage and tool wear. This issue becomes more serious when the workpiece material has great hardness. It means that the UCT has to be small enough to obtain a crack-free surface according to the diamond turning model, which seriously restricts the production efficiency. As a result, auxiliary machining has become a main research branch. This section introduces three typical approaches to improving the machinability of hard and brittle materials, i.e., nanometric machining of ion-implanted materials (NiIM) based on manipulating the lattice structure, laser-assisted nanometric cutting (LAC) based on thermal softening, and ultrasonic vibration-assisted cutting (UVAC) based on modifying the tool kinematics, whose features are summarized in **Table 5**.

Table 5．Features of the auxiliary machining methods.

Method	Workpiece material	Benefits	Limitations	Influence on material surface layer
NiIM	Si [128, 141, 185,	Feasible for nearly	Low efficiency for	Residual

	186, 188], Ge [143], SiC [97, 189, 190], GaP [191], WC [192]	all non-metal crystals	large area implantation	amorphous layer
LAC	Si [193, 196, 198, 200, 201, 204, 205], Ge [202], WC [203], et al.	High machining efficiency; Competitive overall low costs	Risk of diamond graphitization under high temperature	Damage reduction by the laser annealing effect
UVAC	Ferrous metals [222, 223], Si [207, 215], glass [213, 214], KDP [206], WC [208-210], et al.	Chemical wear reduction; Better lubrication	Slow workpiece speed; Sensitive to the vibration locus	Apparent vibration mark under large cutting speed

4.1   Ion implantation-assisted nanometric cutting

For semiconductors and insulators, the brittleness and hardness would decrease when the atom arrangement becomes disordered. This is the key concept of NiIM, as shown in **Figure 14**. Charged particles are first accelerated in an electric field and then directed to the target surface, which is conducted using an ion implanter (for energy up to keV) or tandem accelerator (for energy larger than MeV). During the interaction with workpiece atoms, incident ions lose energy and are slowed down via elastic (nuclear

stopping) and inelastic (electronic stopping) collisions. Workpiece atoms that gain sufficient energy during the collision would be displaced to form lattice defects. With an increase in the dosage, the crystalline lattice is destroyed and an amorphous layer is formed. To fabricate the amorphous layer efficiently, heavy ions are usually preferred due to their strong damage ability. However, they require more energy than light ions to reach the same penetration depth, which could reduce the ion number density and prolong the implantation time. These should be balanced based on the current fluence that can be supplied.
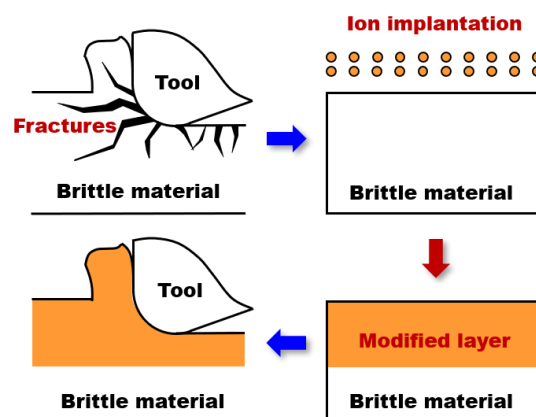
Figure 14. Illustration of NiIM. Formation of the modified layer with plenty of lattice defects is critical for depressing fractures during the cutting.

NiIM was first reported in 2011 [141], where 10 MeV fluorine ions were implanted into monocrystalline Si. As shown in **Figure 15**a, the diffraction rings indicate the formation of amorphous phase in the surface layer. After 6.5 km cutting length, the tool edge shows stable and gradual wear without breakage, and 0.86 nm Ra roughness can be achieved (**Figure 15**b,c). Nanoindentation test reveals the hardness and Young's

modulus are significantly reduced after surface amorphization (**Figure 15**d), and the NOSC depth increases up to 900 nm. MD simulation shows that the material defect induced by implantation acts as the core absorbing the cutting energy, which prevents brittle fractures. The amorphization can be realized through both nuclear collision and electronic stopping process. Electrons that gain energy during the collision would be excited and atoms are ionized, making the lattice temporarily charged and then transforms to amorphous phase via Coulomb explosion. This process is dominant especially in high-energy implantation, and a mixture of crystalline and amorphous phase would be formed caused by large temperature rise. This type of modified layer can stimulate more shear bands for chip formation, so the plastic deformation is enhanced [185]. Machinability can even be modified by the strain confined around the project range of incident ions, without the occurrence of amorphization. However, anisotropy of the NOSC depth and cutting force still exists and such an implantation may bring negative effect on specific cutting directions [186].
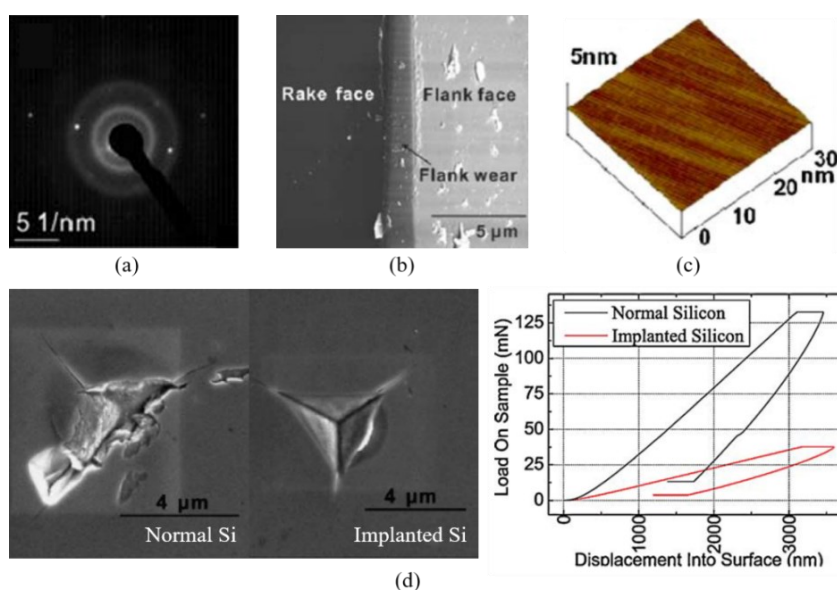
Figure 15. Improving the machinability of monocrystalline Si by F ion implantation. (a) Electron diffraction pattern of the modified layer. (b) Tool edge after cutting on implanted Si (UCT: 30 nm). (c) Machined surface topography of implanted Si. (d) Nanoindentation marks and load-displacement curves for normal and implanted Si [141].

Up to now, the effectiveness of NiIM has been verified on various brittle materials. For example, the NOSC depth of modified Ge can be enhanced to 600–700 nm after Cu ion implantation, and its decrease at large cutting speed was observed [143]. As reported in the study of nanoindentation on amorphous Si [187], the hardness increases with the strain rate which could result in a lower critical UCT according to Equation 1. For the hydrogen implanted Si, the power spectrum density of the cutting force is similar to that of cutting on Al alloy, with an obvious alleviation in the high-frequency vibration [188]. The amorphous layer enhances the ductile-regime cutting and obstructs the crack propagation into the crystalline substrate, which provides an approach to the

damage-free machining of hard and brittle materials, such as SiC, ceramics, and WC [189]. The implanted SiC has smaller subsurface damage and larger NOSC depth than normal SiC, implying a higher machining efficiency [97, 190]. On the Cl-implanted GaP, the micro-pyramid array is machined with high surface quality, and an average 16% increase in the Terahertz radiation power is achieved [191]. After Au ion implantation, the hardness and Young's modulus of binderless WC decrease from 28.6 to 19.9 GPa and from 715.8 to 535.3 GPa, respectively. This leads to an obvious reduction in the surface fracture and tool wear, as well as an enhanced plasticity indicated by the shear bands on the chip surface [192]. Furthermore, multi-implantation is proposed to prepare the amorphous layer more efficiently, by which the total dosage for a 3 μm-thick modified layer on Si is reduced to only one-fifth of that consumed in the single-implantation. The NOSC depth is enhanced from 40 nm to 80–470 nm accompanied by the formation of ductile cutting chips, and micro pillar array is achieved via ductile-regime cutting (**Figure 16**) [128]. Of course, it is difficult to completely remove the modified layer during the cutting. This issue is not critical for those applications where the change of lattice structure has no influence on the surface function, e.g., when the wavelength is much larger than the residual layer thickness for optical components. Otherwise, annealing would be required to recover the damaged lattice.
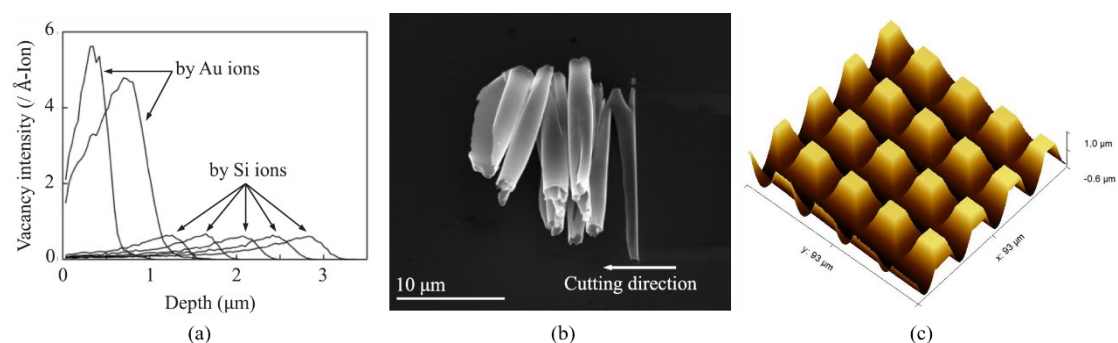
Figure 16. Surface modification by multi-ion implantation. (a) Vacancy distribution of each individual implantation. (b) Cutting chip morphology indicates a significant enhancement in the workpiece ductility [128]. (c) Microstructure array on the implanted Si machined by fly cutting.

4.2 Laser-assisted nanometric cutting

In LAC, the thermal effect of laser is utilized to reduce the material hardness and enhance the plastic deformation. A merit of this method is that the on-machine instrument can be developed to achieve a real-time surface modification. LAC at nanoscale was first reported in 2012, where a 45 W infrared beam was applied to assist the diamond cutting of monocrystalline Si via the "in-process-heat" mode [193]. It takes advantage of the good optical transmittance of diamond, based on which the laser beam can be guided through the diamond body to the cutting edge, as shown in **Figure 17**a. The local area around the tooltip is continuously heated during machining, and the cutting fluid exerts no influence on the laser beam. Moreover, the "pre-heat" mode has recently been proposed based on the macro scale LAC and has achieved preliminary applications [194]. By moving the beam outside the diamond and approaching the rake face, the material close to the cutting edge is locally heated by the laser spot prior to

being removed, as shown in **Figure 17**b. This configuration is simpler and has less restriction on the diamond shape.
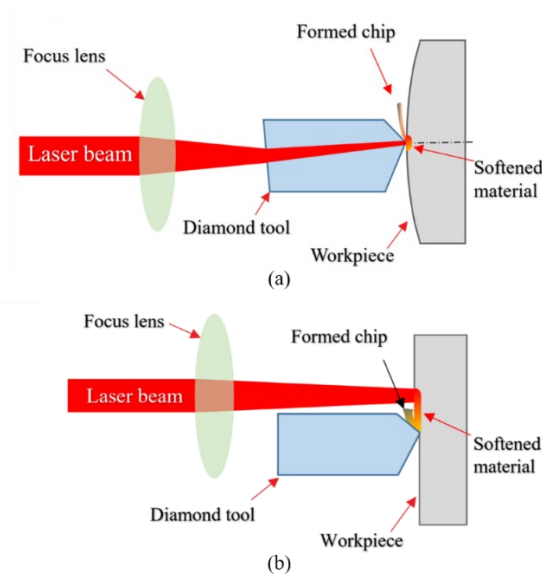
Figure 17. Two types of LAC [194]. (a) Laser in-process-heat-assisted cutting. (b) Laser pre-heat-assisted cutting.

The temperature field in the workpiece is crucial. Material near the tool edge should be locally heated to exceed the softening temperature above which the hardness begins to decrease rapidly (e.g., 400 °C for Si [195]). However, excessive laser power would result in severe residual thermal stress and rapid diamond tool wear because of oxidation and graphitization. To investigate the temperature field, numerical simulation has to be used because the resolution of existing instruments is not capable of imaging the highly localized temperature distribution at the tool tip. It shows that the hydrostatic pressure induced Si-II phase has larger laser absorptivity than the Si-I phase, which makes major contribution to the temperature rise [196]. A laser-assisted orthogonal cutting model that considers the laser heating and material deformation plasticity was

also established to study the cutting force reduction in LAC [197]. Further knowledge from the MD simulation reveals a strong correlation between the cutting anisotropy and the workpiece temperature in Si [198], and a power about 150 eV/ps is estimated for suppressing the diamond tool wear in the laser pre-heat method [199].

Using the optimized processing parameters of in-process-heat mode, a promising surface finish with a roughness of 3.2 nm in Ra was obtained on the (111) surface of Si [200]. Low residual stress, high phase purity, and good relative crystallinity were also revealed by the micro-Raman spectrum [201]. In the laser in-process-heat-assisted turning of monocrystalline Ge, X-ray diffraction analysis shows that the residual stress is reduced nearly by half compared with conventional diamond turning while using a laser power higher than 15 W [202]. In addition to single crystals, LAC shows superiority to be a solution of optical grade surface generation on ultra-hard ceramics. For example, a binderless WC aspheric mold is achieved with a roughness less than 5 nm [203]. Nanometric surface roughness can also be realized on Si using the pre-heat-assisted mode [204]. The subsurface damage in Si is alleviated after laser softening, accompanied by an increase in the NOSC depth from 150 nm to 395 nm [205]. However, cutting fluid cannot be used in this condition because of its disturbance on the laser beam, and the non-coincidence between the laser spot and the cutting edge may weaken the softening effect.

Compared with traditional LAC for hard metals, nanometric LAC is proposed to meet the demands of mirror surface on brittle crystals, glass and ceramics. This leads to distinctive mechanism related to nanometric cutting, such as the absorption

enhancement by the high-pressure phase transition. Although the laser spot becomes bigger relative to the UCT, the thermal affected area must be carefully controlled within a small range to minimize undesired thermal damage in the nanometric LAC, which is not critical for traditional process and makes a big difference in the laser heating strategy. For example, the in-process-heat mode that utilizes the diamond crystal as a focus lens is a unique operation of nanometric LAC, which has a highly localized heating zone and a large soften efficiency.

4.3 Ultrasonic vibration-assisted nanometric cutting

Different from NiIM and LAC that change material properties, UVAC consists in modifying the kinematics of the tool by imposing a vibration at an ultrasonic frequency. It is always applied in combination with diamond turning or grooving process. Small-scale material removal in UVAC is attributed to the superposition of the tool vibration locus and the workpiece linear motion. As shown in **Figure 18**, although the DOC may be several microns, the material to be removed or deformed is determined by the overlap of successive tool paths (blue and red curves), whose size can be much smaller than the DOC and reach nanoscale in the elliptical UVAC. This plays an important role in the ductile-regime cutting of brittle materials. On the basis of the critical UCT of fracture, crack length, and the cutting geometry, a predictive model for the BDT is constructed [206]. It is revealed that the critical DOC, above which cracks can propagate and reach the machined surface, increases with the vibration amplitude in the cutting direction and would reach the maximum level as the amplitude in the thrust direction increases. However, the effect of UCT reduction by the tool path overlap

might not always be sustained once the tool reaches a special position (point E in **Figure 18**), where the UCT suddenly changes from the "overlap region (AEE')" to the distance relative to the uncut surface. This rapid growing becomes a potential risk of fracture. The orientation angle of the vibration ellipse should also be controlled carefully; otherwise, the process may be even worse than conventional cutting [207]. It implies that the UVAC of brittle materials is sensitive to the vibration locus shape.
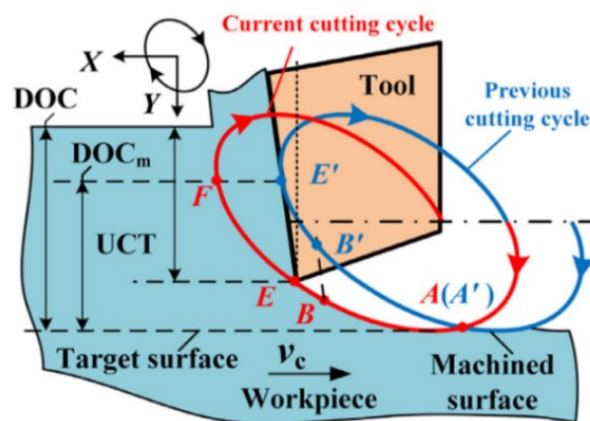
Figure 18. Geometric model of elliptical UVAC**.** The material is intermittently removed in each vibration cycle, and the overlapped tool path makes a nanometric UCT [207]. (*A/A'*: start contacting, *E*: rapid increase in UCT, *F/E'*: disengage)

UVAC has been used to improve the nanometric cutting on various brittle materials [208]. Among them, WC has attracted many research interests because of its prominent properties for mold production. Systematic studies [208-210] indicated that the thrust amplitude should be controlled to avoid pulling out the grains, and small grain size is beneficial for ductile-regime cutting. For the binder phase (Co), it can improve the plastic deformation on one hand, but also accelerate tool wear because Co has three

unpaired-d electrons which makes it affinity to diamond. However, a nanometric surface roughness on WC is still difficult to achieve efficiently because of the brittleness and great hardness inducing fast tool wear. Under the optimized parameters, the maximum UCT in diamond turning should be controlled within only 4 nm to realize the ductile-regime cutting and plastic chip formation for binder-containing and binderless WC. This issue also exists in the UVAC of other ceramics with high strength, e.g., the reaction bonded SiC [211].

An excessively small or large thrust amplitude does not work well in the 2D UVAC of brittle materials [212]. However, 1D UVAC, with zero thrust amplitude, can indeed improve the process. For example, the critical DOC of optical glass can be enhanced to 1.5 μm, and the cleavage fracture of the tool edge can be significantly reduced [213, 214]. Raman spectrum indicates the compressive stress state and polycrystalline structure of the Si chip. Different from conventional nanometric cutting, no amorphous phase is detected in UVAC because of the low strain rate during chip formation, and the chip becomes flocculent rather than continuous ribbon-like [215]. In the cutting of WC (12% Co), linear vibration even leads to less surface fracture and tool wear than elliptical vibration [209]. These results imply some essential differences and complex relationship between the cutting mechanism of 1D and 2D UVAC, which need further investigation. Technical investigations on improving the process stability of UVAC were also conducted and will not be expanded in this review [216-220]. At the end of this section, the improvement in the NOSC depth for typical brittle materials is summarized in **Table 6**.

Table 6. Improvement in the NOSC depth for various brittle materials.

Material	Vibration locus	Frequency (kHz)	NOSC depth (nm)	Ref
Si	1D	103	UVAC: 1030 CC*: 120	[215]
	2D	41.6	UVAC: 475 CC: 38	[212]
	2D	20	UVAC: 628 CC: 176	[207]
KDP	2D	19.68	UVAC: 600 CC: 80-180	[206]
Fused silica	1D	40	UVAC: 1500 CC: 500	[213]
Soda-lime glass	2D	19.8	UVAC: 900 CC: 130-260	[208]
WC	2D	36.2	UVAC: 1500 CC: < 200	[210]
Tungsten alloy	2D	39	UVAC: 800 CC: < 400	[221]

* CC: Conventional cutting

It is well known that the intermittent contact in UVAC makes diamond cutting on

ferrous metals possible. In addition to ceasing the chemical reaction (see Section 3.3), it reduces the average cutting force and enhances the lubrication. For the chip formation mechanism at nanoscale, simulation on iron reveals that the chip has a highly disordered (amorphous) lattice in UVAC, which is quite different from the crystal twinning induced polycrystalline structure in conventional cutting and shows a better viscous material flow [222]. Experiment also indicates the W and V elements should be avoided in mold steel, because of the hard carbides formation which causes abrasive tool wear [223].

There are some differences between the UVAC at nanoscale and micro/macro scale. Remembering that the UCT now is determined by the material removal in each vibration cycle instead of DOC, ductile regime machining of non-metallic crystals can only be achieved using a nanometric UCT. The UCT can be approximately evaluated as the product of workpiece speed and vibration period, which falls into the range of 30-160 nm in most of the experiments in **Table 6**. In contrast, some metallic alloys, such as steel and WC, have applications in both conventional and precision industries, so phenomenological effects caused by the reduction of scale can be observed. For example, a surface roughness less than 10 nm would be realized on steel while using a SCD tool and the UCT of 0.8-0.2 μm [223-225]. In this condition, the tool edge is sharp enough to remove the material via shearing. As the edge becomes blunt, the roughness increases to above 100 nm (polycrystalline diamond tool, 20 nm UCT [226]) or several microns (cemented carbide tool, >10 μm UCT [227]. In addition, metallographic structure deformation layer in the subsurface becomes thicker and larger than that in

conventional cutting for soft steel [224]. These are the result of enhanced plastic deformation by the round edge. For WC, micro UVAC (polycrystalline diamond tool, > 800 nm UCT) leads to a roughness larger than 30 nm and broken chip [228], while nanometric UVAC (SCD tool, 57 nm UCT) achieves <5 nm roughness and continuous chip [210].

In addition to the methods mentioned above, surface defect machining can also be used to improve the machinability of brittle materials and hard metals. In this method, predefined surface defects, such as a series of holes or grooves, are introduced on the workpiece surface prior to the machining process [229]. These defects reduce the workpiece strength and ease the material removal, which was validated via SPDT of Si wafer [230].

5. Nanometric cutting practice and application

5.1 Diamond tool-based nanometric cutting

This section provides examples to illustrate how nanometric cutting appears in the production, especially those using commercial diamond tools and ultra-precision lathe. Different from orthogonal cutting where the UCT is equal to the DOC, nanometric UCT in these methods is realized via specific motion and tool geometry in order to have an acceptable efficiency.
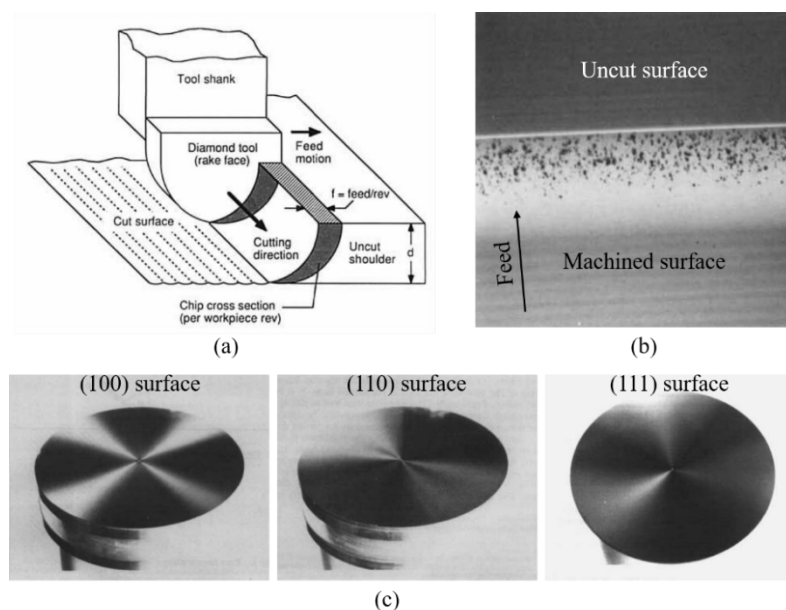
5.1.1 Single-point diamond turning

In SPDT, material is removed through the rotation of workpiece mounted on an air-bearing spindle and its relative linear motion to the tool in the feed and infeed

directions. As illustrated in **Figure 19**a, the nanoscale material removal happens in the dark crescent region [160], which results in a non-uniform UCT along the tool nose shown in **Figure 11**a. The maximum UCT (t_{max}) near the uncut surface can be evaluated by

$$t_{max} = R_{nose} - \sqrt{R_{nose}^2 + f^2 - 2f\sqrt{2R_{nose}D - D^2}} \qquad (2)$$

where R_{nose} is the tool nose radius, f is the feed per revolution, D is the DOC. This expression plays an important role in the machining of brittle materials as it indicates whether the BDT would happen. To verify it, shoulder cutting test is developed in which the face turning would be ceased and the tool would be withdrawn from the surface. As a result, a transition region joining the machined surface and the uncut surface is formed, and the crack distribution can be observed. The brittle defects on the transition shoulder in **Figure 19**b confirm the theoretical statement [231]. SPDT is also commonly used to investigate the anisotropy of the machined surface quality via the distribution of surface pits that concentrate in high-symmetry crystal orientations (**Figure 19**c) [232].

Figure 19. Investigation of nanometric cutting by single-point diamond turning.

(a) Schematic illustration of turning process [160]. (b) Shoulder cutting surface [231].

(c) Pits distribution on diamond-turned Ge with various surface orientations [232].

In SPDT, the surface geometry can be determined by the tool geometry and the modulation of the DOC, respectively [233]. For the later manner, there are two mainstream technologies, slow tool servo (STS) and fast tool servo (FTS) [234], extensively employed in the production of complex optical surfaces. Due to the heavy weight of the sliders and tool holder, the linear motion speed is limited in STS. Despite of this, STS has merit in better surface finish and larger motion amplitude. FTS is developed for improving the efficiency by using a specially designed driver that has fast dynamic respond in the DOC direction. It has been used to machine freeform surfaces on Ge to reduce the lens number and improve the performance of infrared system [235]. FTS is also suitable for machining array structure which requires high-frequency tool motion. For example, **Figure 20**a shows a laser beam integrator on

oxygen-free Cu machined by a high dynamically stiff FTS system [236]. It contains a 2D array of small concave lenses (3 nm roughness) that modify the light intensity distribution. Taking the advantages of piezo ceramic, a nano-FTS system, with an operation frequency as high as 5-10 kHz, is developed to meet the requirement of diffractive optical structure down to submicron scale (**Figure 20**b) [237].

(a)   (b)
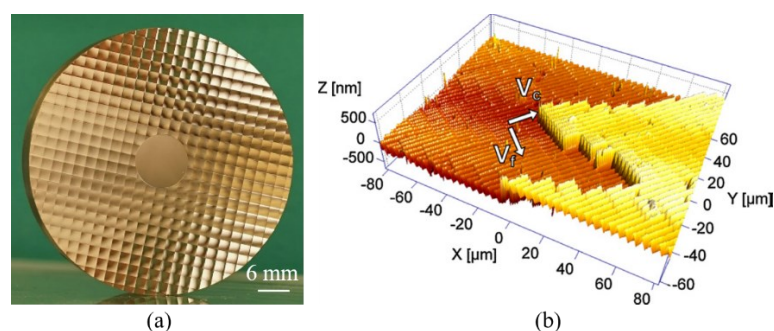
Figure 20. Array structures machined by FTS. (a) Lens array of beam integrator (UCT: 970 nm) [236]. (b) WLI measurement of submicron structure on nickel silver machined by nano-FTS [233].

In some advanced optical systems, a much shorter light wavelength has to be used to achieve ultra-high resolution. One typical example is the next-generation extreme ultraviolet (EUV) lithography machine, which uses a light source at 13.5 nm wavelength. EUV light is first collected after being emitted from the hot plasma. The grazing-incidence collector mirror can be manufactured via a high-precision metal replica using the mandrel, which has the original shape of the mirror shell and is machined through SPDT of aluminum alloy [238]. Diamond turning is also a promising approach for the production of metal illuminator optics because the replacement cost of these mirrors can be significantly reduced. With polyimide smoothing film, the roughness decreases to a sub-nanometric level and meets the specifications required for

EUV lithography [239].

5.1.2 High precision fly-cutting and milling

In fly-cutting, diamond tool, instead of workpiece, rotates with the spindle. Depending on the tool direction, fly-cutting can be classified into end-fly-cutting and radial-fly-cutting, as shown in **Figure 21**a [240]. Because a constant cutting speed and large rotation radius can be realized, it is particularly suitable for large-area machining [241, 242]. The radial fly-cutting is also widely employed to machine micro structure with various shapes. However, as material removal is intermittent, the attainable surface roughness is relatively lower than that of SPDT. As shown in **Figure 21**b [243], a piece of material would be removed in each rotation cycle as the tool advancing in the feed direction, and the UCT is at nanoscale near the machined surface. Actually, this is similar to the configuration of SPDT, where the tool nose radius is replaced by the rotation radius, so Equation 2 is still applicable to estimate the maximum UCT. In the study of BDT via taper cutting test, it is more convenient to cover a wide range of cutting speed by controlling the spindle speed or the tool rotation radius by fly-cutting [170], compared with using only the translational motion of the machine. Combined with multi-degree of freedom motion, fly-cutting can realize very complex optical system and surface structure. For example, a system containing several freeform mirrors can be manufactured using the one alignment-free manufacture approach to eliminate assembly errors. The relative position between individual mirror is assured by a uniform coordinate system and the radial-fly setup of the tool [244]. **Figure 21**c shows a micro–nano hierarchical structure machined by a novel end-fly-cutting-servo

system with four-axis motions. The microstructure is generated by the translational servo motions, whereas the nanostructure is simultaneously constructed by the residual tool marks [245].
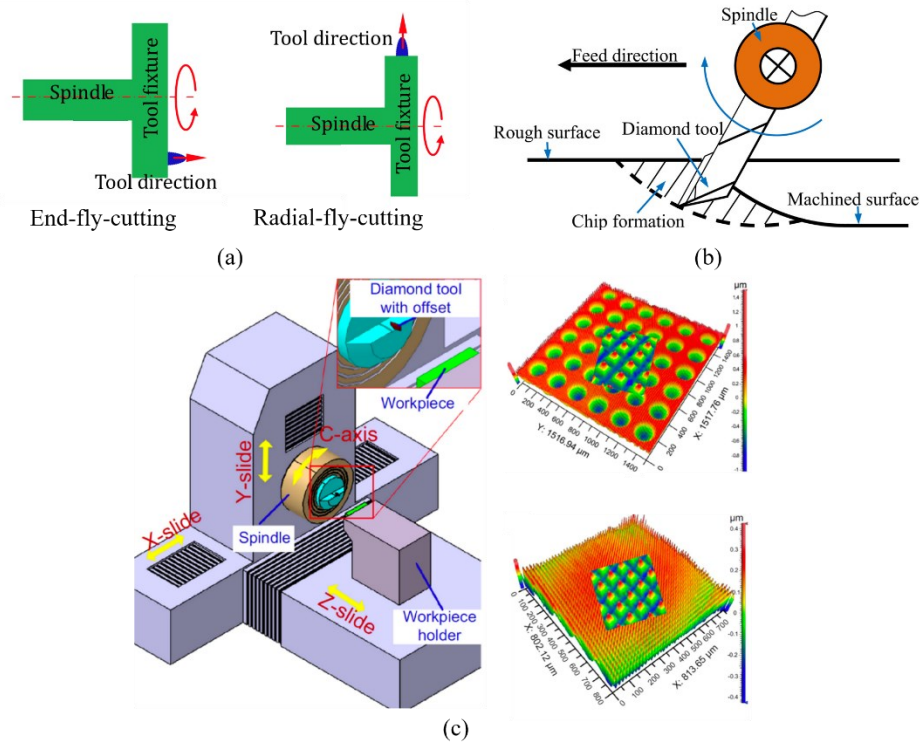
Figure 21. Diamond fly cutting. (a) Setup of two machining modes [240]. (b) Material removal in (radial) fly-cutting [243]. (c) Micro–nano hierarchical structures machined by end-fly-cutting-servo method [245].

Diamond tool also rotates in the milling process. Fly-cutting is actually also named as raster milling, and strictly speaking, what is mentioned here is the ball-end milling or face milling [233]. Different from fly-cutting, the milling tool is mounted on a cylinder rod which coaxially rotates with an extra high-speed milling spindle. The rotation speed can reach tens of thousands rpm, much faster than the common spindle of ultra-precision machine, in order to enhance the machining efficiency. As shown in

Figure 22a, a piece of material is removed when the rotating tool moves from O_{i-1} to O_i in each cycle. Projection of the removed volume on the axis of machined groove is a crescent region (*ABC*), which is exactly the same as that in SPDT, while the difference is that this region shrinks to zero from the centre position (2) to the up/down-milling side (1/3). Again, nanometric material removal takes place near the machined surface. Milling is suitable for machining both array structure and freeform surfaces. Because the tool rotation radius is very small, it can be considered as a point-by-point process [246] and there is almost no limit on the curvature or slope of the target shape. Due to the high speed, milling is also a good solution for ductile-regime cutting of brittle materials. As mentioned in Section 3, a 0.26 m/s cutting speed, which is large for SPDT and fly-cutting, has improved the NOSC depth of Si. The speed can be enhanced by one order of magnitude if a 0.5 mm nose milling tool rotating at 50000 rpm is used. Investigation on Si by a SCD tool with 50 nm edge radius reveals that the weight of amorphous phase in the chip decreases as the feed per tooth increases from 50 nm to 1.2 μm [247], providing a convincing evidence of the nanometric cutting model. Facing the low material removal rate, a novel multi-edge milling tool is developed (**Figure 22**b), based on which an aspheric binderless WC mold with 12 nm Rz roughness and 100 nm PV form error can be achieved [248].
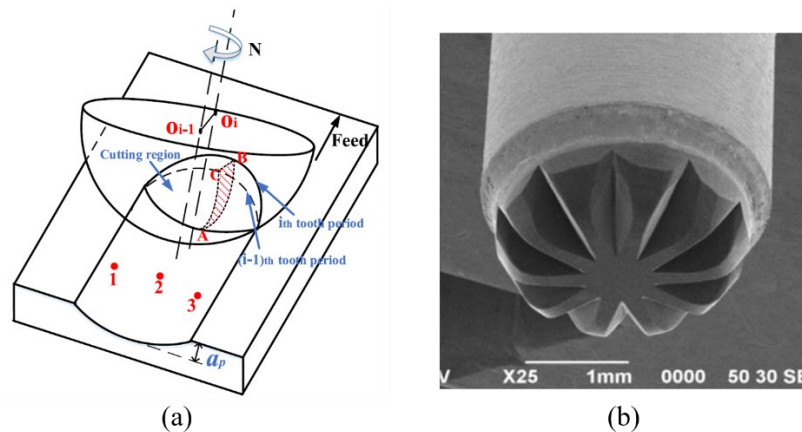
Figure 22. Diamond milling. (a) Material removal model [247]. (b) Multi-edge milling tool [248].

5.1.3 Machining capability

Figure 23 shows various machining techniques covering a wide range of spatial feature size of the target surface. As the feature shapes become increasingly complicated, the machining setup becomes more complex as well. The achievable surface roughness varies from sub-nanometre to tens of nanometres, as shown in Table 7. The form errors of the machined surface depend on many factors, such as the shape, feature depth, rotation speed, and diameter of the workpiece. Comparing different techniques only based on the form error value is very difficult. Motion bandwidth is an alternative indicator of how the positioning system performs at high speeds. It can be seen from the table that FTS is the only way to achieve very high repetitive motion speed, but the resulting surface roughness is usually poorer than the diamond turning or STS. Therefore, studying how to achieve less surface roughness using FTS without reducing the movement speed is valuable. Milling and fly-cutting are more suitable for

array structure, especially that has discontinuous slope (C_0 continuity). Due to the

intermittent feature, the efficiency is relatively lower.
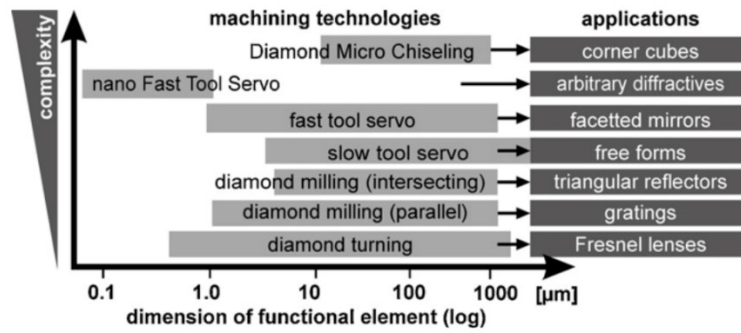
Figure 23. Machining complexity of surfaces with different functional

dimensions [249].

Table 7. Overview of diamond tool-based technologies to fabricate freeform and micro/nano-structured surfaces.

Method	Surface roughness	Limitations	Motion frequency	Reference
SPDT	< 3 nm	Limited to symmetrical parts	Near zero Hz	[250]
STS	< 5 nm	Low efficiency	< 5 Hz 40 Hz (error compensation)	[116, 251]
FTS	< 10 nm	Poorer surface roughness	100 Hz – 20 kHz	[252, 253]
Diamond milling	~ 10 nm	Long machining time & poorer surface	< 2 Hz	[254]
Fly cutting	< 10 nm	For prisms and pyramids	Near zero Hz	[240]

5.2   AFM tip-based nanometric cutting

As the feature size of target structure further decreases to nanoscale, using commercial diamond tool is not feasible any more, and AFM tip becomes an applicable solution. In general, nano-fabrication based on AFM includes local anodic oxidation [255], dip pen nanolithography [256], thermomechanical/chemical nanolithography [257], and mechanical scratching [258]. For the mechanical approach, the interaction force between the AFM tip and the workpiece is large enough to deform the contact area of workpeice. Along with the feedback control of the force, it makes the TBNC possible. As shown in **Figure 24**, different from the nanometric cutting by diamond tool where the relative motion is controlled, the force normal to the workpiece surface is maintained constant during TBNC, so the machined surface is naturally parallel to the inclined original surface, as shown in **Figure 24** [6]. Compared with the diamond tool-based nanometric cutting, TBNC owns its own advantages. It can be used to machine nanostructures with high accuracy due to the small tip (less than 10nm in tip apex) and small normal force (from micro Newton down to nano Newton). Nanostructures can be machined on the surface of existing micro structures, even the surface is curved. TBNC can machine a wide range of materials, such as metal, polymer, semiconductor, etc. Working environments include air, liquid, and even vacuum. The setup of TBNC is low cost and ease of use because commercial AFM systems available in many laboratories. However, due to the normal force feedback control strategy of the AFM system and the tip wear effect, there are also some disadvantages of TBNC. Firstly, AFM tip moves much slower than diamond tool, which results in a low machining efficiency and small

working range. Secondly, the high aspect ratio of the tip structure also induces a strong wear, especially for the common Si tip whose apex radius can be less than 10 nm. Although diamond tip is a substitute, the larger apex radius reduces the minimum achievable feature size.
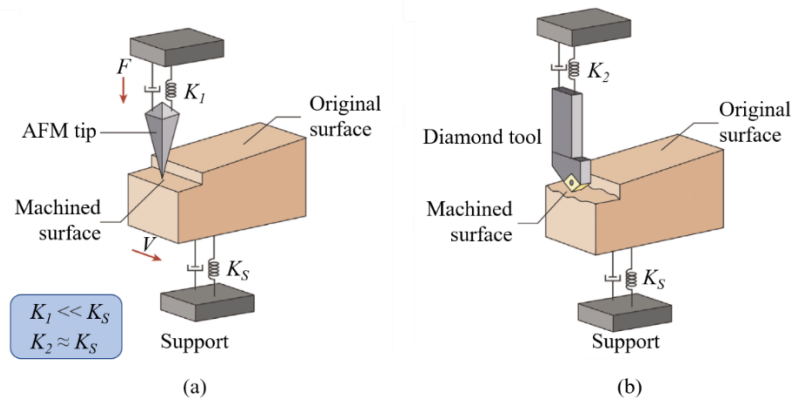

Figure 24. Schematics of two nanometric cutting approaches [6]. (a) Force control in TBNC. (b) Motion control in diamond tool-based nanometric cutting.

The mechanism of TBNC is mainly in agreement with that of diamond nanometric cutting. Specifically, as the UCT and tip radius have similar scale and the shape of AFM tip is conical or pyramidal, the rake angle is always negative. In the TBNC of metal, SEM observation indicates the trace of shear deformation (**Figure 25**a) [259]. The negative rake angle also induces strong ploughing effect, which leads to obvious pile-up and side flow on the machined surface (**Figure 25**b) [260]. A parameter is defined to characterize the manner of chip formation

$$K = \frac{h - 0.07R}{0.07(R - h)} \tag{3}$$

where h and R are the UCT and tip radius respectively. As the UCT increases, this parameter changes from 0–2 to >8, corresponding to the transition from ploughing to cutting-dominant state [261].

The AFM tip is at the end of a flexible cantilever which can undergo bending and torsion deformation. This is quite different from the diamond tool-based machining, where the whole system has great stiffness to keep the motion strictly following the program. Because of the cantilever elastic deformation, the contact area between the tip and the workpiece would change with the feed or cutting direction, which results in a variation of DOC in the TBNC of metals or semiconductors. Thus, the feed motion can also be used to machine 3D nanostructures under a constant normal force. For the nanometric cutting of thermoplastic polymer, as shown in **Figure 25**c, surface nanoripples perpendicular to the cutting direction are formed, and the mechanism lies in the competition between the driving lateral spring force and the plastic response of the workpiece [262]. In the machining of nanostructures with accurate shapes, the corresponding normal force must be determined at first. Therefore, it is necessary to understand the relationship between the normal force and the UCT. Based on fitting the experimental data, a theoretical model feasible for most workpiece materials, various tip shapes, and processing parameters has been proposed [263].


(a)   (b)   (c)
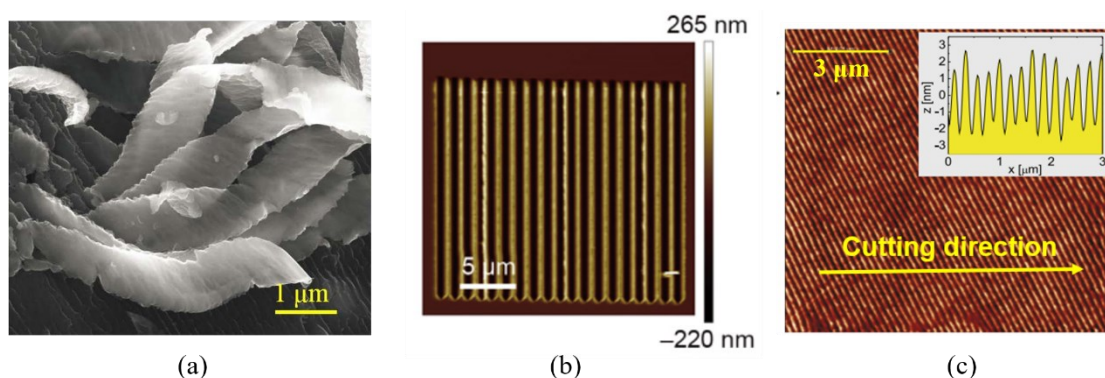
Figure 25. Characterization of TBNC. (a) Chip of Al alloy. UCT: 270-370 nm, tip radius: 110 nm. [259] (b) Periodic structure formed by pile-up [260]. (c) Formation of nanoripples due to the torsion effect of cantilever [262].

The nanometric cutting devices for TBNC can be divided into three types. Firstly, the device is based on the commercial AFM, which is used to perform nanometric cutting on the plane surface. AFM features a 3D PZT tube that drives the tip to perform nanometric cutting. Its disadvantages are the hysteresis, nonlinearity, and small moving range of PZT. Therefore, the commercial AFM with a 3D nano accuracy motion stage was modified [264]. Secondly, the device, AFM-based five-axis nanometric cutting system, likes a conventional machine tool, is used to machine nanostructures on the curved surface. As shown in Figure 26a, an air-bearing spindle is used to rotate the sample, and a rotation stage is utilized to move the AFM head [265]. Thirdly, the device can perform AFM-based vibration-assisted nanometric cutting process. As shown in Figure 26b, the sample is driven by an X-Y nano scanner with a high motion frequency [266-268]. The machined depth is determined by the normal force, and the machined width is controlled by the X-Y amplitude of the scanner. This method significantly improves the machining efficiency, where a cutting speed over 5 m/min could be achieved by a vibration-assisted setup with a 40 kHz frequency of the scanner.

(a)

(b)
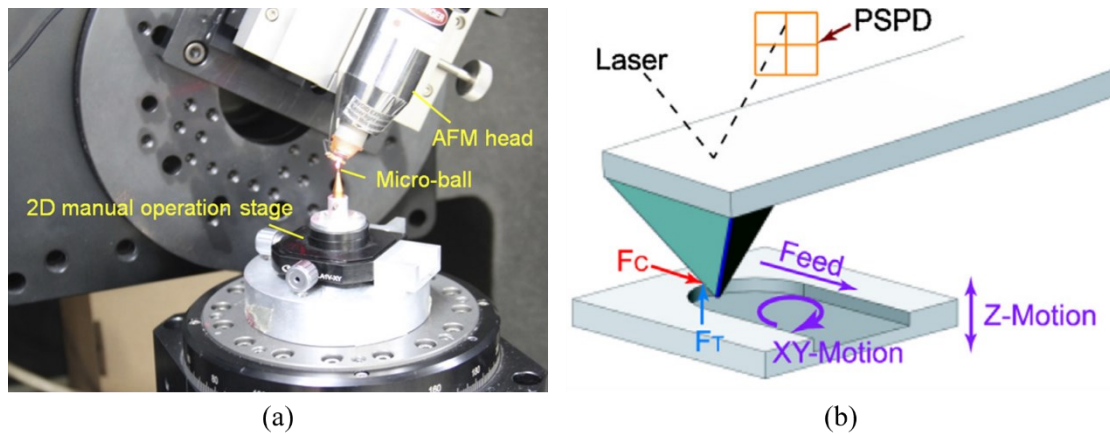
Figure 26. Realization of TBNC. (a) Five-axis AFM-based machining system [265]. (b) Vibration-assisted nanometric cutting method based on an AFM [266].

Nanostructures machined by TBNC have promising potential applications in many fields including nano optics, nano fluidics, and nano sensors. For example, nanodisks and nanotriangles with a highly precise size and shape controllability are realized to modify the plasmonic properties [269]. TBNC is integrated in the fabrication chain of chemical sensor, a single metal nanowire connected with metal electrodes, for octadecanethiol and dodecanethiol molecules measurement [270]. Complex nano-array structure is machined as a label-free surface-enhanced Raman substrate (**Figure 27**), and nano-channel connecting micro-channels is realized as a candidate of chip-based system to detect and quantify charged nanoparticles and biomolecules (such as DNA, proteins) [271, 272]. With development and optimization, the controllability and functionality of TBNC can be expected to be further improved.

(a)   (b)
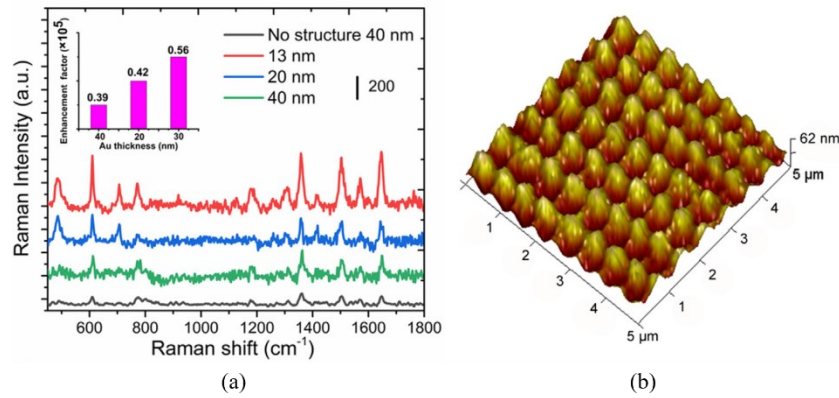
Figure 27. Surface-enhanced Raman substrate [271]. (a) Raman spectrum from substrates with and without array structure. (b) AFM image of the nanodots array substrate deposited with 40 nm Au film.

6. Future research perspectives

Although nanometric cutting mechanism and techniques have been studied and developed for decades, there are still some fundamental issues and challenges to be further investigated and clarified, as shown in **Figure 28**.
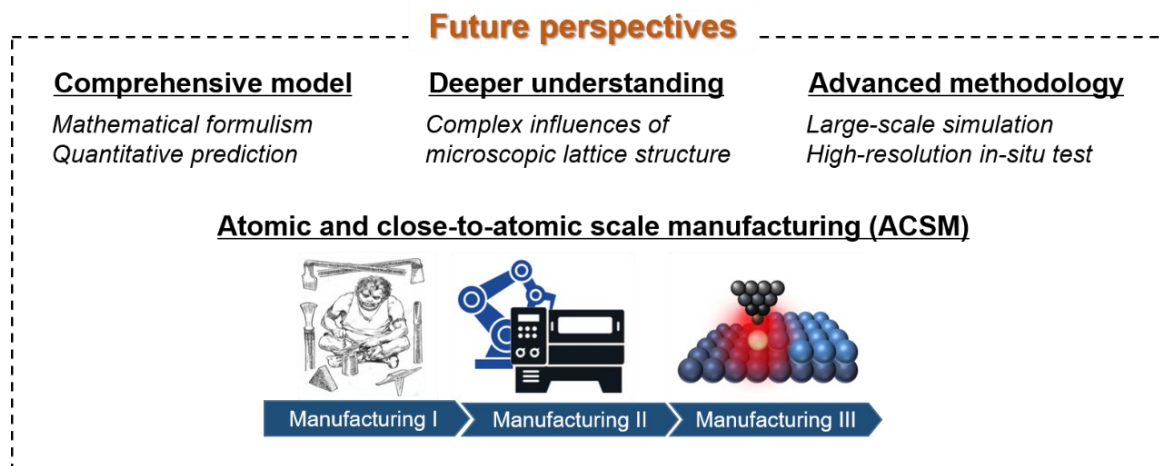
Figure 28. Challenges and future research perspectives of nanometric cutting.

(1) A new comprehensive mathematical model of nanometric cutting

Currently, modelling of nanometric cutting is still phenomenological rather than mathematical. The difficulties come from two aspects: firstly, the geometry of amorphous zone of extrusion has not been described quantitatively; secondly, material

constitutive at nanoscale becomes more complex than that at macroscale. When extrusion is dominant, both the fluid-like and the solid-state material in different regions have to be considered. It requires a comprehensive analytical model that can predict the cutting force and analyse critical stresses. This model should be able to reflect the size effect at small scale and have an asymptotic solution to the shearing model as the UCT increases.

(2) Experimental characterization of defects in nanometric cutting

The subsurface deformation of metals and alloys strongly relies on the initial surface state including crystallization orientation, GB, and TB etc. The present experimental evidences of lattice misorientation, DTL and HAB in the subsurface are mostly from the scratching and micro cutting tests. Currently, experimental characterization results of the evolution of these defects and their relationship with crystalline orientation are still missing when the UCT is less than 100 nm. In addition, GB steps are usually reported to deteriorate surface finish in nanometric cutting practice, which seems related to the grain orientation, GB angle and type, as well as cutting direction. However, the roles of different GBs in the evolution of subsurface defects and surface generation in nanometric cutting are still unclear.

(3) Mechanism of subsurface microcrack propagation

The mechanism of how the subsurface microcrack finally propagates to the machined surface is still unclear during the nanometric cutting of brittle materials. When the UCT increases continuously, the crack nucleation may happen in front of the tool edge and propagate upwards to the uncut surface. It seems that the surface fracture caused by the large UCT and excessively negative rake angle has different morphology, which implies two kinds of BDT processes.

(4) Large-scale MD simulations that is close to practical nanometric cutting scale

By large-scale simulations, many fundamental hypotheses can be justified with more certainty. For example, whether the high-pressure phase transition occurs under the complex stress state of cutting, how the lattice orientation influences surface integrity, and at what extent the extrusion or shearing model is reasonable. All these questions bring great challenge to the simulation technology, because not only the scale of model in all dimensions need enhancing, but also the cutting speed should be thoroughly reduced to the practical values used in real nanometric cutting, which requires significantly advanced algorithm and computer hardware.

(5) Effects of low strain rate on the material deformation mechanism

The pyramid tool shape and low strain rate of indenter and AFM tip-based nanoscratching restrict the applicability of the fundamental study results for diamond-based nanometric cutting practice. SEM-based nanometric cutting shares the same shortcoming of low strain rate. Therefore, the effects of low strain rate on the material deformation mechanism in nanoscale should be carefully evaluated in the future, in order to identify the application scope of these research results. Meanwhile, nanometric cutting experiments with matched strain rate should be designed and characterised as well.

(6) In-situ characterization of subsurface structural evolution

For the sake of better revealing nanometric cutting mechanism, in-situ characterization of subsurface structural evolution is in great demand. Although laser micro-Raman spectroscopy is considered as a potential on-machine measurement method for the subsurface deformation and residual stress of non-metallic material in nanometric cutting, it is still hard to capture the dynamic evolution of subsurface deformation during cutting processes with high strain rate, due to the restricts of measurement location and resolution, as well as the integration time. New methods

applicable to more kinds of workpiece for in-situ characterization of material structural change with high resolution should be developed.

(7) Single atomic layer removal to realise atomic and close-to-atomic scale manufacturing

To meet the ever-increasing requirements for such a variety of very demanding applications, Atomic and Close-to-atomic Scale Manufacturing (ACSM) has been formally proposed as the third phase of manufacturing advancement, i.e., Manufacturing III, existing in parallel with the other paradigms of craft-based Manufacturing I and precision-controllable machinery-enabled Manufacturing II. In ACSM, the objectives and processes focus directly on atoms, spanning macro- through micro- to nanoscale, where manufacturing is based on removal, migration, and addition at the atomic scale [273-276]. Since the next-generation electronic, quantum and optical devices required a precision or functional feature size would be close to the limit of material lattice, single atomic layer removal in a controllable manner by cutting can be of great scientific and engineering significance in the future, which requires further development of machines with ultimate precision and tools with atomically sharp edges.

7. Concluding remarks

Nanometric cutting is a promising manufacturing technology that produces high-end products possessing freeform shapes and micro or nanostructures with sub-nanometric surface finish. As opposed to macro and micro cuttings, the tool edge radius and UCT in nanometric cutting are at the same nanoscale. The strong size effect on material behaviour makes nanometric cutting unique in terms of cutting model, material deformation mechanism, tool wear pattern and relevant practice. This paper reviews the

state-of-the-art cutting mechanisms and models, deformation of different workpiece materials, innovative nanometric cutting approaches for difficult-to-cut materials, and practical applications. The main conclusions can be summarized as follows:

(1) Nanometric cutting can be modelled by an extrusion model concerning the size effect from both the tool edge and the workpiece material property. The essence of extrusion is the amorphous zone, which directly contacts the edge and behaves like viscoelastic fluid. Next to this zone, various kinds of deformation depending on specific workpiece material may take place, including the shear-induced chip formation, phase transition, dislocation activity and so forth. Extrusion is much weak in ductile metals, where the shearing and dislocation activities make major contribution.

(2) Extrusion becomes less dominant as the ratio of UCT to edge radius increases. However, this statement is only valid for nanometric cutting and cannot be extrapolated to micro and macro cuttings where the stress field is not large enough to induce massive amorphization zone and extrusion can be totally neglected. Therefore, the tool sharpness, UCT and workpiece material all together determine the chip formation mechanism at nanoscale. The minimum UCT for stable material removal is expected about 1%~10% of the tool edge radius.

(3) MD and multiscale simulations are important numerical methods to study the mechanism of nanometric cutting, which present atomic details of the structural evolution in various workpiece materials and diamond tool. Despite the small strain rate, nanoscratching and SEM-based nanometric cutting, together with the post characterization provide valuable experimental references of material response in micro and nanoscale. Taper-cutting is an efficient way to estimate the critical UCT of BDT for the nanometric cutting on brittle materials.

(4) For monocrystalline metals, dislocations and stacking faults dominate the material deformation in nanometric cutting, which are greatly influenced by crystalline orientation. The abundant dislocations would induce the lattice misorientation and even the HAB. For polycrystalline metals and alloys, DTL, dislocation-GB interaction, bending and shift of GB, sub-grain formation, as well as nanoscale grain rotation are all observed as subsurface deformation.

(5) For brittle crystals, the analytical model of BDT can be established by formulating the specific cutting energy based on the shearing model and fracture mechanics separately. Brittle-regime cutting originates from the subsurface shear banding/dislocation network where tensile stress concentrates at. At this stage, the micro crack propagates down to the inner of the workpiece that cannot be observed by surface measurement. An excessively small UCT, even less than the critical value, could tear the machined surface, because more cutting energy has to be dissipated in the subsurface, instead of via chip formation, which prompts subsurface defect and crack nucleation.

(6) Thermal-chemical process plays an important role in diamond tool wear in nanometric cutting. It induces the micro breakages of tool edge even during the cutting of ductile metals such as Cu. For brittle materials, it could also result in hard particles that cause abrasive wear. As opposed to what is considered conventionally, recent study reveals the minority elements (W, Cr, V) in ferrous alloy are more critical than Fe for tool wear. Flank wear is generally a common issue in nanometric cutting, accompanied with other types (crater, groove, edge fracture, etc.) for difficult-to-cut materials.

(7) Three innovative nanometric cutting approaches of NiIM, LAC and UVAC are effective in improving the machinability of difficult-to-cut materials. For brittle

materials, the first two approaches aim at enhancing the plastic deformation via ion implantation-induced amorphization and thermal softening by laser, respectively, while the third is to reduce the chip removal in each vibration cycle without an essential change in the material properties. Due to the sensitivity on the vibration locus and the impaction on the tool, UVAC may intensify the surface fracture and tool wear, and has not been used on brittle materials as widely as on ferrous metals. For LAC, an extra merit over the others is the recovery of subsurface damage (annealing effect), while the laser power must be controlled to avoid diamond graphitization.

(8) SPDT, fly cutting and milling are three major technologies for generating high precision freeform surfaces and micro/nano structures, while AFM tip-based nanomachining is another approach to generate nanostructures with even reduced feature size. The force control principle and flexible cantilever make AFM tip-based nanomachining distinct from the diamond tool-based machining, which leads to more operating modes.

(9) Future advancement in nanometric cutting could be made to develop new comprehensive mathematical model, large-scale MD simulation and in-situ subsurface structural characterization methods. Moreover, single atomic layer removal in a controllable manner by cutting is of great scientific and engineering significance in the future to meet the demand of next-generation electronic, quantum and optical devices.

Reference

[1]. E. Brinksmeier, W. Preuss. Micro-machining, Philosophical Transactions of the Royal Society A, 2012, 370(1973): 3973–3992.

[2]. F. Z. Fang, H. Wu, Y. Liu. Modelling and experimental investigation on nanometric cutting of monocrystalline silicon, International Journal of Machine Tools and Manufacture, 2005, 45(15): 1681–1686.

[3]. Korytár, Z. Záprazný, C. Ferrari, et al. Cross-sectional TEM study of subsurface damage in SPDT machining of germanium optics, Applied optics, 2018, 57(8): 1940–1943.

[4]. J. W. Yan, J. Tamaki, K. Syoji, et al. Single-point diamond turning of CaF2 for nanometric surface, The International Journal of Advanced Manufacturing Technology, 2004(9-10), 24: 640–646.

[5]. F. Z. Fang, X. Zhang, W. Gao, et al. Nanomanufacturing - Perspective and applications, CIRP Annals - Manufacturing Technology, 2017, 66(2): 683–705.

[6]. Y. D. Yan, Y. Q. Geng, Z. J. Hu. Recent advances in AFM tip-based nanomechanical machining, International Journal of Machine Tools and Manufacture, 2015, 99: 1–18.

[7]. J. W. Yan, T. Asami, H. Harada, et al. Fundamental investigation of subsurface damage in single crystalline silicon caused by diamond machining, Precision Engineering, 2009, 33(4): 378–386.

[8]. M. Lai, X. Zhang, F. Z. Fang, et al. Fundamental investigation on partially overlapped nano-cutting of monocrystalline germanium, Precision Engineering, 2017, 49: 160–168.

[9]. C. Li, F. H. Zhang, B. B. Meng, et al. Research of material removal and deformation mechanism for single crystal GGG ($Gd_3Ga_5O_{12}$) based on varied-depth nanoscratch testing, Materials & Design, 2017, 125: 180–188.

[10]. R. Komaduri, N. Chandrasekaran, L. M. Raff. Effect of tool geometry in nanometric cutting: a molecular dynamics simulation approach, Wear, 1998, 219(1): 84–97.

[11]. D. A. Lucca, R. L. Rhorer. Energy dissipation in the ultraprecision machining of copper. CIRP Annals - Manufacturing Technology, 1991, 40(1): 69–72.

[12]. J. W. Yan, K. Syoji, J. Tamaki. Some observations on the wear of diamond tools in ultra-precision cutting of single-crystal silicon, Wear, 2003, 255(7-12): 1380–1387.

[13]. K. Cheng, X. Luo, R. Ward, et al. Modeling and simulation of the tool wear in nanometric cutting, Wear, 2003, 255(7-12): 1427–1432.

[14]. G. Feng, D. Sagapuram. A strong basis for friction as the origin of size effect in cutting of metals, International Journal of Machine Tools and Manufacture, 2021, 168: 103741.

[15]. X. Luo, K. Cheng, X. Guo, et al. An investigation on the mechanics of nanometric cutting and the development of its test-bed, International Journal of Production Research, 2003, 41(7): 1449–1465.

[16]. J. D. Kim, D. S. Kim. Theoretical analysis of micro-cutting characteristics in ultra-precision machining, Journal of Materials Processing Technology, 1995, 49(3-4): 387–398.

[17]. A. Mallock. The action of cutting tools, Proceedings of the Royal Society of London, 1881, 33(216-219): 127.

[18]. F. Z. Fang, V. C. Venkatesh. Diamond cutting of silicon with nanometric finish, CIRP Annals - Manufacturing Technology, 1998, 47(1): 45–49.

[19]. E. Brinksmeier, W. Preuss, O. Riemer, et al. Ductile to brittle transition investigated by plunge-cut experiments in monocrystalline silicon, Proceedings of the ASPE 1998 Spring Topical Meeting, 1998, 17: 55–58.

[20]. T. P. Leung, W. B. Lee, X. M. Lu. Diamond turning of silicon substrates in ductile-regime, Journal of Materials Processing Technology, 1998, 73(1-3): 42–48.

[21]. D. Frenkel, B. Smit. Understanding molecular simulation: From algorithms to application, Academic Press, 2001.

[22]. W. G. Hoover, C. G. Hoover, I. F. Stowers, et al. Interface tribology via nonequilibrium molecular dynamics, MRS Online Proceedings Library, 1988, 140(1): 119–124.

[23]. J. F. Belak, I. F. Stowers. A molecular dynamics model of the orthogonal cutting process, Lawrence Livermore National Lab, CA (USA), 1990.

[24]. S. Shimada, N. Ikawa, H. Tanaka, et al. Feasibility study on ultimate accuracy in microcutting using molecular dynamics simulation, CIRP Annals - Manufacturing Technology, 1993, 42(1): 91–94.

[25]. S. Shimada, N. Ikawa, G. Ohmori, et al. Molecular dynamics analysis as compared with experimental result of micromachining, CIRP Annals - Manufacturing Technology, 1992, 41(1): 117–120.

[26]. S. Shimada, N. Ikawa, H. Tanaka, et al. Structure of micromachined surface simulated by molecular dynamics analysis, CIRP Annals - Manufacturing Technology, 1994, 43(1): 51–54.

[27]. S. Shimada, N. Ikawa, T. Inamura, et al. Brittle-ductile transition phenomena in microindentation and micromachining, CIRP Annals - Manufacturing Technology, 1995, 44(1): 523–526.

[28]. T. Inamura, S. Shimada, N. Takezawa, et al. Brittle/ductile transition phenomena observed in computer simulations of machining defect-free monocrystalline silicon, CIRP Annals - Manufacturing Technology, 1997, 46(1): 31–34.

[29]. M. Lai, X. Zhang, F. Z. Fang. Study on critical rake angle in nanometric cutting, Applied Physics A: Materials Science and Processing, 2012, 108(4): 809–818.

[30]. H. T. Liu, X. F. Zhu, Y. Z. Sun, et al. Evolution of stacking fault tetrahedral and work hardening effect in copper single crystals, Applied Surface Science, 2017, 422: 413–419.

[31]. Q. L. Wang, Q. S. Bai, J. X. Chen, et al. Subsurface defects structural evolution in nano-cutting of single crystal copper, Applied Surface Science, 2015, 344: 38–46.

[32]. H. Liu, Y. Guo, P. Zhao. Surface generation mechanism of monocrystalline materials under arbitrary crystal orientations in nanoscale cutting, Materials Today Communications, 2020, 25: 101505.

[33]. F. Xu, F. Z. Fang, X. Zhang. Hard particle effect on surface generation in nano-cutting, Applied Surface Science, 2017, 425: 1020–1027.

[34]. F. Xu, F. Z. Fang, Y. Z. Zhu, et al. Study on crystallographic orientation effect on surface generation of aluminum in nano-cutting, Nanoscale Research Letters, 2017, 12(1): 1–13.

[35]. Y. Gao, H. M. Urbassek. Evolution of plasticity in nanometric cutting of Fe single crystals, Applied Surface Science, 2014, 317: 6–10.

[36]. I. A. Alhafez, H. M. Urbassek. Orientation dependence in nanocutting of Fe single crystals: A molecular-dynamics study, Computational Materials Science, 2018, 143: 286–294.

[37]. J. Ren, M. Hao, M. Lv, et al. Molecular dynamics research on ultra-high-speed grinding mechanism of monocrystalline nickel. Applied Surface Science, 2018, 455: 629–634.

[38]. J. J. Zhang, H. B. Zheng, M. B. Shuai, et al. Molecular dynamics modeling and simulation of diamond cutting of cerium. Nanoscale Research Letters, 2017, 12(1): 1–10.

[39]. A. Sharmaa, S. S. Joshic, D. Datta, et al. Modeling and analysis of tool wear mechanisms in diamond turning of copper beryllium alloy, Journal of Manufacturing Processes, 2020, 56: 439–450.

[40]. K. You, F. Z. Fang, G. Yan. Surface generation of tungsten carbide in laser-assisted diamond turning. International Journal of Machine Tools and Manufacture, 2021, 168: 103770.

[41]. J. S. Wang, X. Zhang, F. Z. Fang, et al. A numerical study on the material removal and phase transformation in the nanometric cutting of silicon, Applied Surface Science, 2018, 455: 608–615.

[42]. Z. Wang, J. Chen, G. Wang, et al. Anisotropy of single-crystal silicon in nanometric cutting, Nanoscale Research Letters, 2017, 12(1): 300.

[43]. S. Goel, A. Kovalchenko, A. Stukowski, et al. Influence of microstructure on the cutting behaviour of silicon, Acta Materialia, 2016, 105: 464–478.

[44]. L. N. Abdulkadir, K. A. Hossein. Observed edge radius behavior during MD nanomachining of silicon at a high uncut chip thickness, International Journal of Advanced Manufacturing Technology, 2019, 101: 1741–1757.

[45]. F. Xu, F. Z. Fang, X. Zhang. Study on surface generation in nano-cutting by large-scale molecular dynamics simulation, International Journal of Advanced Manufacturing Technology, 2019, 104: 4325–4329.

[46]. M. Lai, X. Zhang, F. Z. Fang, et al. Study on nanometric cutting of germanium by molecular dynamics simulation, Nanoscale Research Letters, 2013, 8: 13.

[47]. M. Lai, X. Zhang, F. Z. Fang. Crystal orientation effect on the subsurface deformation of monocrystalline germanium in nanometric cutting, Nanoscale Research Letters, 2017, 12: 296.

[48]. J. S. Wang, X. Zhang, F. Z. Fang, et al. Study on nano-cutting of brittle material by molecular dynamics using dynamic modeling, Computational Materials Science, 2020, 183: 109851.

[49]. S. Goel, X. C. Luo, R. L. Reuben. Shear instability of nanocrystalline silicon carbide during nanometric cutting, Applied Physics Letters, 2012, 100(23): 231902.

[50]. L. Zhao, M. Alam, J. J. Zhang, et al. Amorphization-governed elasto-plastic deformation under nanoindentation in cubic (3C) silicon carbide, Ceramics International, 2020, 46(8): 12470–12479.

[51]. G. B. Xiao, S. To, G. Q Zhang. The mechanism of ductile deformation in ductile regime machining of 6H SiC, Computational Materials Science, 2015, 98: 178–188.

[52]. C. Chen, M. Lai, F. Z. Fang. Study on the crack formation mechanism in nano-cutting of gallium arsenide, Applied Surface Science, 2021, 540: 148322.

[53]. Y. He, M. Lai, F. Z. Fang. A numerical study on nanometric cutting mechanism of lutetium oxide single crystal, Applied Surface Science, 2019, 496: 143715.

[54]. W. K. Kim, B. H. Kim. A molecular dynamics study on atomistic mechanisms of nano-scale cutting process of sapphire, Journal of Mechanical Science and Technology, 2017, 31(9): 4353–4362.

[55]. J. X. Chen, M. Y. Li, F. Wang, et al. Effects of anisotropy on single-crystal SiO_2 in nano-metric cutting, Advances in Mechanical Engineering, 2020, 12(2): 1–9.

[56]. P. Zhu, C. Qiu, F. Z. Fang, et al. Molecular dynamics simulations of nanometric cutting mechanisms of amorphous alloy, Applied Surface Science, 2014, 317: 432–442.

[57]. K. E. Avila, V. H. Vardanyan, I. A. Alhafez, et al. Applicability of cutting theory to nanocutting of metallic glasses: Atomistic simulation, Journal of Non-Crystalline Solids, 2020, 550: 120363.

[58]. P. C. Wang, J. G. Yu, Q. X. Zhang. Nano-cutting mechanical properties and microstructure evolution mechanism of amorphous/ single crystal alloy interface, Computational Materials Science, 2020, 184: 109915.

[59]. V. H. Vardanyan, Z. B. Zhang, I. A. Alhafez, et al. Cutting of Al/Si bilayer systems: molecular dynamics study of twinning, phase transformation, and cracking, The International Journal of Advanced Manufacturing Technology, 2020, 107(3-4): 1297–1307.

[60]. X. G. Guo, C. H. Zhai, R. K. Kang, et al. The mechanical properties of the scratched surface for silica glass by molecular dynamics simulation, Journal of Non-Crystalline Solids, 2015, 420: 1–6.

[61]. P. Erhart, K. Albe. Analytical potential for atomistic simulations of silicon, carbon, and silicon carbide, Physical Review B, 2005, 71(3): 035211.

[62]. J. K. Bording. Molecular dynamics simulation of Ge rapidly cooled from the molten state into the amorphous state. Physical Review B, 2000, 62(11): 7103–7109

[63]. G. B. Xiao, M. J. Ren, H. B. Hong. 50 million atoms scale molecular dynamics modelling on a single consumer graphics card, Advances in Engineering Software, 2018, 124: 66–72.

[64]. G. B. Xiao, S. To, G. Q. Zhang. Molecular dynamics modelling of brittle–ductile cutting mode transition: Case study on silicon carbide, International Journal of Machine Tools and Manufacture, 2015, 88: 214–222.

[65]. J. S. Wang, F. Z. Fang. Nanometric cutting mechanism of silicon carbide, CIRP Annals-Manufacturing Technology, 2021, 70(1): 29–32.

[66]. T. Inamura, S. Shimada, N. Takezawa, et al. Crack initiation in machining monocrystalline silicon, CIRP Annals-Manufacturing Technology, 1999, 48(1): 81–84.

[67]. T. Inamura, N. Takezawa, K. Yamada, et al. Molecular dynamics simulation of micro mechanisms in slip deformation theory of crystals, CIRP Annals - Manufacturing Technology, 2006, 55(1): 51–54.

[68]. T. Inamura, Y. Shishikura, N. Takezawa. Digital microscope observation of the initial stage of cutting monocrystalline silicon, CIRP Annals - Manufacturing Technology, 2009, 58(1): 69–72.

[69]. H. Lu, N. P. Daphalapurkar, B. Wang. Multiscale simulation from atomistic to continuum-coupling molecular dynamics (MD) with the material point method (MPM), Philosophical Magazine, 2006, 86(20): 2971–2994.

[70]. B. Shiari, R. E. Miller, D. D. Klug. Multiscale simulation of material removal processes at the nanoscale, Journal of the Mechanics and Physics of Solids, 2007, 55(11): 2384–2405.

[71]. P. Z. Zhu, Y. Z. Hu, F. Z. Fang, et al. Multiscale simulations of nanoindentation and nanoscratch of single crystal copper, Applied Surface Science, 2012, 258(10): 4624–4631.

[72]. X. Z. Sun, K. Cheng. Multi-scale simulation of the nano-metric cutting process, International Journal of Advanced Manufacturing Technology, 2010, 47(9–12): 891–901.

[73]. H. M. Pen, Y. C. Liang, X. C. Luo, et al. Multiscale simulation of nanometric cutting of single crystal copper and its experimental validation, Computational Materials Science, 2011, 50(12): 3431–3441.

[74]. L. Zhang, H. W. Zhao, W. C. Guo, et al. Quasicontinuum analysis of the effect of tool geometry on nanometric cutting of single crystal copper, Optik - International Journal for Light and Electron Optics, 2014, 125(2): 682–687.

[75]. W. H. Huang, J. W. Yan. Deformation behaviour of soft-brittle polycrystalline materials determined by nanoscratching with a sharp indenter, Precision Engineering, 2021, 72: 717–729.

[76]. J. Q. Wang, Y. D. Yan, B. Jia, et al. Study on the processing outcomes of the atomic force microscopy tip-based nanoscratching on GaAs, Journal of Manufacturing Processes, 2021, 70: 238–247.

[77]. Y. D. Yan, J. Q. Wang, Y. Q. Geng, et al. Implementation of AFM tip-based nanoscratching process on single crystal copper: Study of material removal state, Applied Surface Science, 2018, 459: 723–731.

[78]. D. D. Xu, T. Edwards, Z. R. Liao, et al. Revealing nanoscale deformation mechanisms caused by shear-based material removal on individual grains of a Ni-based superalloy, Acta Materialia, 2021, 212: 116929.

[79]. F. Z. Fang, B. Liu, Z. Xu. Nanometric cutting in a scanning electron microscope, Precision Engineering, 2015, 41: 145–152.

[80]. C. Li, L. C. Zhang. Mechanical behaviour characterisation of silicon and effect of loading rate on pop-in: a nanoindentation study under ultra-low loads, Materials Science and Engineering: A, 2009, 506(1-2): 125–129.

[81]. T. H. Fang, W. J. Chang, C. M. Lin. Nanoindentation and nanoscratch characteristics of Si and GaAs. Microelectronic Engineering, 2005, 77: 389–398.

[82]. J. P. Sun, C. Li, H. Jing, et al. Nanoindentation induced deformation and pop-in events in a silicon crystal: molecular dynamics simulation and experiment, Scientific Reports, 2017, 7: 10282.

[83]. C. Li, Y. Zhang, G. Z. Zhou, et al. Theoretical modelling of brittle-to-ductile transition load of KDP crystals on (001) plane during nanoindentation and nanoscratch tests, Journal of Materials Research and Technology, 2020, 9(6): 14142–14157.

[84]. B. B. Meng, Y. Zhang, F. H. Zhang. Material removal mechanism of 6H-SiC studied by nano-scratching with Berkovich indenter, Applied Physics A, 2016, 122: 247.

[85]. C. Li, F. H. Zhang, X. Wang, et al. Repeated nanoscratch and double nanoscratch tests of Lu_2O_3 transparent ceramics: Material removal and deformation mechanism, and theoretical model of penetration depth, Journal of the European Ceramic Society, 2018, 38(2): 705–718.

[86]. W. P. Lin, J. Shimizu, L. B. Zhou, et al. Investigation of nanoscratch anisotropy of C-plane sapphire wafer using friction force microscope, Precision Engineering, 2022, 73: 51–62.

[87]. B. B. Meng, F. H. Zhang, Z. P. Li. Deformation and removal characteristics in nanoscratching of 6H-SiC with Berkovich indenter, Materials Science in Semiconductor Processing, 2015, 31: 160–165.

[88]. C. Li, Q. Zhang, Y. B. Zhang, et al. Nanoindentation and nanoscratch tests of YAG single crystals: an investigation into mechanical properties, surface formation characteristic, and theoretical model of edge-breaking size, Ceramics International, 2020, 46(3): 3382–3393.

[89]. Y. Q. Wang, X. L. Li, Y. Q. Wu, et al. The removal mechanism and force modelling of gallium oxide single crystal in single grit grinding and nanoscratching, International Journal of Mechanical Sciences, 2021, 204: 106562.

[90]. Z. J. Qiu, C. C. Liu, H. R. Wang, et al. Crack propagation and the material removal mechanism of glass–ceramics by the scratch test, Journal of the Mechanical Behavior of Biomedical Materials, 2016, 64: 75–85.

[91]. C. Li, F. H Zhang, Y. C. Piao. Strain-rate dependence of surface/subsurface deformation mechanisms during nanoscratching tests of GGG single crystal, Ceramics International, 2019, 45(12): 15015–15024.

[92]. J. Y. Feng, X. F. Huang, S. Yang, et al. Speed effect on the material behavior in high-speed scratching of BK7 glass, Ceramics International, 2021, 47: 19978–19988.

[93]. Z. F. Wang, J. J. Zhang, Z. W. Xu, et al. Crystal anisotropy-dependent shear angle variation in orthogonal cutting of single crystalline copper, Precision Engineering, 2020, 63: 41–48.

[94]. Z. F. Wang, J. J. Zhang, Z. W. Xu, et al. Crystal plasticity finite element modeling and simulation of diamond cutting of polycrystalline copper, Journal of Manufacturing Processes, 2019, 38: 187–195.

[95]. B. Liu, F. Z. Fang, R. Li, et al. Experimental study on size effect of tool edge and subsurface damage of single crystal silicon in nano-cutting, The International Journal of Advanced Manufacturing Technology, 2018, 98: 1093–1101.

[96]. D. Y. Tian, Z. W. Xu, L. Liu, et al. In-situ investigation of nanometric cutting of 3C-SiC using scanning electron microscope, The International Journal of Advanced Manufacturing Technology, 2021, 115, 2299–2312.

[97]. Z. W. Xu, L. Liu, Z. D. He, et al. Nanocutting mechanism of 6H-SiC investigated by scanning electron microscope online observation and stress-assisted and ion implant-assisted approaches, The International Journal of Advanced Manufacturing Technology, 2020, 106(9–10): 3869–3880.

[98]. B. P. O'Connor, E. R. Marsh, J. A. Couey. On the effect of crystallographic orientation on ductile material removal in silicon, Precision Engineering, 2005, 29: 124–132.

[99]. W. J. Zong, Z. M. Cao, C. L. He, et al. Theoretical modelling and FE simulation on the oblique diamond turning of ZnS crystal, International Journal of Machine Tools and Manufacture, 2016, 100: 55–71.

[100]. T. Sumomogi, M. Nakamura, T. Endo, et al. Evaluation of surface and subsurface cracks in nanoscale-machined single-crystal silicon by scanning force microscope and scanning laser microscope, Materials Characterization, 2002, 48(2-3): 141–145.

[101]. H. T. Young, H. T. Liao, H. Y. Huang. Surface integrity of silicon wafers in ultra precision machining, The International Journal of Advanced Manufacturing Technology, 2006, 29(3): 372–378.

[102]. M. Lai, X. Zhang, F. Z. Fang, et al. Effects of crystallographic orientation and negative rake angle on the brittle-ductile transition and subsurface deformation in

machining of monocrystalline germanium, Precision Engineering, 2019, 56: 164–171.

[103]. D. J. Oliver. Nanoindentation-induced deformation mechanisms in germanium, Australian National University, 2008.

[104]. S. Goel, X. C. Luo, P. Comley, et al. Brittle-ductile transition during diamond turning of single crystal silicon carbide, International Journal of Machine Tools and Manufacture, 2013, 65: 15–21.

[105]. W. Wu, Z. Xu, F. Z. Fang, et al. Decrease of FIB-induced lateral damage for diamond tool used in nanometric cutting, Nuclear Instruments and Methods in Physics Research Section B: Beam Interactions with Materials and Atoms, 2014, 330: 91–98.

[106]. W. Gao, T. Asai, Y. Arai. Precision and fast measurement of 3D cutting edge profiles of single point diamond micro-tools, CIRP Annals - Manufacturing Technology, 2009, 58(1): 451–454.

[107]. Y. D. Cai, Y. L. Chen, Y. Shimizu, et al. Molecular dynamics simulation of subnanometric tool-workpiece contact on a force sensor-integrated fast tool servo for ultra-precision microcutting, Applied Surface Science, 2016, 369: 354–365.

[108]. Y. L. Chen, Y. D. Cai, M. L. Xu, et al. An edge reversal method for precision measurement of cutting edge radius of single point diamond tools, Precision Engineering, 2017, 50: 380–387.

[109]. J. G. Gigax, J. K. Bladwin, C. J. Sheehan, et al. Microscale shear specimens for evaluating the shear deformation in single-crystal and nanocrystalline Cu and at Cu-Si interfaces, Journal of Materials Research, 2019, 34(9): 1574–1583.

[110]. C. Huag, F. Ruebeling, A. Kashiwar, et al. Early deformation mechanisms in the shear affected region underneath a copper sliding contact, Nature Communications, 2020, 11(1), 839.

[111]. A. Kareer, E. Tarleton, C. Hardie, et al. Scratching the surface: elastic rotations beneath nanoscratch and nanoindentation tests, Acta Materialia, 2020, 200: 116–126.

[112]. Z. W. Xu, Z. D. He, Y. Song, et al. Topic review: application of Raman spectroscopy characterization in micro/nano-machining, Micromachines, 2018, 9(7): 361.

[113]. R. G. Sparks, M. A. Paesler. Micro-Raman analysis of stress in machined silicon and germanium, Precision Engineering, 1988, 10(4): 191–198.

[114]. U. Bismayer, E. Brinksmeier, B. Güttler, et al. Measurement of subsurface damage in silicon wafers, Precision Engineering, 1994, 16(2): 139–144.

[115]. J. W. Yan, T. Asami, T. Kuriyagawa. Nondestructive measurement of the machining-induced amorphous layers in single-crystal silicon by laser micro-Raman spectroscopy, Precision Engineering, 2008, 32(3): 186–195.

[116]. M. Mukaida, J. W Yan. Ductile machining of single-crystal silicon for microlens arrays by ultraprecision diamond turning using a slow tool servo, International Journal of Machine Tools and Manufacture, 2016, 115: 2–14.

[117]. Z. X. Li, X. D. Zhang. Subsurface deformation of germanium in ultra-precision cutting: characterization of micro-Raman spectroscopy, International Journal of Advanced Manufacturing Technology, 2017, 91: 213–225.

[118]. M. E. Merchant. Mechanics of metal cutting process, II. Plasticity conditions in orthogonal cutting, Journal of Applied Physics, 1945, 16(6): 318–324.

[119].   X. L. Jin, Y. Altintas. Slip-line field model of micro-cutting process with round tool edge effect, Journal of Materials Processing Technology, 2011, 211(3): 339–355.

[120].   M. Lai, X. Zhang, F. Z. Fang. Nanoindentation-induced phase transformation and structural deformation of monocrystalline germanium: a molecular dynamics simulation investigation, Nanoscale Research Letters, 2013, 8: 353.

[121].   L. Zhang, J. W. Yan. Evolution of high-pressure metastable phase Si-XIII during silicon nanoindentation: A molecular dynamics study, Computational Materials Science, 2021, 191(11): 110344.

[122].   K. B. Kwon, D. W. Cho, S. J. Lee, et al. A Fluid Dynamic Analysis Model of the Ultra-Precision Cutting Mechanism, CIRP Annals-Manufacturing Technology, 1999, 48(1): 43–46.

[123].   R. G. Jasinevicius, J. G. Duduch, P. S. Pizani. Structure evaluation of submicrometre silicon chips removed by diamond turning, Journal of the Brazilian Society of Mechanical Sciences and Engineering, 2007, 22: 561–573.

[124].   F. Z. Fang, H. Wu, W. Zhou, et al. A study on mechanism of nano-cutting single crystal silicon, Journal of Materials Processing Technology, 2007, 184(1–3): 407–410.

[125].   S. Goel, X. C. Luo, R. L. Reuben, et al. Influence of temperature and crystal orientation on tool wear during single point diamond turning of silicon, Wear, 2012, 284–285: 65–72.

[126].   B. Liu, S. Li, R. Li, et al. Finite element simulation and experimental research on microcutting mechanism of single crystal silicon, International Journal of Advanced Manufacturing Technology, 2020, 110: 909–918.

[127]. P. Zhao, J. Wu, H. Chen, et al. Molecular dynamics simulation study of interaction mechanism between grain boundaries and subgrain boundaries in nano-cutting, Journal of Manufacturing Processes, 2021, 67: 418–426.

[128]. J. S. Wang, X. D. Zhang, F. Z. Fang, et al. Diamond cutting of micro-structure array on brittle material assisted by multi-ion implantation, International Journal of Machine Tools and Manufacture, 2019, 137: 58–66.

[129]. M.A. Rahman, M. Rahman, K.S. Woon, et al. Episodes of chip formation in micro-to-nanoscale cutting of Inconel 625, International Journal of Mechanical Sciences, 2021, 199: 106407.

[130]. X. Ding, A.E.W. Jarfors, G.C. Lim, et al. A study of the cutting performance of poly-crystalline oxygen free copper with single crystalline diamond micro-tools, Precision Engineering, 2012, 36: 141–152.

[131]. M. Efe, B. Gwalani, J. Tao, et al. Nanomechanical scratching induced local shear deformation and microstructural evolution in single crystal copper, Applied Surface Science, 2021, 562:150132.

[132]. D. Sagapuram, K. Viswanathan, A. Mahato, et al. Geometric flow control of shear bands by suppression of viscous sliding, Proceedings of The Royal Society A Mathematical Physical and Engineering Sciences, 2016, 472: 20160167.

[133]. F. Z. Fang, F. Xu. Recent advances in micro/nano-cutting: effect of tool edge and material properties, Nanomanufacturing and Metrology, 2018,1: 4–31.

[134]. N. Ikawa, S. Shimada, H. Tanaka, et al. An atomistic analysis of nanometric chip removal as affected by tool-work interaction in diamond turning, CIRP Annals - Manufacturing Technology, 1991, 40(1): 551–554.

[135]. R. R. Donaldson, C. K. Syn, J. S. Taylor, et al. Minimum thickness of cut in diamond turning of electroplated copper, 1987: UCRL97606.

[136]. R. Komanduri, N. Chandrasekaran, L. M. Raff. Some aspects of machining with negative-rake tools simulating grinding: a molecular dynamics simulation approach, Philosophical Magazine B: Physics of Condensed Matter, 1999, 79(7): 955–968.

[137]. W. K. Xie, F. Z. Fang. Rake angle effect in cutting-based single atomic layer removal, Journal of Manufacturing Processes, 2020, 56: 280–294.

[138]. W. J. Zong, D. Li, T. Sun, et al. The ultimate sharpness of single-crystal diamond cutting tools-Part II: A novel efficient lapping process, International Journal of Machine Tools and Manufacture, 2007, 47(5): 864–871.

[139]. Z. Xu, F. Z. Fang, S. Zhang, et al. Fabrication of micro DOE using micro tools shaped with focused ion beam, Optic Express, 2010, 18(8): 8025–8032.

[140]. G. H. Li, Z. W. Xu, F. Z. Fang, et al. Micro cutting of V-shaped cylindrical grating template for roller nano-imprint, Journal of Materials Processing Technology, 2013, 213(6): 895–904.

[141]. F. Z. Fang, Y. Chen, X. Zhang, et al. Nanometric cutting of single crystal silicon surfaces modified by ion implantation, CIRP Annals - Manufacturing Technology, 2011, 60(1): 527–530.

[142]. J. S. Wang, X. Zhang, F. Z. Fang. Molecular dynamics study on nanometric cutting of ion implanted silicon, Computational Materials Science, 2016, 117: 240–250.

[143]. J. S. Wang, F. Z. Fang, X. Zhang. An experimental study of cutting performance on monocrystalline germanium after ion implantation, Precision Engineering, 2015, 39: 220–223.

[144]. P. Y. Zhao, Q. Zhang, Y. Guo, et al. Atomistic simulation study of nanoparticle effect on nano-cutting mechanisms of single-crystalline materials, Micromachines, 2020, 11(3): 265.

[145]. V. Yamakov, D. Wolf, S. R. Phillpot, et al. Dislocation processes in the deformation of nanocrystalline aluminium by molecular-dynamics simulation, Nature Materials, 2002, 1: 45–49.

[146]. I. A. Alhafez, H. M. Urbassek. Influence of the rake angle on nanocutting of Fe single crystals: A molecular-dynamics Study, Crystals, 2020, 10(6): 516.

[147]. Q. L. Wang, Q. S. Bai, J. X. Chen, et al. Influence of cutting parameters on the depth of subsurface deformed layer in nano-cutting process of single crystal copper, Nanoscale Research Letters, 2015, 10(1): 396.

[148]. D. A. Hughes, J. S. Korellis, High load sliding, deformation microstructures, strength, and hardening for cutting and metal forming, International Journal of Machine Tools and Manufacture, 2021, 168: 103766.

[149]. J. Li, B. Liu, H. Luo, et al. A molecular dynamics investigation into plastic deformation mechanism of nanocrystalline copper for different nanoscratching rates. Computational Materials Science, 2016, 118: 66-76.

[150]. D. H. Liu, G. Wang, J. C. Yu, et al. Molecular dynamics simulation on formation mechanism of grain boundary steps in micro-cutting of polycrystalline copper, Computational Materials Science, 2017, 126: 418–425.

[151]. W. H. Huang, J. W. Yan. Surface formation mechanism in ultraprecision diamond turning of coarse-grained polycrystalline ZnSe. International Journal of Machine Tools and Manufacture, 2020, 153:103554

[152]. R. F. King, D. Tabor. The strength properties and frictional behaviour of brittle solids, Proceedings of the Royal Society A: Mathematical, Physical and Engineering Sciences,, 1954, 223(1153): 225–238.

[153]. D.M. Marsh, Plastic flow in glass, Proceedings of the Royal Society of London A: Mathematical, 1964.

[154]. T. Nakasuji, S. Kodera, S. Hara, et al. Diamond turning of brittle materials for optical components, CIRP Annals - Manufacturing Technology, 1990, 39(1): 89–92.

[155]. B. R. Lawn, D.B. Marshall. Hardness, toughness, and brittleness: an indentation analysis, Journal of the American Ceramic Society, 1979, 62(7-8): 347–350.

[156]. T. G. Bifano, T. A. Dow, R. O. Scattergood. Ductile-regime grinding: a new technology for machining brittle materials, Journal of Engineering for Industry, 1991, 113(2): 184–189.

[157]. B. B. Meng, F. H. Zhang, Z. P. Li. Deformation and removal characteristics in nanoscratching of 6H-SiC with Berkovich indenter, Materials Science in Semiconductor Processing, 2015, 31: 160–165.

[158]. A. Muhammad, X. Zhang, R. Mustafizur, et al. A predictive model of the critical undeformed chip thickness for ductile–brittle transition in nano-machining of brittle materials, International Journal of Machine Tools and Manufacture, 2013, 64: 114–122.

[159]. L. Yao, L. Zhang, Q. Jiang, et al. Prediction of critical undeformed chip thickness for ductile mode to brittle transition in the cutting of single-crystal silicon, Semiconductor Science and Technology, 2020, 35: 095010.

[160]. P. N. Blake, R. O. Scattergood. Ductile-regime machining of germanium and silicon, Journal of the American Ceramic Society, 1990, 73(4): 949–957.

[161]. J. W. Yan, K. Syoji, T. Kuriyagawa, et al. Ductile regime turning at large tool feed, Journal of Materials Processing Technology, 2002, 121: 363–372.

[162]. C. Li, F. Zhang, Y. Piao. Strain-rate dependence of surface/subsurface deformation mechanisms during nanoscratching tests of GGG single crystal, Ceramics International, 2019, 45(12): 15015–15024.

[163]. D.R. Clarke, M.C. Kroll, P.D. Kirchner, et al. Amorphization and Conductivity of Silicon and Germanium Induced by Indentation, Physical Review Letters, 1988, 60(21): 2156–2159.

[164]. B. Meng, Y. Zhang, F. Zhang. Material removal mechanism of 6H-SiC studied by nano-scratching with Berkovich indenter, Applied Physics A, 2016, 122(3): 247.

[165]. F. Z. Fang, G. Zhang. An experimental study of edge radius effect on cutting single crystal silicon, International Journal of Advanced Manufacturing Technology, 2003, 22(9–10): 703–707.

[166]. X. Chen, J. Xu, H. Fang, et al. Influence of cutting parameters on the ductile-brittle transition of single-crystal calcium fluoride during ultra-precision cutting, The International Journal of Advanced Manufacturing Technology, 2017, 89: 219–225.

[167]. J. W. Yan, T. Asami, H. Harada, et al. Crystallographic effect on subsurface damage formation in silicon microcutting, CIRP Annals - Manufacturing Technology, 2012, 61(1): 131–134.

[168]. T. Shibata, S. Fujii, E. Makino, et al. Ductile-regime turning mechanism of single-crystal silicon, Precision Engineering, 1996, 18: 129–137.

[169]. J. W. Yan, K. Maekawa, J. I. Tamaki, et al. Experimental study on the ultraprecision ductile machinability of single-crystal germanium, JSME International Journal, Series C: Mechanical Systems, Machine Elements and Manufacturing, 2004, 47(1): 29–36.

[170]. H. T. Liu, W. K. Xie, Y. Z. Sun, et al. Investigations on brittle-ductile cutting transition and crack formation in diamond cutting of mono-crystalline silicon, International Journal of Advanced Manufacturing Technology, 2018, 95: 317–326.

[171]. K. W. K. Leung, Z. L. Pan, D. H. Warner. Atomistic-based predictions of crack tip behavior in silicon carbide across a range of temperatures and strain rates, Acta Materialia, 2014, 77: 324–334.

[172]. Y. I. Golovin, Y. L. Iunin, A. I. Tyurin. Strain-rate sensitivity of the hardness of crystalline materials under dynamic nanoindentation, Doklady Physics, 2003, 48: 505–508.

[173]. Z. A. Liang, A. Wh, Z. A. Qiang, et al. Atomistic origin of brittle-to-ductile transition behavior of polycrystalline 3C-SiC in diamond cutting, Ceramics International, 2021, 47(17): 23895–23904.

[174]. S. J. Zhang, S. To, G. Q. Zhang. Diamond tool wear in ultra-precision machining, International Journal of Advanced Manufacturing Technology, 2017, 88(1-4): 613–614.

[175]. J. Guo, J. G. Zhang, Y. N. Pan, et al. A critical review on the chemical wear and wear suppression of diamond tools in diamond cutting of ferrous metals, International Journal of Extreme Manufacturing, 2020, 2(1): 012001.

[176]. D. X. Wu, B. Wang, F. Z. Fang. Effects of tool wear on surface micro-topography in ultra-precision turning, International Journal of Advanced

Manufacturing Technology, 2019, 102: 4397–4407.

[177].   H. Tanaka, S. Shimada, M. Higuchi, et al. Mechanism of cutting edge chipping and its suppression in diamond turning of copper, CIRP Annals - Manufacturing Technology, 2005, 54(1): 51–54.

[178].   G. J. Dong, X. Wang, S. D. Gao. Molecular dynamics simulation and experiment research of cutting-tool wear mechanism for cutting aluminum alloy, International Journal of Advanced Manufacturing Technology, 2018, 96(1–4): 1123–1137.

[179].   S. Goel, X. C. Luo, R. L. Reuben. Wear mechanism of diamond tools against single crystal silicon in single point diamond turning process, Tribology International, 2013, 57: 272–281.

[180].   C. L. Liu, X. Chen, J. G. Zhang, et al. Molecular dynamic simulation of tool groove wear in nanoscale cutting of silicon, AIP Advances, 2020, 10(1): 015327.

[181].   J. W. Yan, Z. Y. Zhang, T. Kuriyagawa. Mechanism for material removal in diamond turning of reaction-bonded silicon carbide. International Journal of Machine Tools and Manufacture, 2009, 49(5):366–374.

[182].   E. Paul, C. J. Evans, A. Mangamelli, et al. Chemical aspects of tool wear in single point diamond turning, Precision Engineering, 1996, 18(1): 4–19.

[183].   S. Fukumori, F. Itoigawa, S. Maegawa, et al. Suppression mechanism of diamond tool wear in ultrasonic vibration cutting, Proceedings of the 22nd International Esaform Conference on Material Forming: Esaform 2019, 2113:080020.

[184]. X. Q. Zhang, H. Deng, K. Liu. Oxygen-shielded ultrasonic vibration cutting to suppress the chemical wear of diamond tools, CIRP Annals - Manufacturing Technology, 2019, 68: 69–72.

[185]. J. S. Wang, R. T. Chen, X. D. Zhang, et al. Study on machinability of silicon irradiated by swift ions, Precision Engineering, 2018, 51: 577–581.

[186]. G. B. Xiao, S. To, E. V. Jelenkovic. Effects of non-amorphizing hydrogen ion implantation on anisotropy in micro cutting of silicon, Journal of Materials Processing Technology, 2015, 225: 439–450.

[187]. D. M. Jarzbek, M. Milczarek, S. Nosewicz, et al. Size effects of hardness and strain rate sensitivity in amorphous silicon measured by nanoindentation, Metallurgical and Materials Transactions A, 2020, 51: 1625–1633.

[188]. S. To, H. Wang, E. V. Jelenkovic. Enhancement of the machinability of silicon by hydrogen ion implantation for ultra-precision micro-cutting, International Journal of Machine Tools and Manufacture, 2013, 74: 50–55.

[189]. H. Tanaka, S. Shimada. Damage-free machining of monocrystalline silicon carbide, CIRP Annals - Manufacturing Technology, 2013, 62(1): 55–58.

[190]. B. Liu, Z. W. Xu, Y. Wang, et al. Effect of ion implantation on material removal mechanism of 6H-SiC in nano-cutting: A molecular dynamics study, Computational Materials Science, 2020, 174: 109476.

[191]. X. Hu, Y. Li, F. Z. Fang, et al. Enhancement of terahertz radiation from GaP emitters by subwavelength antireflective micropyramid structures, Optics Letters, 2013, 38(12): 2053–2055.

[192]. J. S. Wang, F. Z. Fang, G. Yan, et al. Study on diamond cutting of ion implanted tungsten carbide with and without ultrasonic vibration, Nanomanufacturing and Metrology, 2019, 2: 177–185.

[193]. D. Ravindra, M. K. Ghantasala, J. Patten. Ductile mode material removal and high-pressure phase transformation in silicon during micro-laser assisted machining, Precision Engineering, 2012, 36(2): 364–367.

[194]. K. You, G. Yan, X. C. Luo, et al. Advances in laser assisted machining of hard and brittle materials, Journal of Manufacturing Processes, 2020, 58: 677–692.

[195]. V. Domnich, Y. Aratyn, W. M. Kriven, et al. Temperature dependence of silicon hardness: experimental evidence of phase transformations, Reviews on Advanced Materials Science, 2008, 17: 33–41.

[196]. K. J. Suthar, J. Patten, L. Dong, et al. Estimation of temperature distribution in silicon during micro laser assisted machining, Proceedings of the 2008 International Manufacturing Science and Engineering Conference, 2008, 2: 72195.

[197]. S. S. Park, Y. Wei, X. L. Jin. Direct laser assisted machining with a sapphire tool for bulk metallic glass, CIRP Annals - Manufacturing Technology, 2018, 67(1): 193–196.

[198]. S. Z. Chavoshi, S. Goel, X. C. Luo. Influence of temperature on the anisotropic cutting behaviour of single crystal silicon: a molecular dynamics simulation investigation, Journal of Manufacturing Processes, 2016, 23: 201–210.

[199]. Z. W. Liu, L. Bin, X. H. Liang, et al. Study on the effect of laser-assisted machining on tool wear based on molecular dynamics simulation, Diamond and Related Materials, 2020, 109: 108022.

[200]. H. Mohammadi, D. Ravindra, S. K. Kode, et al. Experimental work on micro laser-assisted diamond turning of silicon (111), Journal of Manufacturing Processes, 2015, 19: 125–128.

[201]. S. M. Langan, D. Ravindra, A. B. Mann. Process parameter effects on residual stress and phase purity after microlaser-assisted machining of silicon, Materials and Manufacturing Processes, 2018, 33(14): 1578–1586.

[202]. H. Shahinian, D. Kang, J. Navare, et al. Ultraprecision laser-assisted diamond machining of single crystal Ge, Precision Engineering, 2020, 65: 149–155.

[203]. K. You, F. Z. Fang, G. Yan, et al. Experimental investigation on laser assisted diamond turning of binderless tungsten carbide by in-process heating, Micromachines, 2020, 11(12): 1104.

[204]. Y. J. Guo, X. J. Yang, J. Kang, et al. Experimental investigations on the laser-assisted machining of single crystal Si for optimal machining, Optics & Laser Technology, 2021, 141: 107113.

[205]. X. Chen, C. L. Liu, J. Y. Ke, et al. Subsurface damage and phase transformation in laser-assisted nanometric cutting of single crystal silicon, Materials & Design, 2020, 190: 108524.

[206]. W. H. Huang, D. P. Yu, X. Q. Zhang, et al. Ductile-regime machining model for ultrasonic elliptical vibration cutting of brittle materials, Journal of Manufacturing Processes, 2018, 36: 68–76.

[207]. J. J. Wang, W. H. Liao, P. Guo. Modulated ultrasonic elliptical vibration cutting for ductile-regime texturing of brittle materials with 2-D combined resonant and non-resonant vibrations, International Journal of Mechanical Sciences, 2020, 170: 105347.

[208]. N. Suzuki, S. Masuda, M. Haritani, et al. Ultraprecision micromachining of brittle materials by applying ultrasonic elliptical vibration cutting, Proceedings of the 2004 International Symposium on IEEE, 2004: 133–138.

[209]. X. Q. Zhang, R. Huang, K. Liu, et al. Suppression of diamond tool wear in machining of tungsten carbide by combining ultrasonic vibration and electrochemical processing, Ceramics International, 2018, 44(4): 4142–4153.

[210]. J. G. Zhang, N. Suzuki, Y. L. Wang, et al. Fundamental investigation of ultra-precision ductile machining of tungsten carbide by applying elliptical vibration cutting with single crystal diamond, Journal of Materials Processing Technology, 2014, 214(11): 2644–2659.

[211]. L. Han, J. J. Zhang, J. C. Chen, et al. Influence of vibration parameters on ultrasonic elliptical vibration cutting of reaction-bonded silicon carbide, The International Journal of Advanced Manufacturing Technology, 2020, 108: 427–437.

[212]. J. G. Zhang, J. J. Zhang, T. Cui, et al. Sculpturing of single crystal silicon microstructures by elliptical vibration cutting, Journal of Manufacturing Processes, 2017, 29: 389–398.

[213]. M. Zhou, X. J. Wang, B. K. A. Ngoi, et al. Brittle–ductile transition in the diamond cutting of glasses with the aid of ultrasonic vibration, Journal of Materials Processing Technology, 2002, 121(2–3): 243–251.

[214]. M. Zhou, B. K. A. Ngoi, M. N. Yusoff, et al. Tool wear and surface finish in diamond cutting of optical glass, Journal of Materials Processing Technology, 2006, 174(1–3): 29–33.

[215]. J. Y. Chen, T. Y. Jin, X. C. Luo. Key machining characteristics in ultrasonic vibration cutting of single crystal silicon for micro grooves, Advances in Manufacturing, 2019, 007(3): 303–314.

[216]. E. Shamoto, N. Suzuki, T. Moriwaki, et al. Development of ultrasonic elliptical vibration controller for elliptical vibration cutting, CIRP Annals-Manufacturing Technology, 2002, 51(1): 327–330.

[217]. H. J. Jung, T. Hayasaka, E. Shamoto. Study on process monitoring of elliptical vibration cutting by utilizing internal data in ultrasonic elliptical vibration device, International Journal of Precision Engineering Manufacturing-Green Technology, 2018, 5(5): 571–581.

[218]. N. Suzuki, H. Yokoi, E. Shamoto. Micro/nano sculpturing of hardened steel by controlling vibration amplitude in elliptical vibration cutting, Precision Engineering, 2011, 35(1): 44–50.

[219]. J. Zhang, N. Suzuki, E. Shamoto. Investigation on machining performance of amplitude control sculpturing method in elliptical vibration cutting, Procedia CIRP, 2013, 8: 328–333.

[220]. J. G. Zhang, N. Suzuki, Y. L. Wang, et al. Ultra-precision nano-structure fabrication by amplitude control sculpturing method in elliptical vibration cutting, Precision Engineering, 2015, 39: 86–99.

[221]. N. Suzuki, M. Haritani, J. Yang, et al. Elliptical vibration cutting of tungsten alloy molds for optical glass parts, CIRP Annals - Manufacturing Technology, 2007, 56(1): 127–130.

[222]. S. Goel, F. D. Martinez, S. Z. Chavoshi, et al. Molecular dynamics simulation of the elliptical vibration assisted machining (EVAM) of pure iron, Journal of Micromanufacturing, 2018: 1–14.

[223]. B. Bulla, F. Klocke, O. Dambon, et al. Influence of different steel alloys on the machining results in ultrasonic assisted diamond turning, Key Engineering Materials, 2012, 523–524:203–208.

[224]. M. Willert, T. Zielinski, K. Rickens, et al. Impact of ultrasonic assisted cutting of steel on surface integrity, Procedia CIRP, 2020, 87: 222–227.

[225]. J. S. Wang, F. Z. Fang, X. D. Zhang, et al. Investigation on controlling diamond tool edge and wear by ultrasonic vibration, Applied Acoustics, 2021, 176: 107896.

[226]. Y. Yuan, D. Zhang, X. Jing, et al. Freeform surface fabrication on hardened steel by double frequency vibration cutting, Journal of Materials Processing Technology, 2020, 275: 116369.

[227]. P. Zou, Y. Xu, Y. He, et al. Experimental Investigation of Ultrasonic Vibration Assisted Turning of 304 Austenitic Stainless Steel, Shock and Vibration, 2015, 817598.

[228]. C. Nath, M. Rahman, K. S. Neo. Machinability study of tungsten carbide using PCD tools under ultrasonic elliptical vibration cutting, International Journal of Machine Tools and Manufacture, 2009, 49: 1089–1095.

[229]. S. Goel, W. B. Rashid, X. C. Luo, et al. A Theoretical assessment of surface defect machining and hot machining of nanocrystalline silicon carbide, Journal of Manufacturing Science and Engineering, 2014, 136(2): 325–325.

[230]. N. Khatri, B. M. Barkachary, B. Muneeswaran, et al. Surface defects incorporated diamond machining of silicon, International Journal of Extreme Manufacturing, 2020, 2: 045102.

[231]. W. S. Blackley, R. O. Scattergood. Ductile-regime machining model for diamond turning of brittle materials, Precision Engineering, 1991, 13(2): 95–103.

[232]. W. S. Blackley, R. O. Scattergood. Crystal orientation dependence of machining damage-a stress model, Journal of the American Ceramic Society, 1990, 73(10): 3113–3115.

[233]. E. Brinksmeier, R. Glabe, L. Schönemann. Review on diamond-machining processes for the generation of functional surface structures, CIRP Journal of Manufacturing Science and Technology, 2012, 5(1): 1–7.

[234]. F. Z. Fang, X. Zhang, A. Weckenmann, et al. Manufacturing and measurement of freeform optics, CIRP Annals - Manufacturing Technology, 2013, 62 (2): 823–846.

[235]. Z. X. Li, F. Z. Fang, J. J. Chen, et al. Machining approach of freeform optics on infrared materials via ultra-precision turning, Optics Express, 2017, 25(3): 2051–2062.

[236]. F. Ding. Design, control and error analysis of a fast tool positioning system for ultra-precision machinign of freeform surface, PhD thesis, University of Strathclyde, 2019.

[237]. E. Brinksmeier, O. Riemer, R. GläBe, B. Lünemann, et al. Submicron functional surfaces generated by diamond machining. CIRP Annals - Manufacturing Technology, 2010, 59(1): 535–538.

[238]. V. Bakshi. Euv Lithography (second edition), SPIE press, 2018.

[239]. R. Soufli, E. Spiller, M. A. Schmidt, et al. Smoothing of diamond-turned substrates for extreme-ultraviolet lithography illuminators, International Society for Optics and Photonics, 2004.

[240]. S. J. Zhang, S. To, Z.W. Zhu, et al. A review of fly cutting applied to surface generation in ultra-precision machining, International Journal of Machine Tools and Manufacture, 2016, 103: 13–27.

[241]. R. C. Montesanti, S. F. Locke, S. L. Thompson, et al. Vertical-axis diamond flycutting machine for producing flat half-meter-scale optics, Optical Fabrication and Testing, 2000.

[242]. W. Q. Chen, Y. C. Liang, X. C. Luo, et al. Multi-scale surface simulation of the KDP crystal fly cutting machining, International Journal of Advanced Manufacturing Technology, 2014, 73(1–4): 289–297.

[243]. G. Q. Zhang, S. To, S. J. Zhang, Evaluation for tool flank wear and its influences on surface roughness in ultra-precision raster fly cutting, International Journal of Mechanical Sciences, 2016, 118: 125–134.

[244]. Z. X. Li, X. L. Liu, F. Z. Fang, et al. Integrated manufacture of a freeform off-axis multi-reflective imaging system without optical alignment, Optics Express, 2018, 26(6): 7625–7637.

[245]. Z. W. Zhu, S. To, S. J. Zhang. Theoretical and experimental investigation on the novel end-fly-cutting-servo diamond machining of hierarchical micro-nanostructures, International Journal of Machine Tools and Manufacture, 2015, 94: 15–25.

[246]. S. J. Zhang, Y. P. Zhou, H. J. Zhang, et al. Advances in ultra-precision machining of micro-structured functional surfaces and their typical applications, International Journal of Machine Tools and Manufacture, 2019, 142: 16–41.

[247]. M. H. Yang, F. Y. Peng, R. Yan, et al. Study on the surface damage mechanism of monocrystalline silicon in micro ball-end milling, Precision Engineering, 2019, 56: 223–234.

[248]. H. Suzuki, M. Okada, K. Fujii, et al. Development of micro milling tool made of single crystalline diamond for ceramic cutting, CIRP Annals – Manufacturing Technology, 2013, 62: 59–62.

[249]. C. Flucke, J. Osmer, B. Lünemann, et al. Scaling in Machining of Optics with Reflective to Diffractive Function, Proceedings of the 9th International Euspen Conference, 2009, 1: 17–20.

[250]. J. B. Bryan. Design and construction of an ultraprecision 84 inch diamond turning machine, Precision Engineering, 1979, 1(1): 13–17.

[251]. C. C. Chen, Y. C. Cheng, W. Y. Hsu, et al. Slow tool servo diamond turning of optical freeform surface for astigmatic contact lens, Proceedings of SPIE - The International Society for Optical Engineering, 2011, 8126(812617): 1–9.

[252]. S. J. Ludwick, D. A. Chargin, J. A. Calzaretta, et al. Design of a rotary fast tool servo for ophthalmic lens fabrication, Precision Engineering, 1999, 23(4): 253–259.

[253]. S. Rakuff, J. F. Cuttino. Design and testing of a long-range, precision fast tool servo system for diamond turning, Precision Engineering, 2009, 33(1): 18–25.

[254]. S. Scheiding, A. Y. Yi, A. Gebhardt, et al. Diamond milling or turning for the fabrication of micro lens arrays: comparing different diamond machining technologies, Proceedings of SPIE - The International Society for Optical Engineering, 2011, 7927(79270N): 1–11.

[255]. J. A. Dagata. Device fabrication by scanned probe oxidation, Science, 1995, 270(5242): 1625–1626.

[256]. R. D. Piner, J. Zhu, F. Xu, et al. "Dip-Pen" nanolithography, Science, 1999, 283(5402): 661–663.

[257]. G. Binnig, M. Despont, U. Drechsler, et al. Ultrahigh-density atomic force microscopy data storage with erase capability, Applied Physics Letters, 1999, 74(9): 1329–1331.

[258]. X. Lin, W. N. Unertl. Submicrometer modification of polymer surfaces with a surface force microscope, Applied Physics Letters, 1992, 61(6): 657–659.

[259]. Y. Geng. Study on AFM-based nanomachining models of machined depth and processing technology of multi-scale nanostructures, PhD thesis, Harbin Institute of Technology, 2016.

[260]. Y. Q. Geng, Y. D. Yan, J. Q. Wang, et al. Fabrication of periodic nanostructures using AFM tip-based nanomachining: combining groove and material pile-up topographies, Engineering, 2018, 4: 787–795.

[261]. Y. D. Yan, T. Sun, S. Dong, et al. Molecular dynamics simulation of processing using an AFM pin tool, Applied Surface Science, 2006, 252(20): 7523–7531.

[262]. E. Gnecco, P. Pedraz, P. Nita, et al. Surface rippling induced by periodic instabilities on a polymer surface, New Journal of Physics, 2015, 17: 032011.

[263]. Z. X. Dong, U. C. Wejinya. Atomic force microscopy based repeatable surface nanomachining for nanochannels on silicon substrates, Applied Surface Science, 2012, 258: 8689–8695.

[264]. S. H. Lee. Analysis of ductile mode and brittle transition of AFM nanomachining of silicon. International Journal of Machine Tools and Manufacture. 2012, 61: 71–79.

[265]. Y. Q. Geng, Y. Z. Wang, Y. D. Yan, et al. A novel AFM-based 5-axis nanoscale machine tool for fabrication of nanostructures on a micro ball, Review of Scientific Instruments, 2017, 88: 115109.

[266]. S. S. Park, M. G. Mostofa, C. I. Park, et al. Vibration assisted nano mechanical machining using AFM probe, CIRP Annals - Manufacturing Technology, 2014, 63: 537–540.

[267]. L. Zhang, J. Y. Dong. High-rate tunable ultrasonic force regulated nanomachining lithography with an atomic force microscope, Nanotechnology, 2012, 23(8): 085303.

[268]. Y. Q. Geng, E. B. Brousseau, X. S. Zhao, et al. AFM tip-based nanomachining with increased cutting speed at the tool-workpiece interface, Precision Engineering, 2018, 51: 536–544.

[269]. J. Kim, J. S. Lee, J. W. Kim, et al. Fabrication of plasmonic arrays of nanodisks and nanotriangles by nanotip Indentation lithography and their optical properties, Nanoscale, 2021, 13(8): 4475–4484.

[270]. H. Y. Lin, H. A. Chen, H. N. Lin. Fabrication of a single metal nanowire connected with dissimilar metal electrodes and its application to chemical sensing, Analytical Chemistry, 2008, 80(6): 1937–1941.

[271]. J. Q. Wang, Y. D. Yan, S. Y. Chang, et al. Label-free surface-enhanced Raman spectroscopy detection of absorption manner of lysozyme based on nanodots arrays, Applied Surface Science, 2020, 509: 145332.

[272]. Z. Wang, D. Wang, N. Jiao, et al. Nanochannel system fabricated by MEMS microfabrication and atomic force microscopy, IET Nanobiotechnology, 2011, 5(4): 108–113.

[273]. F. Z. Fang, N. Zhang, D. Guo, et al. Towards atomic and close-to-atomic scale manufacturing, International Journal of Extreme Manufacturing, 2019, 1: 4–36.

[274]. P. T. Mathew, B. J. Rodriguez, F. Z. Fang. Atomic and close-to-atomic scale manufacturing: A review on atomic layer removal methods using atomic force microscopy, Nanomanufacturing and Metrology, 2020, 3: 167–186.

[275]. F. Z. Fang. On atomic and close-to-atomic scale manufacturing-development trend of manufacturing technology, China Mechanical Engineering, 2020, 31(9): 1009–1021.

[276]. F. Z. Fang. Atomic and close-to-atomic scale manufacturing: perspectives and measures. International Journal of Extreme Manufacturing, 2020, 2(03): 5–18.